USGS
science for a changing world

Prepared in cooperation with the Miami-Dade County Water and Sewer Department

Geologic and Hydrogeologic Frameworks of the Biscayne Aquifer in Central Miami-Dade County, Florida

Scientific Investigations Report 2014–5138

U.S. Department of the Interior
U.S. Geological Survey

Cover. Data-collection activities and well sites in the Snapper Creek Well Field study area.
Photographs by Michael A. Wacker and Jeffery F. Robinson, U.S. Geological Survey.

Geologic and Hydrogeologic Frameworks of the Biscayne Aquifer in Central Miami-Dade County, Florida

By Michael A. Wacker, Kevin J. Cunningham, and John H. Williams

Prepared in cooperation with the Miami-Dade County Water and Sewer Department

Scientific Investigations Report 2014–5138

U.S. Department of the Interior
U.S. Geological Survey

U.S. Department of the Interior
SALLY JEWELL, Secretary

U.S. Geological Survey
Suzette M. Kimball, Acting Director

U.S. Geological Survey, Reston, Virginia: 2014

Suggested citation:
Wacker, M.A., Cunningham, K.J., and Williams, J.H., 2014, Geologic and hydrogeologic frameworks of the Biscayne aquifer in central Miami-Dade County, Florida: U.S. Geological Survey Scientific Investigations Report 2014–5138, 66 p., *http://dx.doi.org/10.3133/sir20145138*.

ISSN 2328-0328 (online)

Acknowledgments

The authors extend thanks to Maria MacFarlane, Sonia Villamil, and Virginia Walsh of the Miami-Dade County Water and Sewer Department for providing logistical support and assistance in the collection of field data.

The contributions of Robert A. Renken, the original U.S. Geological Survey (USGS) project chief—in particular his insight into the overall objectives of the Snapper Creek Well Field project—are much appreciated. Jeffery F. Robinson, Barclay W. Shoemaker, and Richard L. Westcott of the USGS Florida Water Science Center, Davie office, contributed to this report. Specifically, Jeffery F. Robinson assisted in the data collection and analysis, Barclay W. Shoemaker provided information on past and current studies as well as guidance on report writing, and Richard L. Westcott contributed significantly to development of a 3-dimensional geomodel of the cyclostratigraphy and sonic-log porosity of the Snapper Creek Well Field area. Rick Spechler, Louis Murray, and Leel Knowles of the USGS Florida Water Science Center, Orlando office, provided field assistance during monitoring-well construction. Thanks are also extended to the USGS Office of Groundwater, Branch of Geophysics, for use of their winch and flowmeter, and for technical assistance in the collection of flowmeter data.

Contents

Plates

[Available for download at *http://pubs.usgs.gov/sir/2014/5138/*]

1. Cross-hole flowmeter results *A*–*A*'.
2. Geologic section *B*–*B*' showing cyclostratigraphy, lithology, and depositional environments for the Biscayne aquifer in Central Miami-Dade County, Florida.
3. Hydrogeologic section *B*–*B*' showing cyclostratigraphy, lithology, and groundwater pore classes for the Biscayne aquifer in Central Miami-Dade County, Florida.

Figures

Tables

Conversion Factors

Inch/Pound to SI

Multiply	By	To obtain
	Length	
inch (in.)	25.4	millimeter (mm)
foot (ft)	0.3048	meter (m)
mile (mi)	1.609	kilometer (km)
	Area	
square mile (mi^2)	2.590	square kilometer (km^2)
	Flow rate	
cubic foot per second (ft^3/s)	0.02832	cubic meter per second (m^3/s)
gallon per minute (gal/min)	0.06309	liter per second (L/s)
million gallons per day (Mgal/d)	0.04381	cubic meter per second (m^3/s)
	Hydraulic conductivity	
foot per day (ft/d)	0.3048	meter per day (m/d)
	Transmissivity*	
foot squared per day (ft^2/d)	0.09290	meter squared per day (m^2/d)

Temperature in degrees Fahrenheit (°F) may be converted to degrees Celsius (°C) as follows:

$$°C=(°F-32)/1.8$$

Vertical coordinate information is referenced to the National Geodetic Vertical Datum of 1929 (NGVD 29).

Horizontal coordinate information is referenced to the North American Datum of 1983 (NAD 83).

Altitude, as used in this report, refers to distance above the vertical datum.

*Transmissivity: The standard unit for transmissivity is cubic foot per day per square foot times foot of aquifer thickness [$(ft^3/d)/ft^2$]ft. In this report, the mathematically reduced form, foot squared per day (ft^2/d), is used for convenience.

Abbreviations

ABI	acoustic borehole imaging tool
bls	below land surface
CHFC	composite high-frequency cycle
EM	electromagnetic
FLASH	Flow-Log Analysis of Single Holes computer program
FWS	full waveform sonic
GWSI	Groundwater Site Identification
HFC	high-frequency cycle
HFS	high-frequency sequence
ID	internal diameter
K	hydraulic conductivity
kHz	kilohertz
MIS	Marine Isotope Stage
OBI	optical borehole imaging tool
PVC	polyvinyl chloride
SCWF	Snapper Creek Well Field
SFWMD	South Florida Water Management District
SWWF	Southwest Well Field
T	transmissivity
TD	total depth
USGS	U.S. Geological Survey

Geologic and Hydrogeologic Frameworks of the Biscayne Aquifer in Central Miami-Dade County, Florida

By Michael A. Wacker, Kevin J. Cunningham, and John H. Williams

Abstract

Evaluations of the lithostratigraphy, lithofacies, paleontology, ichnology, depositional environments, and cyclostratigraphy from 11 test coreholes were linked to geophysical interpretations, and to results of hydraulic slug tests of six test coreholes at the Snapper Creek Well Field (SCWF), to construct geologic and hydrogeologic frameworks for the study area in central Miami-Dade County, Florida. The resulting geologic and hydrogeologic frameworks are consistent with those recently described for the Biscayne aquifer in the nearby Lake Belt area in Miami-Dade County and link the Lake Belt area frameworks with those developed for the SCWF study area. The hydrogeologic framework is characterized by a triple-porosity pore system of (1) matrix porosity (mainly mesoporous interparticle porosity, moldic porosity, and mesoporous to megaporous separate vugs), which under dynamic conditions, produces limited flow; (2) megaporous, touching-vug porosity that commonly forms stratiform groundwater passageways; and (3) conduit porosity, including bedding-plane vugs, decimeter-scale diameter vertical solution pipes, and meter-scale cavernous vugs. The various pore types and associated permeabilities generally have a predictable vertical spatial distribution related to the cyclostratigraphy.

The Biscayne aquifer within the study area can be described as two major flow units separated by a single middle semiconfining unit. The upper Biscayne aquifer flow unit is present mainly within the Miami Limestone at the top of the aquifer and has the greatest hydraulic conductivity values, with a mean of 8,200 feet per day. The middle semiconfining unit, mainly within the upper Fort Thompson Formation, comprises continuous to discontinuous zones with (1) matrix porosity; (2) leaky, low permeability layers that may have up to centimeter-scale vuggy porosity with higher vertical permeability than horizontal permeability; and (3) stratiform flow zones composed of fossil moldic porosity, burrow related vugs, or irregular vugs. Flow zones with a mean hydraulic conductivity of 2,600 feet per day are present within the middle semiconfining unit, but none of the flow zones are continuous across the study area. The lower Biscayne aquifer flow unit comprises a group of flow zones in the lower part of the aquifer. These flow zones are present in the lower part of the Fort Thompson Formation and in some cases within the limestone or sandstone or both in the uppermost part of the Pinecrest Sand Member of the Tamiami Formation. The mean hydraulic conductivity of major flow zones within the lower Biscayne aquifer flow unit is 5,900 feet per day, and the mean value for minor flow zones is 2,900 feet per day. A semiconfining unit is present beneath the Biscayne aquifer. The boundary between the two hydrologic units is at the top or near the top of the Pinecrest Sand Member of the Tamiami Formation. The lower semiconfining unit has a hydraulic conductivity of less than 350 feet per day.

The most productive zones of groundwater flow within the two Biscayne aquifer flow units have a characteristic pore system dominated by stratiform megaporosity related to selective dissolution of an *Ophiomorpha*-dominated ichnofabric. In the upper flow unit, decimeter-scale vertical solution pipes that are common in some areas of the SCWF study area contribute to high vertical permeability compared to that in areas without the pipes. Cross-hole flowmeter data collected from the SCWF test coreholes show that the distribution of vuggy porosity, matrix porosity, and permeability within the Biscayne aquifer of the SCWF is highly heterogeneous and anisotropic.

Groundwater withdrawals from production well fields in southeastern Florida may be inducing recharge of the Biscayne aquifer from canals near the well fields that are used for water-management functions, such as flood control and well-field pumping. The SCWF was chosen as a location within Miami-Dade County to study the potential for such recharge to the Biscayne aquifer from the C–2 (Snapper Creek) canal that roughly divides the well field in half. Geologic, hydrogeologic, and hydraulic information on the aquifer collected during construction of monitoring wells within the SCWF could be used to evaluate the groundwater flow budget at the well-field scale.

Introduction

The Biscayne aquifer consists mainly of highly transmissive karst limestone of Pleistocene age. The aquifer serves as a sole source of drinking water (Federal Register Notice, 1979) for about 3 million residents in Miami-Dade, Broward, and southeastern Palm Beach Counties, Florida. Some of the production wells in the Biscayne aquifer are

adjacent to water-management canals that are used for flood control, for recharge to the Biscayne aquifer, and to create hydraulic barriers to saltwater intrusion when used in conjunction with control structures near the coast. As part of a study to determine if withdrawals from the wells may be interacting with the water-management functions of the canals, Sunderland and Krupa (2007) attempted to quantify freshwater flow to Biscayne Bay that was being intercepted from the C–2 (Snapper Creek) canal by pumping from the Snapper Creek Well Field (SCWF) in Miami-Dade County (fig. 1). On the basis of analyses of measurements of flow in the canal and water levels in the wells, Sunderland and Krupa (2007) attributed a loss of 20 cubic feet per second from a reach of the C–2 canal that includes the SCWF to withdrawals from the well field. They recommended further research, however, due to uncertainty in their results created by wind, low canal-flow velocities, and inexact well-field pumping rates. Swain (2012) also reported a statistical relation between well-field pumping and water levels in the C–2 canal.

As part of a 20-year, drinking-water permit application, Miami-Dade County is required by the State of Florida to construct artificial recharge systems in the Biscayne aquifer, using reclaimed wastewater to ensure production-well groundwater withdrawals do not reduce surface-water conveyance from the Everglades wetlands to Biscayne Bay. Water-quality and fiscal issues associated with development of an artificial recharge infrastructure are yet to be resolved. A rigorous, quantitative accounting of potential surface-water depletion due to well-field pumping could help improve Miami-Dade County water-management strategies.

One of the uncertainties in quantifying the effect of groundwater pumping on the groundwater/surface-water exchange in the canals is the hydraulic connectivity between the aquifer units from which the production wells are pumping and the canal. Understanding the distribution and connectivity of flow zones can improve predictions of the response of the hydrologic system to water-resource management activities. Currently, the South Florida Water Management District's (SFWMD) Lower East Coast Groundwater Flow Model (South Florida Water Management District, 2000) is being used to assess the impact of well-field pumping on canals near the Alexander Orr, Snapper Creek, and Southwest Well Fields (SWWF; fig. 1). The model is designed to address regional-scale groundwater-management and assessment issues and is likely too coarse to accurately assess the more localized effects of well-field pumping on canal leakage.

To address this localized uncertainty, the U.S. Geological Survey (USGS), in cooperation with Miami-Dade County Water and Sewer Department, began a study in 2009 to evaluate canal leakage in response to well-field pumping at the well-field scale. Specifically, the study included a detailed characterization of the hydrogeology and hydraulic properties at the well field, long-term monitoring of canal flows and calculation of leakages, controlled field-scale experiments of hydraulic response to well-field stresses, and simulation of canal-aquifer exchanges for known conditions at the SCWF in central Miami-Dade County. This report presents the geologic and hydrologic frameworks of central Miami-Dade County that were developed for this study. These frameworks provide information on the heterogeneity of hydraulic properties and spatial distribution of geologic and hydrologic units at the scale of the well field, allowing more accurate evaluations of the effects of local groundwater stresses on canal leakage and providing insight on the scale of processes and properties important to the development of conceptual and quantitative flow models of the Biscayne aquifer.

Purpose and Scope

This report describes the geologic and hydrogeologic frameworks of the Biscayne aquifer for an approximate 32 square mile (mi^2) study area in central Miami-Dade County (fig. 1). Geologic, borehole geophysical, and hydraulic study methods previously developed for aquifer characterization within this unique karst aquifer (Cunningham, 2004; Cunningham and others, 2004b, 2004c, 2006a, 2006b; Wacker and Cunningham, 2008) were used to develop an understanding of the spatial distribution of physical and hydraulic properties of the Biscayne aquifer throughout much of the study area. The geologic and hydrogeologic frameworks developed in this study can be used as input into a numerical model that can be used to quantify leakage from the canal to the production wells.

Geologic and hydrogeologic data collected at the SCWF were integrated with existing geologic and hydrogeologic frameworks for the Biscayne aquifer outside of the SCWF developed by Cunningham (2004), Cunningham and others (2004b, 2004c, 2006a, 2006b, 2009, 2012), and Cunningham and Sukop (2011). This report presents detailed geologic, borehole geophysical, and hydraulic property data of the Biscayne aquifer collected from six test coreholes at the SCWF and also links the two frameworks at the SCWF to those at five other test coreholes in the study area (fig. 1) to develop a consistent model of the spatial distribution of physical and hydraulic properties of the Biscayne aquifer pore system throughout the study area.

In addition to the six coreholes drilled at the SCWF, three additional test coreholes (G–3883, G–3884, and G–3889; fig. 1) were drilled outside the SCWF to collect additional borehole geophysical data. These three coreholes were not completed as monitoring wells to allow access for future investigations. Two test coreholes (G–3883 and G3884) are at the Southwest Well Field (SWWF) and were used to develop the geologic and hydrogeologic frameworks. Borehole geophysical data displays, lithologic descriptions, and core photographs of these three coreholes are included in the appendixes. A core description (app. 1) and core photographs (app. 2) were produced for the G–3889 test corehole at the proposed South Miami Heights Well Field. Detailed analysis of this test corehole was not incorporated as part of the framework because the well is outside of the study area. Three previously drilled test coreholes (G–3790, G–3834, and G–3840) were used in this study to develop the geologic and hydrogeologic frameworks; however, descriptive data for these wells are not included in this report.

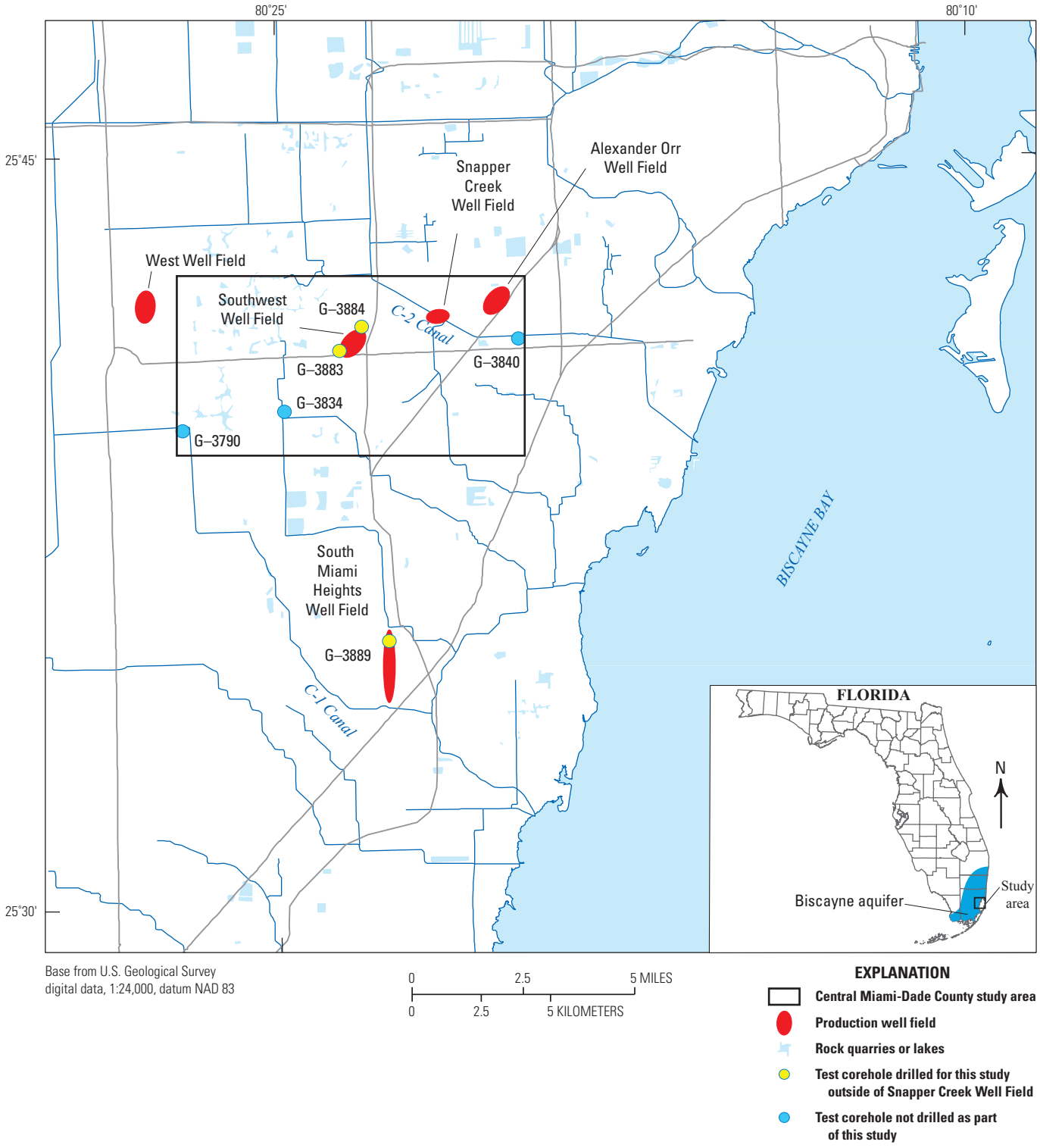

Figure 1. Location of Snapper Creek Well Field and other well fields in Miami-Dade County, and test coreholes drilled for or used as part of this study outside of the Snapper Creek Well Field.

Description of the Study Area

The study area is in central Miami-Dade County (fig. 1). The surficial aquifer system within the study area (fig. 2) and southeast Florida consists of Pliocene to Holocene age siliciclastic and carbonate sediments with a depth of 200 feet (ft); Fish and Stewart, 1991; Reese and Cunningham, 2000). The Biscayne aquifer forms the top or water-table aquifer of the surficial aquifer system and is the principal water supply for southeast Florida. Within the study area, limestone of the Fort Thompson Formation and Miami Limestone compose the Biscayne aquifer, and confining to semiconfining sand and limestone of the Pinecrest Sand Member of the Tamiami Formation forms the base of the aquifer (fig. 2). The Biscayne aquifer is one of the most productive karst aquifers in the world (Parker and others, 1955; Fish and Stewart, 1991) with measured transmissivities ranging from 500,000 to 2,000,000 feet squared per day (ft^2/d).

The focus of this study, the Snapper Creek Well Field, is located in the eastern part of the study area. A reach of the C–2 canal flowing from west-northwest to east-southeast divides the SCWF into a northeastern area and southwestern area (figs. 1 and 3). Four production wells each cased to 50 ft below land surface (S–3011, S–3012, S–3013, and S–3014, fig. 3) are located in the SCWF. Two of the wells (S–3011 and S–3012) are on the northeastern side of the C–2 canal, and the other two wells (S–3013 and S–3014) are on the southwestern side of the canal. Each well is rated at producing 10 million gallons per day (Mgal/d) giving a total capacity for the well field of 40 Mgal/d, although typically only one well is being pumped at any time. Test coreholes G–3883 and G–3884 are located at either end of the SWWF, west of the SCWF (fig. 1). Existing coreholes included in the study area, G–3834 and G–3790, are southwest of the SWWF and SCWF and provide a link to areas studied previously (Cunningham and others, 2004b; 2006a, 2006b). Existing test corehole G–3840 is east of the SCWF along the C–2 canal.

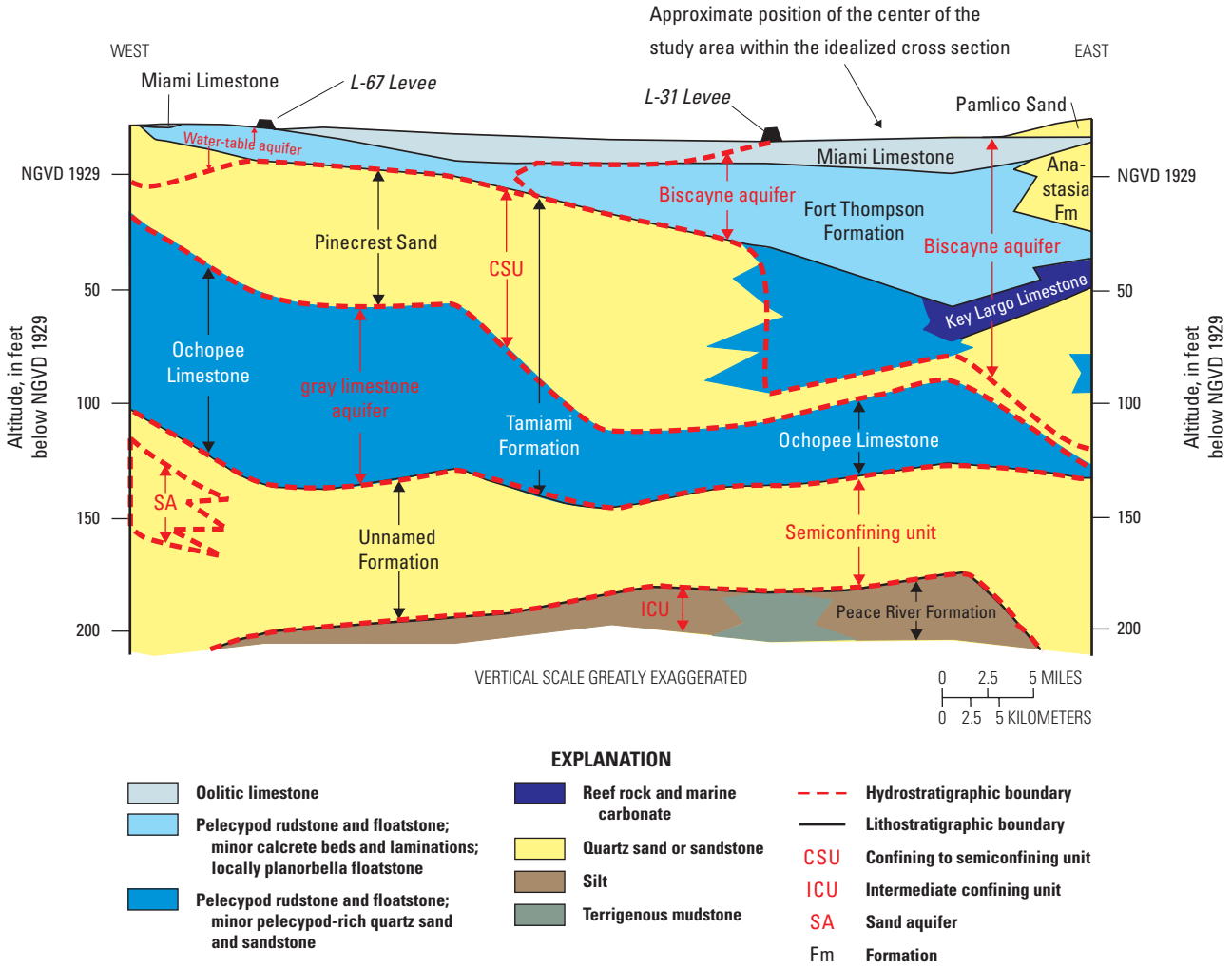

Figure 2. Relation of geologic and hydrogeologic units of the surficial aquifer system across central Miami-Dade County, north of the Snapper Creek Well Field study area (original modified from Reese and Cunningham, 2000; Cunningham and others, 2006b).

Previous Studies

Studies that focused on the SCWF include those by Sherwood and Leach (1962), Goodson (2005), Sunderland and Krupa (2007), and Swain (2012). These studies focused on surface-water/groundwater interactions, especially between canals and production well fields, and attempted to quantify canal leakage. These studies assumed simplified geologic and hydrogeologic frameworks based on available existing data.

The heterogeneity of porosity and permeability in the Biscayne aquifer elsewhere in Miami-Dade County, including central Miami-Dade County, has been investigated in numerous studies. In an area of north-central Miami-Dade County, Klein and Sherwood (1961) first suggested the presence of a low-permeability zone near the top of the Biscayne aquifer, consisting of dense limestone that impeded the downward movement of surface water. In other areas of Miami-Dade County, later studies confirmed the existence of this zone and described similar hydrogeologic units within the aquifer (Shin and Corcoran, 1988; Gaurdiario, 1996, Brown and Caldwell Environmental Engineers and Consultants, 1998; Genereux and Gaurdiario, 1998; Kaufman and Switanek, 1998; Nemeth and others, 2000; Sonenshein, 2001; Cunningham and others, 2004b, 2004c, 2006a, 2006b; Krupa and Mullen, 2005). Cunningham and others (2004b, 2006a, 2006b) related aquifer heterogeneity to cyclostratigraphy within the Miami Limestone and the Fort Thompson Formation and established methods for characterizing hydrogeologic properties within the Biscayne aquifer. A forced gradient convergent tracer test conducted at the Miami-Dade County Northwest Well Field (Cunningham and others, 2006a; Renken and others, 2005) showed that groundwater in the Biscayne aquifer within the well field moved preferentially along stratiform flow zones of touching-vug porosity that were most commonly present at the base of high-frequency depositional cycles.

Geophysical methods, such as borehole imaging, have been used to quantify vuggy porosity and to identify zones of high fluid flow (Hickey, 1993; Newberry and others, 1996; Hurley and others, 1998, 1999; Williams and Johnson, 2000; Cunningham, 2004; Cunningham and others, 2004a). Cunningham and others (2004b, 2004c, 2006b) used borehole images to determine the cyclostratigraphy of preferential flow and low-permeability zones, from which they created two-dimensional cross sections among test coreholes drilled in the Lake Belt area of north-central Miami-Dade County, and developed a three-dimensional hydrogeologic model of the Biscayne aquifer in that area. Additional geophysical techniques using flowmeters and water-quality probes are described by Wacker and Cunningham (2008) for characterizing flow within the Biscayne aquifer. Cunningham

Figure 3. Aerial photograph of Snapper Creek Well Field showing locations of test coreholes drilled for this study and production wells and the C–2 canal.

and others (2009), Cunningham and Sukop (2011), and Cunningham and others (2012) have shown that ichnofabric-related megaporosity can exert a major control on groundwater flow in many areas of the Biscayne aquifer.

Methods of Investigation

A variety of types of data and analyses were integrated to characterize the geology and hydrogeology of the Biscayne aquifer within central Miami-Dade County. These characterizations included (1) core examination for analyses of lithology, paleontology, cyclostratigraphy, ichnology, and paleoenvironments; (2) borehole geophysical surveys (especially borehole image and flowmeter data); and (3) single-well aquifer tests.

Drilling, Core Acquisition, and Construction of Monitoring Wells

Data collected from six continuously cored SCWF test holes that fully penetrate the Biscayne aquifer are the foundation for this study (fig. 3). Four-inch (in.) diameter core was acquired from each of the six coreholes to a depth of 5 to 10 ft below the base of the Biscayne aquifer. Existing data from test coreholes drilled for previous USGS studies in central Miami-Dade County to the east and west of SCWF were integrated with data from the SCWF.

Monitoring-well clusters were constructed at the SCWF several months after hydraulic testing of the coreholes was completed for each of the six coreholes by drilling two to three additional monitoring wells adjacent to each corehole for a total of 23 monitoring wells (app. 3; table 1). Intervals in the monitoring wells within or near the Pinecrest Sand Member of the Tamiami Formation were screened to prevent infilling of the interval, and other depth intervals were left open except for well G–3903, which was also screened. The monitoring wells were pumped until the water produced was clear of particulates, after which borehole image and caliper data were collected in each well to verify completion within the desired intervals (table 1).

Borehole-Geophysical Data Collection

Borehole-geophysical data were collected in each test corehole and monitoring well to characterize the geology and hydrology of the Biscayne aquifer within central Miami-Dade County and verify monitoring-well completion (app. 4). Continuous digital borehole-wall images, full waveform sonic, natural gamma, electromagnetic (EM) induction, water-quality, and caliper data were collected in each test corehole. Additional geophysical data, mainly flowmeter and borehole-fluid data, were collected in each test corehole during periods of well-field shutdown to determine hydraulic properties of the aquifer (Wacker and Cunningham, 2008).

Natural gamma data typically are used for lithologic identification and stratigraphic correlation (Keys, 1990). Natural gamma data were collected to support stratigraphic correlation among coreholes and identify lithologies high in phosphorite grain content, which increased in the Tamiami Formation compared to the Fort Thompson Formation and Miami Limestone.

Electromagnetic induction data indicate the bulk electrical conductivity of rock matrix and formation water and are influenced by formation porosity, groundwater specific conductance, and temperature. Formation resistivity is the reciprocal of conductivity, so EM induction data are comparable to resistivity data.

Fluid data were collected several times in each test corehole under steady-state (no pumping within the SCWF), stressed steady-state (while pumping from either the test corehole or a production well), and transient (while changing from steady state in SCWF to pumping from a SCWF production well) conditions. Two instruments were used to collect fluid data in the test coreholes: (1) a water-quality probe that measures the temperature, specific conductance, pH, percentage dissolved oxygen, and oxidation reduction potential (redox) of the borehole fluid and (2) a fluid probe that measures borehole-fluid temperature and fluid resistivity. Fluid data, in addition to providing water-quality information, can be used to identify the depth intervals that produce water by indicating changes in fluid properties related to permeability and hydraulic head (Keys, 1990). Changes in the conductance and temperature of borehole fluid also may indicate that the probe is at or near the base of the Biscayne aquifer. Borehole fluid properties are markedly different below the base of the Biscayne aquifer owing to a lack of mixing of the immobile borehole fluid due to lower permeability in this unit compared to the upper part of the test corehole within the aquifer where flow in this higher permeability zone is more vigorous.

The mechanical-caliper probe used in this investigation calculates a mean borehole diameter, which can indicate zones in which secondary porosity is present (Keys, 1990) if confirmed by other borehole information, such as a digital optical image. In addition to collecting caliper data in each test corehole, once monitoring-well construction was completed, caliper data were collected in each open-hole monitoring zone to determine the open-hole borehole diameter.

Two types of tools were used to generate an oriented image of the borehole wall in each test corehole: (1) a high-resolution optical borehole imaging tool (OBI) and (2) an acoustic borehole imaging tool (ABI). The OBI data have been used in studies of the Biscayne aquifer of south Florida (Cunningham, 2004; Cunningham and others, 2004b, 2004c, 2006a, 2006b; Cunningham and Sukop, 2011; Cunningham and others, 2012; Wacker and Cunningham, 2008) to identify lithofacies and provide a stratigraphic correlation among boreholes and to delineate megapore; bedding geometries and thicknesses; lithostratigraphic, depositional, and cycle boundaries; and to define depositional and post-depositional features such as grain size and ichnofabrics (Cunningham and

Table 1. Snapper Creek Well Field monitoring-well construction information.

The completion date indicates when coring was completed in the test coreholes or the date the open interval was drilled in the monitoring wells. Top of screen depths in parentheses are bottom of grout or top of limestone. Casing was not fully installed to the bottom of the borehole so some grout was drilled through during construction of the open hole. [MW, monitoring well; NAD 83, North American Datum of 1983; NGVD 29, National Geodetic Vertical Datum of 1929; ft, foot; in., inch; " —" indicates the well was not cored or did not penetrate the base of the Biscayne aquifer]

MW cluster ID	USGS local well number	USGS site identification number	End date of coring or drilling of open hole	Latitude (North) (NAD 83)	Longitude (West) (NAD 83)	Altitude of ground surface (ft) (NGVD 29)	Altitude of top of casing (ft) (NGVD 29)	Total depth cored from surface (ft)	Base of Biscayne aquifer from land surface (ft)	Open hole or screen slot size (in)	Casing internal diameter (in)	Top of screen or open hole from land surface (ft)	Bottom of screen or open hole from land surface (ft)
G–3877	G–3877	254150080215501	04/03/09	25°41′50.74″	080°21′55.03″	8.94	8.45	106	91.65	0.020	4.0	87.1	92.1
	G–3902	254150080215502	01/25/10	25°41′50.66″	080°21′54.99″	8.82	8.45	—	—	Open	4.0	68.0	75.5
	G–3903	254150080215503	01/26/10	25°41′50.67″	080°21′54.90″	8.92	8.46	—	—	0.010	3.0	6.0	19.5
G–3878	G–3878	254151080214301	04/09/09	25°41′51.78″	080°21′43.23″	7.13	6.70	101	86.40	0.020	4.0	73.5	80.5
	G–3904	254151080214302	01/29/10	25°41′51.94″	080°21′43.20″	7.16	6.82	—	—	Open	4.0	63.1	72.3
	G–3905	254151080214303	01/14/10	25°41′51.87″	080°21′43.14″	7.06	6.76	—	—	Open	4.0	29.5	33.6
	G–3906	254151080214304	01/15/10	25°41′51.86″	080°21′43.23″	7.08	6.77	—	—	Open	4.0	4.9	14.4
G–3879	G–3879	254153080213901	03/25/09	25°41′53.47″	080°21′39.93″	7.01	6.78	101	85.60	0.020	4.0	84.1	94.1
	G–3907	254153080213902	01/04/10	25°41′53.42″	080°21′39.91″	7.12	6.75	—	—	Open	4.0	62.9	74.6
	G–3908	254153080213903	01/06/10	25°41′53.51″	080°21′39.95″	7.24	6.90	—	—	Open	4.0	44.6 (45.1)	56.6
	G–3909	254153080213904	01/06/10	25°41′53.55″	080°21′39.98″	7.20	6.66	—	—	Open	4.0	35.2 (37.4)	39.1
G–3880	G–3880	254154080213704	05/06/09	25°41′54.68″	080°21′37.71″	8.13	7.60	102	88.40	Open	4.0	8.4	14.1
	G–3910	254154080213702	02/09/10	25°41′54.71″	080°21′37.74″	8.27	7.65	—	—	Open	4.0	65.1	78.2
	G–3911	254154080213703	02/08/10	25°41′54.75″	080°21′37.77″	8.07	7.62	—	—	Open	4.0	59.6	62.5
	G–3912	254154080213701	02/02/10	25°41′54.67″	080°21′37.70″	8.11	7.54	—	—	0.020	4.0	80.7	87.7
G–3881	G–3881	254155080243501	04/16/09	25°41′55.88″	080°21′34.96″	7.23	6.69	105.5	87.80	0.020	4.0	80.2	95.2
	G–3913	254155080243502	03/08/10	25°41′55.88″	080°21′35.04″	7.44	6.94	—	—	Open	4.0	63.3	75.1
	G–3914	254155080243503	03/05/10	25°41′55.96″	080°21′35.04″	7.19	6.68	—	—	Open	4.0	52.7	60.4
	G–3915	254155080243504	03/08/10	25°41′55.96″	080°21′34.96″	7.19	6.54	—	—	Open	4.0	7.7	17.8
G–3882	G–3882	254158080212201	03/19/09	25°41′58.33″	080°21′22.26″	7.45	6.90	100	85.00	0.020	4.0	78.4	90.4
	G–3916	254158080212202	03/23/10	25°41′58.55″	080°21′22.26″	7.83	7.10	—	—	Open	4.0	68.5 (68.8)	77.3
	G–3917	254158080212203	02/25/10	25°41′58.49″	080°21′22.26″	7.54	7.13	—	—	Open	4.0	36.4	43.9
	G–3918	254158080212204	02/19/10	25°41′58.44″	080°21′22.26″	7.66	7.02	—	—	Open	4.0	7.6	18.3

others, 2004a). The OBI data were used at the SCWF to assist in developing a cyclostratigraphy, which helped to define the geologic and hydrogeologic frameworks. The data were also used to assist in determining the base of the Biscayne aquifer in each test corehole (table 1).

Acoustic borehole image (ABI) data complement the OBI data by displaying physical features on the borehole wall that may be difficult to distinguish optically (Williams and Johnson, 2004). Two types of ABI data are generated—one based on the travel time of the acoustic signal and one based on the amplitude of the acoustic signal reflected from the borehole wall and is a measure of density of the borehole wall (Prensky, 1999; Williams and Johnson, 2004). The travel time ABI data can be used to produce a high-resolution borehole caliper log. Amplitude ABI data can be used to detect variations in rock properties, such as quality of cementation and matrix porosity that are not apparent on the OBI image, as well as stratigraphic cycle boundaries in rock of similar color, fabric, and texture that may not be apparent on OBI data. Thus, amplitude ABI data can be used to interpret qualitative variations in porosity values that can be compared with flowmeter and fluid property data to determine the existence and vertical extent of flow zones. The optical and acoustic images complement caliper data providing additional detail about the distribution of matrix porosity and megapores that can be used to estimate porosity in zones where there is no core recovery.

Full waveform sonic (FWS) data, including compressional- and Stoneley-wave data, were collected in each test corehole. Two logging runs over the total depth of each corehole were made with the sonic tool, one with an acoustic signal transmitted at 15 kilohertz (kHz; data used for porosity calculations) and a second with the signal transmitted at 1 kHz (data used for relative permeability estimations). Compressional wave data were used for calculation of sonic porosity, and Stoneley-wave amplitude was computed from the 1 kHz FWS data to provide an estimation of relative permeability.

After the test coreholes were cased as monitoring wells at SCWF, it was discovered that the acoustic output from the FWS tool transmitter varied during data collection due to an intermittent instrument malfunction and was less than required for optimal performance in some test coreholes at SCWF. In test coreholes drilled for other studies, however, and in the other three test coreholes (G–3883, G–3884, and G–3889) drilled as part of this study but not at SCWF, new FWS data with the designed level of acoustic output were obtained and compared with the previous data with the weakened signal. Even though the signal for the compressional wave in each of the previously collected FWS data was weak and difficult to process, the arrival time of the recomputed compressional wave was unchanged. Thus, porosity calculations, which are based on the compressional-wave arrival time, remained unchanged; only the signal strength varied.

The Stoneley-wave amplitude data, however, were affected by the low signal strength. Weaker amplitude data falsely indicate greater permeability and produce less contrast in wave amplitude among lithologic units of different permeabilities. The test coreholes in which the wave amplitude data appeared to be most affected by the low signal strength when compared with other borehole geophysical data were G–3878, G–3879, and G–3880. The Stoneley-wave amplitude data in the other three test coreholes at SCWF were also collected with the lower strength acoustic signal, but the amplitude data were able to be interpreted.

Flowmeter Testing

Three types of flowmeters—spinner, heat-pulse, and EM—were used to measure vertical borehole fluid flow in the test coreholes at SCWF. The impellor or spinner flowmeter is the oldest and most commonly used type of flowmeter. The spinner flowmeter spins with vertical flow velocity and is most accurate in boreholes with high fluid flow. The heat-pulse flowmeter detects the movement of a pulse of heated borehole fluid up or down and is most accurate in boreholes with low flow velocity. The EM flowmeter detects the movement of borehole fluid through an electromagnetic field and is accurate for intermediate flow velocities. Borehole image and caliper data were used to select the intervals within each borehole for use in making stationary flow measurements.

Pumping from a production well in a well field can create vertical flow of fluid within a borehole near the pumping well at velocities that exceed the upper measurement limit of the heat-pulse and EM flowmeters. Because the pumping of production wells in the SCWF could not be discontinued (well-field shutdown) without advanced notice, flowmeter data were collected in two phases (table 2) to minimize interference with well-field operations. For phase 1 flowmeter testing, at least one production well was being pumped, and stressed steady-state conditions were assumed for the SCWF. The pumping production well could not be turned off or changed for flowmeter testing. Flowmeter (heat-pulse and spinner)

Table 2. Types of flowmeter testing conducted at Snapper Creek Well Field.

[Phase 1, typical conditions in well field with at least one production well pumping; Phase 2, ambient conditions assumed in well field with no pumping in the last 16 hours; PMP well, borehole or production well from which water is being pumped; OBS well, observation borehole where flowmeter data are being collected; "—, only one test type was conducted"]

Phase	Test type	PMP well	OBS well	Well-field condition observed
1	—	Production well	Test corehole	Stressed steady state
2	1	None	Test corehole	Unstressed ambient
2	2	Test corehole	Test corehole	Stressed steady state
2	3	Production well	Test corehole	Transient and stressed steady state

data, both stationary and trolling flowmeter measurements, were collected to profile flow within five test coreholes at SCWF to provide preliminary identification of flow zones for use in planning monitoring-well construction. Phase 1 flowmeter testing is similar to cross-hole flowmeter testing (phase 2 type 3) in that the resultant flow within the test corehole depends on the connectivity of the open section of the pumping production well to the test corehole, which creates a short circuit that does not exist elsewhere in the larger well field. Single-well flowmeter testing, under ambient and while pumping from the test corehole when the well field is shutdown, more accurately reflects the hydrological conditions in the test corehole for determining flow zones and there relative contributions to total vertical flow within the corehole.

For phase 2 flowmeter testing, production wells could be turned off and on, or changed as needed for flowmeter testing. Borehole flow data for phase 2 were collected using an EM flowmeter for all three test types in each test corehole (table 2). In addition to measuring vertical flow in the borehole, the EM flowmeter also incorporates a sensor to measure borehole fluid temperature and resistivity, providing data used for further identification of flow zones. A pressure transducer with a temperature sensor was placed in the corehole to measure water levels and temperature changes in the shallow part of the hole during the collection of EM flowmeter data. These data documented background water levels and water-level changes during trolling of the EM flowmeter under ambient and steady-state conditions and were useful in determining when steady-state conditions were achieved during the transient cross-hole testing. Additionally, for test coreholes near the C–2 canal, temperature and specific conductance measurements of the canal water were also made for comparison with those values in the borehole fluid. Also, during cross-hole flowmeter data collection in corehole G–3880, it was noticed early in the test that the C–2 canal stage was being lowered for water-management activities. Testing was continued to observe the effects of a lowered canal stage level on flow within the test corehole. The cross-hole flowmeter test was repeated 11 days later when the canal stage was returned to normal.

Phase 2 testing for all six test coreholes at SCWF began with shutting down all pumping from the well field for at least 16 hours, so that unstressed ambient conditions could be measured. During phase 2 type 1 testing (table 2), flowmeter data were collected while no production wells at SCWF were being pumped, and water levels in the well field were considered to be at ambient conditions. During the phase 2 type 2 testing, single-hole, stressed steady-state conditions were induced in each of the six coreholes by pumping from the corehole (with a 2-inch diameter, small-capacity pump), while none of the production wells were being pumped, and unstressed ambient conditions were assumed for the rest of the well-field area. After phase 2 type 2 testing, no pumping was permitted for 16 hours in the well field prior to the start of phase 2 type 3 testing to allow unstressed ambient conditions to develop.

Phase 2 type 3 testing (cross-hole flowmeter testing) was conducted while individual production wells at SCWF were pumped, in turn, to observe stressed transient and steady-state conditions in the test corehole. The objective in this case was to examine the connectivity between the coreholes and the SCWF production wells during conditions of controlled short-term pumping and recovery cycles in individual production wells, to determine intervals and magnitude of flow in the corehole, and to determine if flows varied depending on which production well was being pumped. Where possible, the flowmeter was placed in the same cyclostratigraphic interval in all six test coreholes, based on correlation of high-frequency cycles throughout the SCWF area.

At the SWWF, only phase 1 flowmeter data were collected in test coreholes G–3883 and G–3884, because well-field shutdown was not possible and multiple production wells in the field were being pumped during data collection. Unstressed ambient conditions were assumed for corehole G–3889 and coreholes G–3790, G–3834, and G–3840, and only phase 2 type 1 and 2 flowmeter testing was conducted on these coreholes, because they are not located near any well field. Detailed descriptions and results of flowmeter testing for the test coreholes at SCWF are provided in appendix 5.

Display of Borehole Geophysical Data

Borehole geophysical data with lithologic descriptions and interpreted geologic and hydrologic units are presented at three different scales (app. 4): (1) Borehole geophysical data display of each monitoring-well cluster at 1:12 scale (for example, G–3878 CLUSTER.pdf, app. 4–1), which is best for viewing borehole images of each test corehole and open-hole monitoring zones; (2) Display at 1:96 scale (for example, G–3878 COMBO Flowmeter.pdf, app. 4–2), showing corehole flowmeter and fluid data; and (3) Borehole geophysical data displays of the SCWF cross-hole, EM flowmeter data were plotted at 1:240 scale (for example, G–3878 Xhole.pdf, app. 4–3). Final monitoring-well completion zones shown on the borehole geophysical data displays are listed in table 1, and construction data are provided in appendix 3. Borehole geophysical data displays of the two coreholes G–3883 and G–3884, at the SWWF, and the corehole G–3889, south of the study area, were created at 1:12 scale only (for example, G–3883 COMBO.pdf, app. 4–2). Borehole geophysical data displays of the SCWF cross-hole EM flowmeter data were analyzed to determine the unstressed ambient and stressed pumping flow rate at each test depth and the change in the flow rate (app. 5–1). These data can be used to determine the contribution of the interval above or below the test depth to flow into or out of the borehole. Detailed descriptions of the lithologies shown on the borehole geophysical data displays for each corehole are presented in appendix 1, and photographs of the boxed, slabbed core are presented in appendix 2.

The cross-hole flowmeter data (app. 4–3) for all coreholes were normalized to zero for pump start time, vertical flow, and temperature. Plots of the change in flow rate and temperature, versus time from when each production well pump was turned on, were created for each test corehole and each tested depth

below land surface to facilitate comparison of cross-hole test data in the SCWF (app. 5, table 5–1). Plate 1 was prepared using data from table 5–1 and depicts intervals of net inflow and outflow in each SWCF test corehole during cross-hole flowmeter testing of transient and stressed steady-state production well pumping.

Full waveform sonic data collected at the SCWF were processed to determine the primary compressional- and Stoneley-wave velocities. The compressional-wave velocity was used as input into the Raymer-Hunt porosity equation for calculation of sonic porosity (Raymer and others, 1980) using free LogCruncher software (Mercury Geophysics, 2009) and is displayed on the borehole geophysical data displays (app. 4). The Raymer-Hunt equation:

$$(V_p = (1–\phi)2\ V_m + \phi V_f),$$

where ϕ is total porosity, V_p is the compressional-wave velocity, V_m is the compressional-wave velocity of the matrix and V_f is the compressional-wave velocity of the fluid, was computed using a solver function in LogCruncher. Although the time-average equation (Wyllie and others, 1956) is used to calculate porosity in rocks such as consolidated sandstones having uniformly distributed interparticle-pore spaces (Keys, 1990), the pore system of the eogenetic karst lithology of the Biscayne aquifer is heterogeneous and complex (Cunningham and others, 2004b, 2006b). Therefore, the time-average equation may not be suitable for use in calculating sonic porosity. Instead, the Raymer-Hunt equation may provide a more accurate estimation of porosity in rocks with heterogeneous distribution of pore types and sizes (Raymer and others, 1980). Stoneley-wave velocities were used to determine the amplitude of the Stoneley wave, which can be qualitatively related to permeability (Paillet and White, 1982; Keys, 1990; and Wacker and Cunningham, 2003) and, in turn, can be used to make an estimate of the permeability of the rock surrounding the borehole (Burns and others, 1988; Tang and Cheng, 1988, 1993; Keys, 1990). Generally, low Stoneley-wave amplitudes are indicative of high permeability, and high Stoneley-wave amplitudes are a signpost for low permeability. Stoneley-wave amplitude data collected at the SCWF can thus be used in a qualitative manner to estimate vertical intervals of high and low permeability.

Borehole-Flow Analysis

The hydraulic character of the flow zones penetrated by the SCWF test coreholes was characterized through the analysis of the various types of flowmeter data collected. Each of the coreholes penetrated multiple flow zones with different vertical hydraulic heads. The composite head of a multizone borehole is the transmissivity-weighted mean of the hydraulic heads of the individual flow zones (Bennett and others, 1982). Inflow zones have a hydraulic head that is greater than the composite head, and outflow zones have a head that is less than the composite head.

Analytical and numerical methods can be used to quantitatively analyze single-hole flow data to estimate the transmissivity and hydraulic head of individual flow zones penetrated by a multizone borehole (Paillet, 2000; Halford, 2009; Day-Lewis and others, 2011). In the current study, local aquifer characteristics, corehole conditions, and equipment capabilities limited this type of analysis. The high transmissivity of the karstic Miami Limestone in the uppermost borehole intervals, small-diameter and rugose boreholes, and relatively low pumping rates (100 gallons per minute [gal/min]) resulted in small drawdowns and minimal hydraulic stress on the lower flow zones in the coreholes. The computer program FLASH (Flow-Log Analysis of Single Holes) (Day-Lewis and others, 2011), which is based on an analytical solution for steady-state, multilayer radial flow to a borehole derived from the Theim equation (Theim, 1906), was used to define the relative hydraulic heads of the flow zones penetrated by the boreholes and to estimate their relative transmissivity as a percentage of the total transmissivity exclusive of the Miami Limestone.

Cross-hole flow data can be analyzed to investigate the hydraulic character of the connectedness of individual flow zones penetrated by multiflow-zone boreholes (Paillet, 1993; Williams and Paillet, 2002; and Paillet and others, 2012). In the cross-borehole flow analysis method developed by Paillet (1998), a numerical model is used to simulate transient changes in vertical flow above each flow zone in an observation borehole in response to pumping and recovery cycles in an adjacent borehole. In the current study, transient flow datasets were collected from five (G–3878, G–3879, G–3880, G–3881, and G–3882) of the six coreholes during pumping from and recovery in an individual selected SCWF production well. The exception, corehole G–3877 at the westernmost edge of the SCWF, did not show a response during the 10-minute period when two production wells (S–3012 and S–3013 at 1,806 and 1,527 ft measured lateral distance from test corehole G–3877, respectively) were pumped. In the Paillet (1998) model, the transmissivity of each flow zone is specified on the basis of results of single-borehole flow test analysis. Various possible hydraulic-connection geometries between the flow zones were evaluated, and the storage coefficient of those hydraulic connections was varied to provide a reasonable match between measured and simulated flows in the observation borehole.

The cross-hole flow model program by Paillet (2011) allows for leakage between flow zones. Leakage is simulated using a model factor that is proportional to the ratio of the vertical hydraulic conductivity and the product of the storage and hydraulic-head difference between the two hypothetical flow zones. In general, the greater the leakage rate, the less variable the change in borehole flow during the test (fig. 4). The hypothetical example in figure 4 represents two aquifer flow zones in which the observation borehole is open to both aquifer flow zones, the flowmeter collecting the data is positioned between the upper and lower aquifer flow zones, and the pumping borehole is open only to the lower aquifer flow

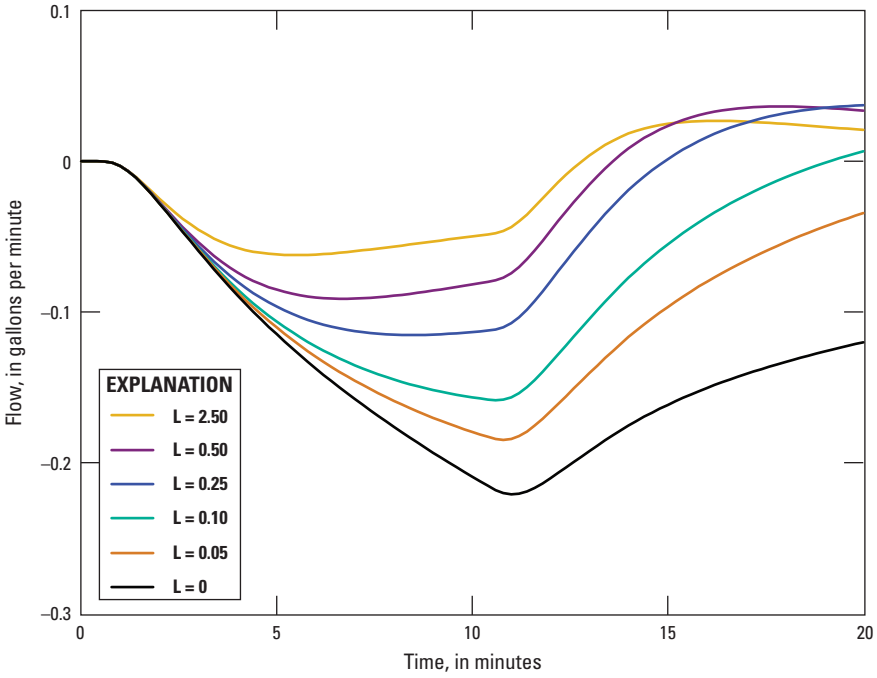

Figure 4. Hypothetical two-aquifer flow-zone model of borehole flow in which the lower zone is the primary hydraulic connection to the observation borehole, and the effect of various rates of vertical leakage (leakage proportional factor L in minutes^{-1}) (modified from Paillet, 2011).

zone. In the current study, the lack of flow-zone transmissivity estimates for the test coreholes and production wells limited the quantitative application of the Paillet (2011) model in the analysis of the cross-hole test data. Analyses of the cross-hole flow data, however, were used to define the primary hydraulic connectedness of the flow zones and whether those connections were isolated or leaky.

Single-Well Slug Tests

Hydraulic conductivity and transmissivity values can be determined by means of slug tests made in a single well. In such tests, a known volume of water is added to or removed from the borehole or, in this case, air pressure is used to depress the water level by a distance that represents a known volume of water, and measurements of the rate at which the borehole water level returns to the original level are used to calculate a transmissivity (T) and hydraulic conductivity (K). Slug tests were conducted at 20 of the 23 monitoring wells at SCWF to determine the hydraulic properties of 20 vertical aquifer intervals. The water levels in three of the shallow monitoring wells (G–3880, G–3903, and G–3906) were below or too close to the bottom of the casing and were not testable or the result was rated as poor. The results of these slug tests are presented in appendix 6. The water-level data were analyzed using methods developed by Halford and Kuniansky, (2002) that incorporate the equations for (1) the Bouwer and Rice (1976) method for unconfined aquifers with an exponential decay response and (2) the Van der Kamp (1976) method for highly permeable formations or those with an oscillatory response. Results from the multiple tests were averaged to obtain a mean estimate of horizontal hydraulic conductivity and transmissivity for each of the 20 aquifer intervals tested.

Construction of the monitoring wells and slug tests were completed prior to a detailed hydrostratigraphy being finalized; thus, reported interval type in the slug-test report, which was based on preliminary data, may not be accurate when compared to the final hydrostratigraphy. The slug-test results were analyzed to determine if the reported test interval for the slug test was fully within the reported flow unit, aquifer matrix, or semiconfining unit as indicated by the final hydrostratigraphy, or if the reported interval was in a mix of each unit. To accomplish the analysis, the slug-test results were compared with the final monitoring-well completion interval based on the OBI, lithostratigraphy, and pore type (table 3). Additionally, G–3879 was not included in this table because the slug-test results may have been influenced by a cavity created by airlifting of material during well construction.

Hydrologic Analysis

The hydrologic and hydraulic properties of the flow zones in the test coreholes—porosity, permeability, hydraulic conductivity, and transmissivity—were estimated on the basis of visual examination of thin sections of recovered core (apps. 1 and 2), borehole geophysical data (app. 4), and results of single-well slug tests (app. 6). On the basis of the results of these analyses, permeable zones of inflow and outflow, and the base of the Biscayne aquifer in each test corehole were identified. The proximity of the upper Biscayne aquifer flow unit to the ground surface required that the pump intake be placed within this unit, which prevented trolling of the flowmeter across the upper flow unit and collection of stationary flow measurements above the unit. As a result, the upper flow unit could not be separated into individual flow zones, so the upper Biscayne aquifer flow unit is considered as a single flow zone.

Table 3. Comparison of slug-test results with monitoring zone lithostratigraphy and pore type at the Snapper Creek Well Field (modified from table 1 of appendix 6).

[K, hydraulic connectivity, in feet per day (ft/d); T, transmissivity, in feet squared per day (ft²/d); FM, Formation; HFS, high-frequency sequence; HFC, high-frequency cycle; ft, feet; NA, not available]

Cluster ID	Monitoring well ID	Test date	Bottom of test interval	Top of test interval	Individual tests for K (ft/d)	Mean K (ft/d)	Mean T (ft²/d)	HFS	HFC	Hydrologic unit	Pore type	Comments
G–3877	G–3877	3/4/2010	92.1	87.1	100; 100; 100	100	500	Tamiami FM and HFS 2	Tamiami FM and HFC 2d2	Lower semiconfining unit and minor flow zone in lower Biscayne aquifer flow unit	Burrow and matrix	Sand may have infilled annular space. Most of monitoring zone is Pore Class III and II. Part of monitoring zone is a minor flow zone (Pore Class 1b).
	G–3902	8/4/2010	75.5	68.0	8,600; 8,400; 8,900	9,000	64,800	HFS 2	HFC 2e2 and 2f1	Major flow zone in lower Biscayne aquifer flow unit	Burrow	0.9 ft of monitoring zone is in Pore Class III. Most of monitoring zone is a major flow zone (Pore Class 1a).
G–3878	G–3878	8/4/2010	80.5	73.5	7,600; 7,600; 7,500	8,000	53,000	HFS 2	HFC 2d2 and 2e2	Major flow zone in lower Biscayne aquifer flow unit	Burrow, irregular vug, and vertical solution pipe	Monitoring zone is in a major flow zone (Pore Class 1a).
	G–3904	8/4/2010	72.3	63.1	3,900; 3,900; 3,900	4,000	35,900	HFS 2	HFC 2e2 and 2f1	Minor flow zone in lower Biscayne aquifer flow unit	Burrow, fossil moldic, irregular vug, and matrix	Monitoring zone is in a minor flow zone (Pore Class 1b). Lower 1.5 ft of monitoring zone is in Pore Class II.
	G–3905	8/4/2010	33.6	29.5	2,000; 2,000, 2,100	2,000	8,300	HFS 2 and 3	HFC 2h1-2 and 3a	Minor flow zone in middle semiconfining unit and aquifer matrix	Matrix, fossil moldic, and irregular vug	Upper half of monitoring zone is Pore class II, lower half is a minor flow zone (Pore Class 1b).
G–3879	G–3907	8/3/2010	74.6	62.9	2,100; 2,000; 2,000	2,000	23,800	HFS 2	HFC 2e2 and 2f1	Minor flow zone in lower Biscayne aquifer flow unit	Burrow, fossil moldic, irregular vug, vertical solution pipe, and matrix	Upper 0.7 ft of monitoring zone is in Pore class III and lower 2.2 ft is in Pore Class II. Most of the monitoring zone between these two intervals is a minor flow zone (optical borehole image of G–3907 shows Pore Class 1b). In test corehole G–3879, test interval is a major flow zone with higher porosity (Pore Class 1a).
	G–3908	8/3/2010	56.5	45.1	660; 660; 680	700	22,600	HFS 2	HFC 2f1 and 2f2 and 2g2a and 2g2b	Minor flow zone in middle semiconfining unit	Uncertain, irregular vug, fossil moldic, and burrow	Minor flow zones (Pore Class 1b) bounded by Pore Class III above and Pore Class II below.
	G–3909	3/3/2010	39.1	37.4	40; 40; 40	40	70	HFS 2	HFC 2h1-2	Aquifer matrix	Matrix	Upper 2.2 ft of monitoring zone is grout (not part of test interval). Lower part (test interval) is Pore Class II

Table 3. Comparison of slug-test results with monitoring zone lithostratigraphy and pore type at the Snapper Creek Well Field (modified from table 1 of appendix 6).—Continued

[K, hydraulic connectivity, in feet per day (ft/d); T, transmissivity, in feet squared per day (ft^2/d); FM, Formation; HFS, high-frequency sequence; HFC, high-frequency cycle; ft, feet; NA, not available]

Cluster ID	Monitoring well ID	Test date	Bottom of test interval	Top of test interval	Individual tests for K (ft/d)	Mean K (ft/d)	Mean T (ft^2/d)	HFS	HFC	Hydrologic unit	Pore type	Comments
G–3880	G–3910	3/31/2010	78.2	65.1	2,500; 2,800; 2,900	3,000	35,800	HFS 2	HFC 2e2 and 2f1	Minor flow zone in lower Biscayne aquifer flow unit	Burrow, irregular vug, interparticle and intergranular, fossil moldic, and vertical solution pipe	Upper 0.9 ft is Pore Class III. Most of monitoring zone is in a minor flow zone (Pore Class 1b).
	G–3911	3/31/2010	62.5	59.6	8,600; 8,600; 8,600	9,000	24,900	HFS 2	HFC 2f1	Minor flow zone in middle semiconfining unit and may be connected to minor flow unit above monitoring zone	Mostly fossil moldic; flow zone above is burrow and irregular vug	Monitoring zone is in Pore Class II, but top of zone is in a minor flow zone (Pore Class 1b). Inadequate casing grout may connect monitoring zone to thick minor flow zone just above giving a high K for the monitoring zone.
	G–3912	8/4/2010	87.7	80.7	3,500; 3,500; 3,600	4,000	24,700	Tamiami FM and HFS 2	Tamiami FM and HFC 2d2	Major flow zone in lower Biscayne aquifer flow unit	Burrow and matrix	Upper 2.2 ft of monitoring zone is Pore Class II. Most of zone is in a major flow zone (Pore Class 1a)
G–3881	G–3881	3/31/2010	95.2	80.2	1,000; 1,000; 930	1,000	14,600	Tamiami FM and HFS 2	Tamiami FM and HFC 2d2	Lower semiconfining unit and major flow zone in lower Biscayne aquifer flow unit	Matrix, burrow, fossil moldic, and vertical solution pipe	Upper 2.2 ft of monitoring zone is Pore Class II. Lower 6.9 ft is in Pore Class II. Middle 5.7 ft is in a major flow zone (Pore Class 1a).
	G–3913	3/31/2010	75.1	63.3	3,100; 3,300; 3,300	3,000	38,200	HFS 2	HFC 2d2 and 2e2 and 2f1	Minor flow zone in lower Biscayne aquifer flow unit	Burrow, fossil moldic, irregular vug, bedding-plane vugs, vertical solution pipe, and matrix	Upper 0.5 ft of monitoring zone is in Pore Class III. Remaining monitoring zone is in a minor flow zone (Pore Class 1b).
	G–3914	3/31/2010	60.4	52.7	6,400; 6,400; 6,300	6,000	49,400	HFS 2	HFC 2f1 and 2f2	Minor flow zone in middle semiconfining unit and aquifer matrix	Matrix and fossil moldic	Mostly in Pore Class II. Some Pore Class III and 1.9 ft of minor flow zone (Pore Class 1b).
	G–3915	3/31/2010	17.8	7.7	9,500; 9,900; 9,900	10,000	98,600	HFS 4/5	HFS and HFC 4a and 4b	Upper Biscayne flow unit	Burrow, vertical solution pipe, and matrix	Monitoring zone mostly in a major flow zone (Pore Class 1a). Lower 1.7 ft is in Pore Class III

Table 3. Comparison of slug-test results with monitoring zone lithostratigraphy and pore type at the Snapper Creek Well Field (modified from table 1 of appendix 6).—Continued

[K, hydraulic connectivity, in feet per day (ft/d); T, transmissivity, in feet squared per day (ft²/d); FM, Formation; HFS, high-frequency sequence; HFC, high-frequency cycle; ft, feet; NA, not available]

Cluster ID	Monitoring well ID	Test date	Bottom of test interval	Top of test interval	Individual tests for K (ft/d)	Mean K (ft/d)	Mean T (ft²/d)	HFS	HFC	Hydrologic unit	Pore type	Comments
G–3882	G–3882	3/30/2010	90.4	78.4	390; 420; 440	400	5,000	Tamiami FM and HFS 2	Tamiami FM and HFC 2d2	Lower semiconfining unit and minor flow zone in lower Biscayne aquifer flow unit	Matrix, burrow, and fossil moldic	Two minor flow zones (Pore Class Ib) in upper part of monitoring zone. Remaining monitoring zone is Pore Class II and III.
	G–3916	3/30/2010	77.3	68.8	5,800; 4,700; Poor result	5,000	44,600	HFS 2	HFC 2d2 and 2e2	Major flow zone in lower Biscayne aquifer flow unit	Burrow, irregular vug, and matrix	Major flow zone (Pore Class 1a) in middle of monitoring zone. Remainder of monitoring zone is Pore Class II and III.
	G–3917	3/30/2010	43.9	36.4	5,300; 5,500; 5,300	5,000	40,300	HFS 2	HFC 2h1-2	Minor flow zone in middle semiconfining unit	Matrix, fossil moldic, and irregular vugs	Minor flow zone (Pore Class Ib) in middle of monitoring zone. Above the minor flow zone is Pore Class III and below is Pore Class II.
	G–3918	3/30/2010	18.3	7.6	7,000; 6,800; 6,600	7,000	76,200	HFS 5	NA	Upper Biscayne aquifer flow unit	Burrow and vertical solution pipe	Monitoring zone is completely in a major flow zone (Pore Class 1a).

Borehole images display rock fabric and textures, and megaporosity at the borehole wall; therefore, in intervals of no core recovery, the image log was inspected to make estimates of megaporosity and permeability. Slug-test data were used to calculate hydraulic conductivity and transmissivity for the 20 aquifer intervals. The percentages of megaporosity estimated in the borehole image data were then used to compare to the Raymer-Hunt sonic-porosity data and to provide assurance that the log-calculated values were realistic. Raymer-Hunt sonic-porosity data were used with ROXAR RMS™ geomodeling software to construct a cross section and a three-dimensional conceptualization of the distribution of porosity in the Biscayne aquifer at the SCWF (fig. 5).

Geologic Framework of the Biscayne Aquifer in Central Miami-Dade County

Analysis of the lithostratigraphy, lithofacies, paleontology, ichnology, cyclostratigraphy, depositional environments, and OBI data defines a geologic framework for the rocks and unconsolidated sediments that compose the Biscayne aquifer and the uppermost part of an underlying semiconfining unit for central Miami-Dade County (plate 2). This analysis builds on the geologic framework for the Lake Belt area (fig. 6) delineated by Cunningham and others (2004b, 2004c, 2006a, 2006b, 2009, 2012), Renken and others (2005, 2008), and Cunningham and Sukop (2011).

Lithostratigraphy

Neuendorf and others (2005) define lithostratigraphy as the description and systematic organization of rocks and sediments into distinct units based on the lithologic character of the rocks and sediments, and their stratigraphic relations. The eight coreholes at the SCWF and SWWF partially penetrate the Pinecrest Sand Member of the Tamiami Formation and completely penetrate the Fort Thompson Formation and the Miami Limestone (plate 2). The Pinecrest Sand Member is mostly medium to very thickly bedded skeletal quartz sandstone and skeletal quartz sand with minor units of arenaceous skeletal wackestone and packstone, quartz sandstone, and quartz sand (plate 2). Molluscan paleontology indicates a Pliocene age for the Pinecrest Sand Member of the Tamiami Formation in the Lake Belt area (Cunningham and others, 2006a), and it is assumed to be of the same age in the SCWF and SWWF study area. The Fort Thompson Formation consists mainly of medium to very thick beds of limestone and arenaceous limestone with some medium to very thick beds of

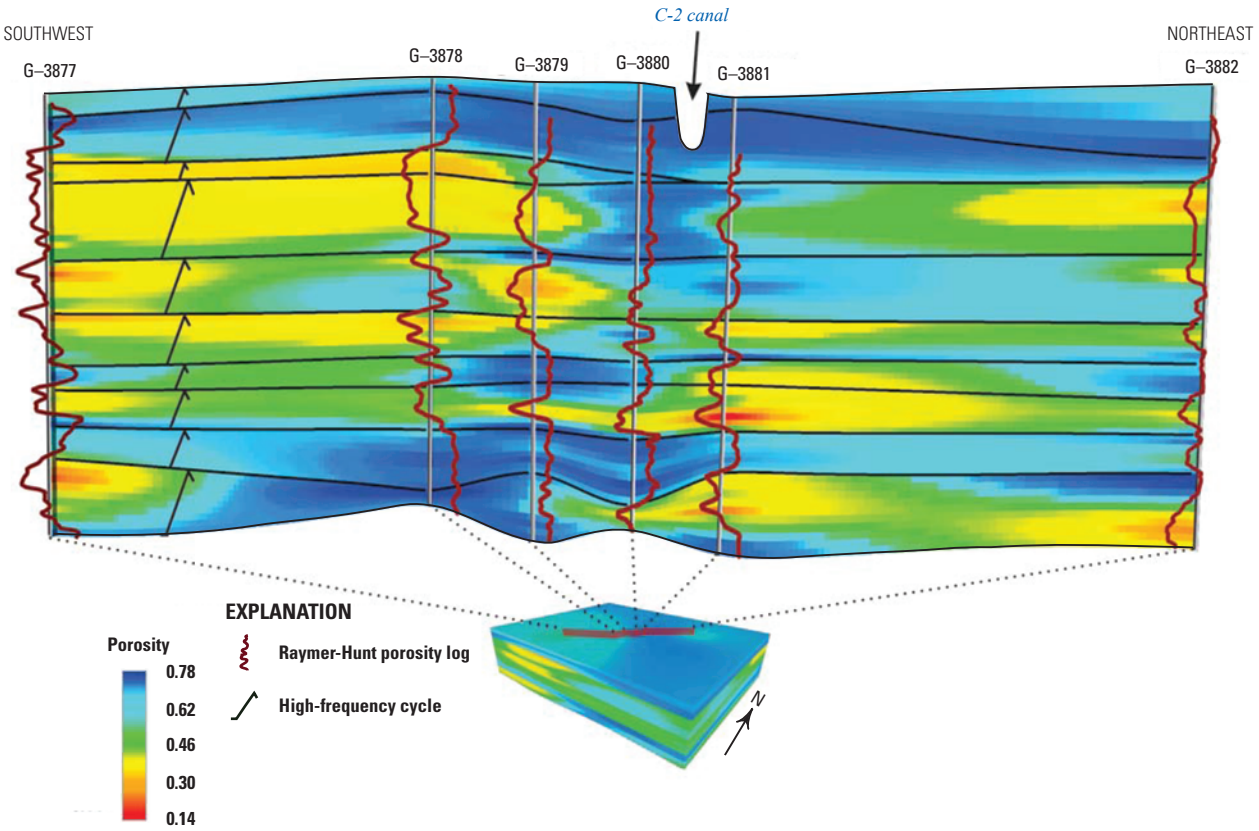

Figure 5. Cross section and three-dimensional conceptualization showing the distribution of porosity calculated using the Raymer-Hunt equation for sonic log data acquired in the six coreholes at the Snapper Creek Well Field study area (fig. 3). High-frequency cycle boundaries of Pleistocene age delineated by examination of core samples and optical borehole wall images are shown as black lines.

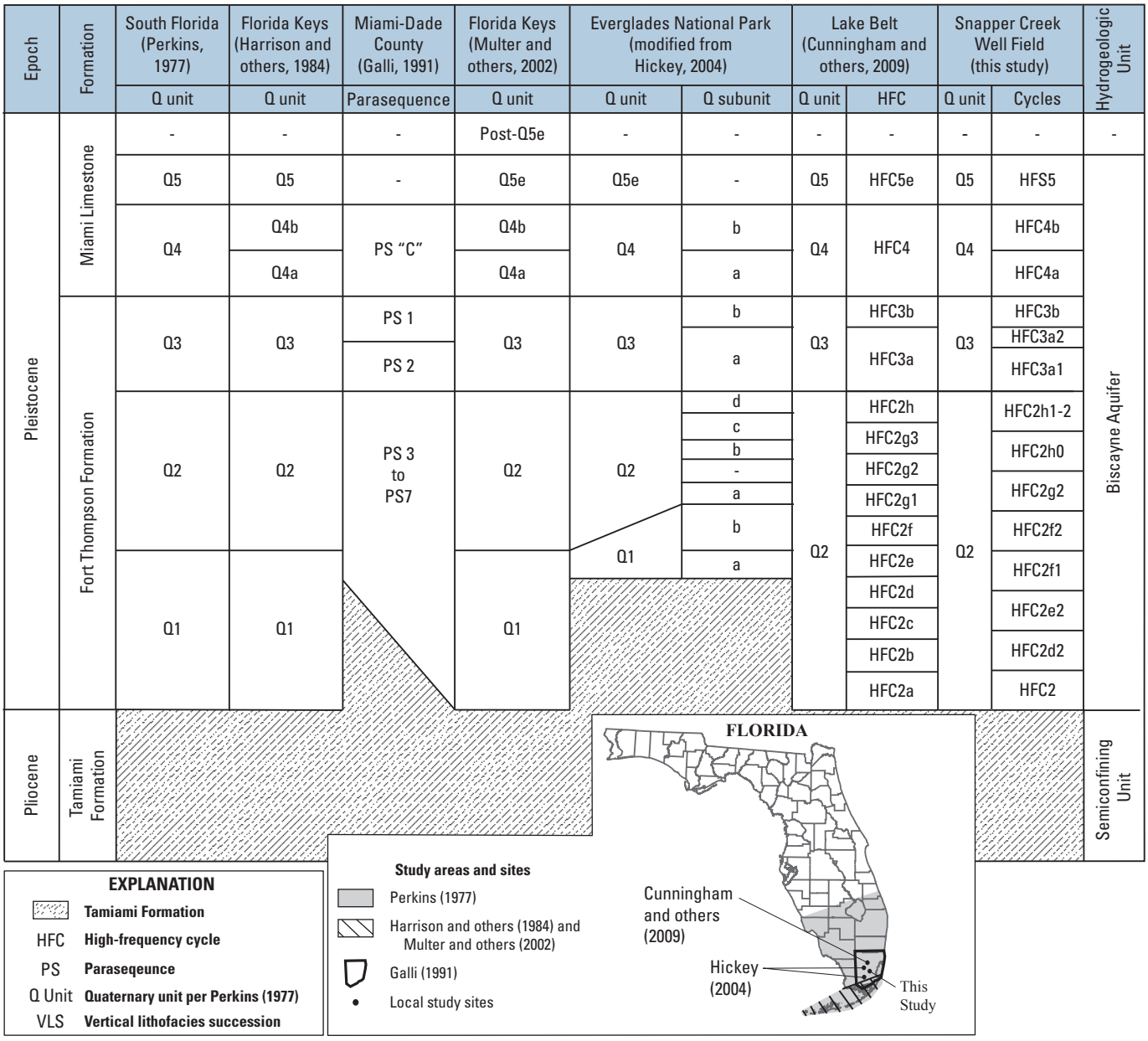

Figure 6. Correlation of ages, formations, stratigraphy, and hydrogeologic units of the Tamiami Formation, Fort Thompson Formation, and Miami Limestone by various authors and this study (modified from Cunningham and others, 2006b).

skeletal quartz sandstone and minor amounts of quartz sand. The rocks and sediments of the Fort Thompson Formation are equivalent to rocks of the Key Largo Formation that have been assigned a middle Pleistocene age by Multer and others (2002), but the Fort Thompson rocks could range in age from early to middle Pleistocene (Cunningham and others, 2006b; Hickey and others, 2010). The middle to late Pleistocene Miami Limestone consists entirely of medium to very thick beds of limestone and minor amounts of arenaceous limestone.

An unconformity separates the Pinecrest Sand Member of the Tamiami Formation and the Fort Thompson Formation. In core samples recovered from 11 test coreholes in the SCWF and SWWF study area (plate 2; app. 4), rhizoliths (root molds or tubes lined with concentric micrite and microspar) or laminated calcretes, or both, were observed below the unconformity, indicating the unconformity is associated with subaerial exposure. In some cases, the rhizoliths are abundant enough to form a pedotubule calcrete (Wright and Tucker, 1991). Lithoclasts (fig. 7) composed of a distinct lithology representative of the Pinecrest Member of the Tamiami Formation are present within the lower several feet of the base of the Fort Thompson Formation. Some of the lithoclasts contain pedotubule calcretes. The presence of the lithoclasts is consistent with subaerial exhumation and erosion of rocks from the Pinecrest Member of the Tamiami Formation and their deposition as sediments of

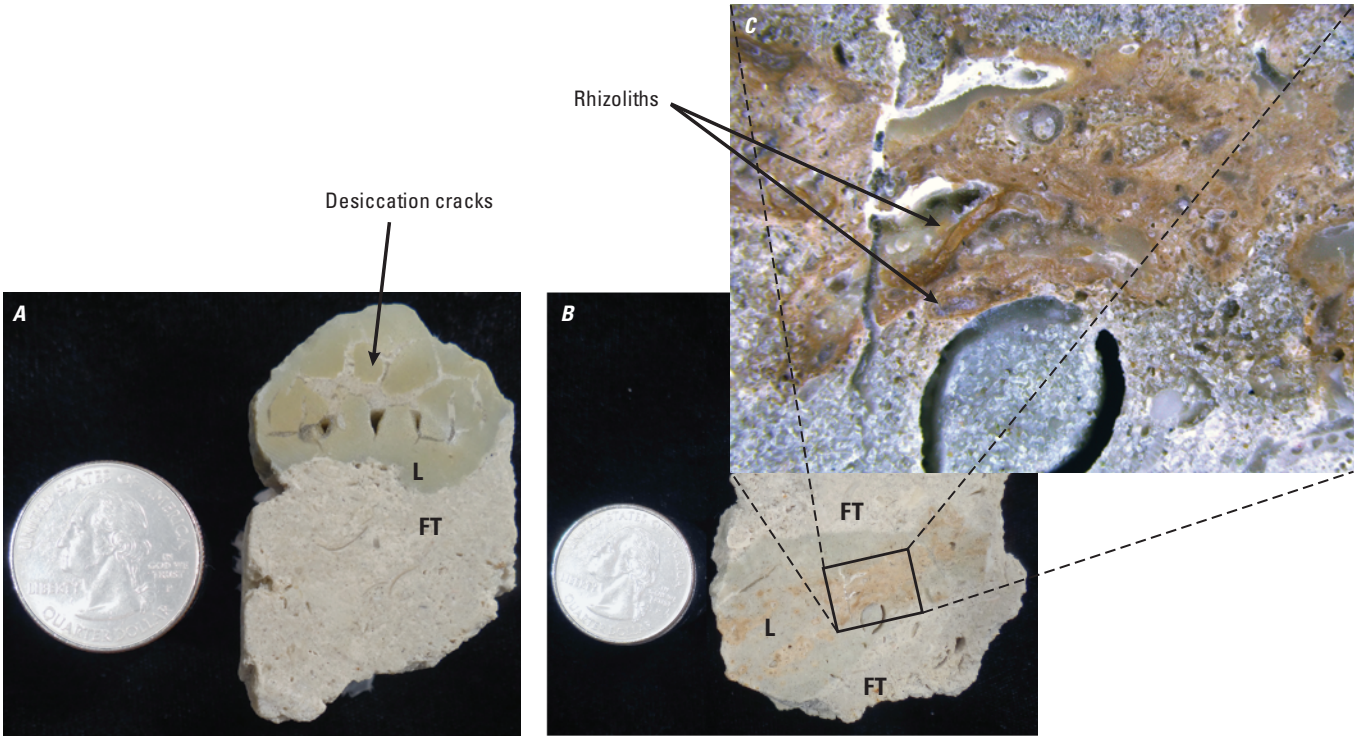

Figure 7. Examples of lithoclasts (L) derived from erosion of the Tamiami Formation and within a rock matrix of the Fort Thompson Formation (FT) observed in core rubble from test corehole G–3878 at about 86 feet below land surface above an unconformity and sequence boundary between the Tamiami Formation and Fort Thompson Formation. The (*A*) lime mudstone and (*B*) quartz sandstone lithoclasts eroded from the Tamiami Formation are contained in younger arenaceous skeletal packstone and grainstone. The lithoclasts in A contain desiccation cracks and (*C*) rhizoliths, which are evidence for subaerial exposure for the Tamiami Formation.

the Fort Thompson Formation during marine reflooding of the subaerial unconformity. This same subaerial unconformity that separates the Pinecrest Member of the Tamiami and the Fort Thompson Formation was identified by Cunningham and others (2006a, 2006b) in cores from a number of wells in the Lake Belt area. Missimer (1993) recognized a disconformity that bounds the top of the Pinecrest Member of the Tamiami Formation. The disconformity probably correlates to the depositional sequence boundary recognized at the contact between the Pinecrest Sand Member of the Tamiami Formation and the Fort Thompson Formation shown in plate 2. The observations of Missimer (1993) provide corroborating evidence that this surface recognized in Miami-Dade County is a widespread major unconformity.

Lithofacies

A lithofacies is a laterally mappable subdivision of a stratigraphic unit established on the basis of mineralogic, petrographic, and paleontologic characteristics of rocks and sediments (Neuendorf and others, 2005). The main component identified and mapped on hydrogeologic cross sections in this study (plates 2 and 3) is the lithofacies. A vertical lithofacies succession is defined by Kerans and Tinker (1997) as a distinctive stack of lithofacies that indicates either an upward shallowing, or an amalgamation of a persistent depositional environment, as accommodation fills within a cycle-scale sea-level rise. Lithofacies were organized into vertical successions that represent either upward-shallowing depositional cycles or depositional cycles composed entirely or mostly of a discrete lithofacies representative of a predominant depositional water depth. In the study area, these cycles are typically from 2 to about 10 ft thick. Sedimentary characteristics, paleontology, and ichnology of lithofacies were evaluated to establish their vertical organization within cyclic vertical lithofacies successions and their relation to bounding surfaces at the top and bottom of the cycles. Using Walther's law of correlation of facies (Middleton, 1973), Cunningham and others (2006b; table 4) organized the lithofacies within vertical lithofacies successions to delineate environments of deposition.

Eighteen lithofacies, four of which are newly defined or modified here, describe the sedimentary rocks and sediments that form the Pinecrest Sand Member of the Tamiami Formation, the Fort Thompson Formation, and the Miami Limestone throughout the study area (table 4). Cunningham and others (2006a) delineated the Tamiami Formation, Fort Thompson Formation, and Miami Limestone on the basis of 16 lithofacies. The four newly defined or modified lithofacies (table 4) include (1) ooid grainstone and packstone, (2) skeletal wackestone and packstone, (3) coral boundstone (modified from framestone), and (4) skeletal quartz sand. The vuggy wackestone and packstone of Cunningham and others (2006b) were

Table 4. Summary of lithofacies of the Miami Limestone, Fort Thompson Formation, and selected lithofacies of the Tamiami Formation in north-central Miami-Dade County including the Snapper Creek Well Field (updated data originally developed for the Lake Belt area from Cunningham and others, 2006a).

[Color, based on Geological Society of America rock color chart (1995); Ichnofabric, based on index developed by Droser and Bottjer (1986); NDA, no laboratory measurements available; mm, millimeter; cm, centimeter; *, lithology applies to Tamiami Formation only]

Lithofacies	Description
Peloid packstone and grainstone	**Color:** Very pale orange 10YR 8/2, grayish orange 10YR 7/4 and pale yellowish orange 10YR 8/6 matrix **Depositional texture:** Burrow-mottled pelmold and peloid packstone and grainstone **Sedimentary structures/textures:** Very thickly bedded **Ichnofabrics:** Abundant *Ophiomorpha*, common ichnofabric index 5 **Carbonate and accessory grains:** Mainly pelmolds and peloids; minor pelecypods, gastropods, and *Schizoporella* bryozoans, miliolids, quartz grains, intraclasts, archaiasinids, agglutinating foraminifera, oomolds **Helium porosity (percent):** Common pore types include pelmoldic, *Ophiomorpha*-related megaporosity, interparticle, intraparticle, irregular vugs, fossil moldic, and root-mold porosity. Mean porosity is 44.5, n = 26, range from 37.2 to 49.4 **Air permeability (millidarcies):** Mean maximum horizontal is 9,187, n = 24, range from 1,116 to 25,764; mean vertical is 4,719, n = 26, range from 220 to 14,750 **Lattice Boltzmann methods permeability (darcies)**: n = 1, vertical 1.3 x 10^6 and horizontal 2.1 x 10^6 **Paleoenvironment:** Inner-shelf peloidal lagoon **Pore class:** I
Ooid grainstone and packstone	**Color:** Very pale orange (10YR 8/2), and minor dark yellowish orange 10YR 6/6 **Depositional texture:** Burrow-mottled ooid grainstone and packstone **Sedimentary structures/textures:** Very thickly bedded, cross laminated **Ichnofabrics:** Abundant *Ophiomorpha*, common ichnofabric index 5 **Carbonate and accessory grains:** Mainly ooids and oomolds; minor peloids, pelecypods, *Halimeda*, gastropods, miliolids, *Favreina*, *Schizoporella* bryozoans **Helium porosity (percent):** Common pore types include oomoldic, Ophiomorpha-related megaporosity, interparticle, intraparticle, pelmoldic, and fossil-moldic porosity NDA for porosity values **Air permeability (millidarcies):** NDA for permeability values **Paleoenvironment:** Middle-shelf ooid shoals **Pore class:** I
Peloid wackestone and packstone	**Color:** Very pale orange 10YR 8/2, dark yellowish orange 10YR 6/6, moderate yellowish brown 10YR 5/4, pale yellowish brown 10YR 6/2, and light brown 5YR 5/6 matrix **Depositional texture:** Mainly mud-dominated fabric characterized by pelecypod, benthic foraminifera lime floatstone with a peloid lime wackestone to mud-dominated lime packstone matrix, but minor grain-dominated fabric characterized by peloid lime grainstone or skeletal grain-dominated lime packstone matrix; minor solution-enlarged burrows filled with peloid grainstone or packstone **Sedimentary structures/textures:** Medium to very thickly bedded **Ichnofabrics:** Abundant *Thalassinoides*, minor ~0.5–1-mm diameter rhizoliths and less common up to 5-cm wide subvertical root molds, common ichnofabric index 5 **Carbonate and accessory grains:** Mainly peloids, pelecypods (including *Chione*) and benthic foraminifera (including archaiasinids, soritids, miliolids, peneroplids, *Cyclorbiculina*), ostracods, and minor *Schizoporella* bryozoans, quartz grains, *Favreina*, intraclasts, and stick-shaped *Porites*, *Halimeda* **Helium porosity (percent):** Common pore types include pelmoldic and skeletal moldic porosity, *Thalassinoides*-related megaporosity, irregular vugs, root-mold porosity, bedding-plane vugs, and intraparticle porosity. Mean porosity is 18.4, n = 12, range from 11.0 to 27.3 **Air permeability (millidarcies):** Mean maximum horizontal is 2,611, n = 12, range from 13.8 to 11,017; mean vertical is 596, n = 12, range from 11 to 1,750 **Paleoenvironment:** Micrite-rich middle shelf **Pore class:** III

Table 4. Summary of lithofacies of the Miami Limestone, Fort Thompson Formation, and selected lithofacies of the Tamiami Formation in north-central Miami-Dade County including the Snapper Creek Well Field (updated data originally developed for the Lake Belt area from Cunningham and others, 2006a).—Continued

[Color, based on Geological Society of America rock color chart (1995); Ichnofabric, based on index developed by Droser and Bottjer (1986); NDA, no laboratory measurements available; mm, millimeter; cm, centimeter; *, lithology applies to Tamiami Formation only]

Lithofacies	Description
Planorbella floatstone and rudstone	**Color:** Pale yellowish brown 10YR 6/2, very pale orange 10YR 8/2, light gray N7 to medium dark gray N4 **Depositional texture:** Moldic *Planorbella* floatstone and rudstone with skeletal wackestone and packstone matrix; local lime wackestone **Sedimentary structures/textures:** Local desiccation cracks, very thinly to very thickly bedded **Ichnofabrics:** Uncommon ~0.5–1-mm diameter rhizoliths Ichnofacies: In some cases *Gastrochaenolites*, *Entobia* **Carbonate and accessory grains:** Mainly gastropod molds including *Planorbella*, *Pomacea*, *Physa*, *Hydrobiidae*?, smooth-walled ostracods, and skeletal fragments; minor quartz sand, pelecypods, freshwater-algae *Charophyta*, uncommon benthic foraminifera (including *Ammonia*, *Elphidium*, peneroplids), echinoids **Helium porosity (percent):** Common pore types include skeletal-moldic separate vugs, solution-enlarged semivertical root molds, and minor vertical or irregular vugs, and bedding plane vugs. Mean porosity is 21.8, n = 31, range from 13.0 to 41.5 **Air permeability (millidarcies):** Mean maximum horizontal is 3,458, n = 31, range from 0.02 to 19,323; mean vertical is 5,354, n = 30, range from 1 to 17,428 **Paleoenvironment:** Freshwater paralic (mainly freshwater ponds or marshes) **Pore class:** III
Gastropod floatstone and rudstone	**Color:** Very pale orange 10YR 8/2 **Depositional texture:** Moldic gastropod floatstone and rudstone with skeletal wackestone and packstone matrix or skeletal packstone matrix; local lime wackestone **Sedimentary structures/textures:** Thinly to medium bedded **Ichnofabrics:** Common thalassinidean and (or) thalassinidean-like crustacean produced burrows **Carbonate and accessory grains:** Mainly gastropods molds including skeletal fragments (*Turritella* can be common); minor quartz sand, pelecypods, ostracods, large discoid benthic foraminifera (including archaiasinids), peloids, serpulid tubes, uncommon *Sideastrea* and *Schizoporella* **Helium porosity (percent):** Common pore types include skeletal-moldic separate vugs and minor irregular vugs. Mean porosity is 20.8, n = 4, range from 11.2 to 29.7 **Air permeability (millidarcies):** Mean maximum horizontal is 1,101, n =4, range from 43 to 2,350; mean vertical is 3,775, n = 4, range from 317 to 13,272 **Paleoenvironment:** Grain-rich middle shelf **Pore class:** I or II
Conglomerate	**Color:** Very pale orange 10YR 8/2 and pale yellowish brown 10YR 6/2 matrix, and very pale orange 10YR 8/2, dark yellowish orange 10YR 6/6, moderate yellowish brown 10YR 5/4, pale yellowish brown 10YR 6/2, moderate brown 5YR 4/4, light brown 5YR 6/4, grayish orange pink 5YR 7/2 and dark gray N3 to light gray N7 intraclasts **Depositional texture:** Intraclast lime rudstone with quartz sandstone matrix or quartz sand-rich lime grainstone or mud-dominated lime packstone matrix **Sedimentary structures/textures:** Thinly to medium bedded **Ichnofabrics:** Common ~0.5–1-mm diameter rhizoliths **Carbonate and accessory grains:** Mainly intraclasts and quartz grains; local minor peloids, pelecypods, gastropods, echinoids, and benthic foraminifera (including *Elphidium*, *Ammonia*, miliolids, soritids, rotaliforms, amphistiginids, *Nonion*) **Helium porosity (percent):** Common pore types include intergrain porosity, separate- and touching-vug porosity, and local root- mold porosity. Mean porosity is 15.5, n = 10, range from 6.9 to 26.0 **Air permeability (millidarcies):** Mean maximum horizontal is 968, n = 10, range from 1 to 3,813; mean vertical is 1,009, n = 10, range from 0 to 5,624 **Paleoenvironment:** Fluvial?, restricted inner shelf (shoreface?), platform margin-to-outer platform **Pore class:** III

Table 4. Summary of lithofacies of the Miami Limestone, Fort Thompson Formation, and selected lithofacies of the Tamiami Formation in north-central Miami-Dade County including the Snapper Creek Well Field (updated data originally developed for the Lake Belt area from Cunningham and others, 2006a).—Continued

[Color, based on Geological Society of America rock color chart (1995); Ichnofabric, based on index developed by Droser and Bottjer (1986); NDA, no laboratory measurements available; mm, millimeter; cm, centimeter; *, lithology applies to Tamiami Formation only]

Lithofacies	Description
Autobreccia	**Color:** Very pale orange 10YR 8/2 and light gray N7 **Depositional texture:** Angualar clasts forming a rudstone **Sedimentary structures/textures:** Commonly thinly to medium bedded **Carbonate and accessory grains:** Mostly autoclasts, fossils include mollusks, ostracods, echinoids, benthic foraminifera (including *Ammonia*, archaiasinids?, miliolids, soritids, rotaliforms, bolvinids, *Spaerogypsina*, amphistiginids) **Helium porosity (percent):** Common pore types include minor microporosity; interclast porosity, and vuggy porosity. Mean porosity is NDA **Air permeability (millidarcies):** Mean maximum horizontal is NDA and mean vertical is NDA **Paleoenvironment:** Subaerial exposure **Pore class:** III
Pedogenic limestone	**Color:** (1) Very pale orange 10YR 8/2, dark yellowish orange 10YR 6/6, moderate yellowish brown 10YR 5/4, pale yellowish brown 10YR 6/2 and grayish orange 10YR 7/4; (2) very pale orange 10YR 8/2 and grayish orange 10YR 7/4; and (3) dark yellowish orange 10YR 6/6, grayish orange 10YR 7/4, pale yellowish brown 10YR 6/2, moderate yellowish brown 10YR 5/4 and very pale orange 10YR 8/2 **Depositional texture:** Three principal types: (1) laminated calcrete, (2) massive calcrete, and (3) pedotubule limestone **Sedimentary structures/textures:** (1) Thinly to very thickly bedded and drapes over microtopography; (2) very finely laminated; and (3) thinly to very thickly bedded or poorly bedded, desiccation cracks, uncommon alveolar septal fabric **Ichnofabrics:** Common rhizoliths **Carbonate and accessory grains:** (1) Minor quartz grains, uncommon miliolids, ostracods; (2) minor intraclasts, pelecypods, skeletal fragments, quartz grains, benthic foraminifera including *Ammonia*, *Elphidium*, miliolids, soritids, arachaiasinids, peneroplids, rotaliforms; and (3) skeletal fragments and local miliolids, minor quartz sand **Helium porosity (percent):** (1) Minor microporosity and uncommon bedding-plane vugs; (2) 20 to 30 percent root-mold porosity, 5 to 10 percent vuggy porosity (including uncommon bedding-plane vugs), 5 percent pelmoldic and skeletal moldic porosity; and (3) 2 to 5 percent skeletal moldic porosity, 2 to 5 percent desiccation crack porosity and common bedding-plane vugs **Air permeability (millidarcies):** (1) Low, (2) moderate to high, and (3) matrix very low to low **Paleoenvironment:** Subaerial exposure **Pore class:** III
Mudstone and wackestone	**Color:** Very pale orange 10YR 8/2, grayish orange pink 5YR 7/2, pale yellowish brown 10YR 6/2, grayish orange 10YR 7/4 **Depositional texture:** Lime mudstone and wackestone **Sedimentary structures/textures:** Common subvertical cracks, thinly to thickly bedded **Ichnofabrics:** Common burrow mottling and rhizoliths **Carbonate and accessory grains:** (1) Brackish: mainly ostracods, skeletal fragments, gastropods (including *Planorbella*), benthic foraminifera (including *Ammonia*, *Elphidium*, miliolids, soritids, archaiasinids, peneroplids, *Androsina*, rotaliforms); minor pelecypods quartz sand, charophytes; and (2) mud mound: peloids, pelecypods, benthic foraminifera (including miliolids), quartz sand, intraclasts, ostracods **Helium porosity (percent):** Common pore types include skeletal mold porosity, root-mold porosity, separate vug porosity, semivertical touching-vug porosity, irregular vugs, bedding-plane vugs, and desiccation-crack porosity. Mean porosity is 15.7, n = 50, range from 5.5 to 31.1 **Air permeability (millidarcies):** Mean maximum horizontal is 2,292, n = 49, range from 0.001 to 20,592; mean vertical is 1,880, n = 50, range from 0 to 18,223 **Paleoenvironment:** Brackish paralic **Pore class:** III

Table 4. Summary of lithofacies of the Miami Limestone, Fort Thompson Formation, and selected lithofacies of the Tamiami Formation in north-central Miami-Dade County including the Snapper Creek Well Field (updated data originally developed for the Lake Belt area from Cunningham and others, 2006a).—Continued.

[Color, based on Geological Society of America rock color chart (1995); Ichnofabric, based on index developed by Droser and Bottjer (1986); NDA, no laboratory measurements available; mm, millimeter; cm, centimeter; *, lithology applies to Tamiami Formation only]

Lithofacies	Description
Laminated peloid packstone and grainstone	**Color:** Very pale orange 10YR 8/2 **Depositional texture:** Peloid grainstone and packstone **Sedimentary structures/textures:** Thinly laminated to very thinly bedded **Ichnofabrics:** Generally low ichnofabric index 2 **Carbonate and accessory grains:** Mainly peloids; minor quartz grains, skeletal fragments, and benthic foraminifera (including miliolids, *Elphidium*, archaiasinids, *Androsina*, rotaliforms), mollusk fragments **Helium porosity (percent):** Common pore types include moldic porosity, intergrain porosity, and bedding-plane vug porosity. Mean porosity is 20.2, n = 1 **Air permeability (millidarcies):** Mean maximum horizontal is 5,268, n = 1; mean vertical is 533, n = 1 **Paleoenvironment:** Restricted platform interior (tidal flat) **Pore class:** I
Skeletal wackestone and packstone	**Color:** Very pale orange 10YR 8/2, grayish orange 10YR 7/4, yellowish gray 5Y 8/1 **Depositional texture:** Skeletal wackestone and packstone **Sedimentary structures/textures:** Principally massive and thickly to very thickly bedded **Ichnofabrics:** Typically highly burrowed by mostly by thalassinidean or thalassinidean-like crustaceans **Carbonate and accessory grains:** Mainly pelecypods, benthic foraminifera (including archaiasinids, soritids, miliolids, peneroplids, *Elphidium*), peloids, mollusks (including *Chione*), skeletal fragments, peloids, ostracods, gastropods, echinoids; minor to abundant quartz grains **Helium porosity (percent):** Common pore types include burrow-related megaporosity, intraparticle porosity, irregular vugs, bedding-plane vugs, fossil-moldic, and root-mold porosity. Mean porosity is NDA **Air permeability (millidarcies):** Mean maximum horizontal is NDA and mean vertical is NDA **Paleoenvironment:** Mainly micrite-rich middle shelf **Pore class:** III
Skeletal packstone and grainstone	**Color:** Very pale orange 10YR 8/2, pale yellowish brown 10YR 6/2, grayish orange 10YR 7/4; light gray N7 to very light gray N8 **Depositional texture:** Skeletal grainstone and packstone **Sedimentary structures/textures:** Principally massive and thickly to very thickly bedded **Ichnofabrics:** Common to abundant ichnofabrics probably produced by thalassinideans or thalassinidean-like crustaceans, and less common rhizoliths that have a less than 1-mm diameter inner wall **Carbonate and accessory grains:** Mainly skeletal fragments, benthic foraminifera (including archaiasinids, soritids, miliolids, peneroplids, *Elphidium*, *Ammonia*, *Androsina*, *Amphistegina*, rotaliforms, *Gypsina*, *Parasorites*, *Cyclorbiculina*, *Cycloputeolina*), peloids, mollusks (including *Chione*, *Modulus*, *Turritella*, *Codakia*, *Lucina*, *Trachycardium*, *Anodontia*, *Lirophora*, *Pyrazisinus*, *Tagelus*, *Anomalocardia*, *Melongena*, *Lucinisca*, *Carditimera*, *Codakia*, *Cerithium*), skeletal fragments, peloids, ostracods, gastro- pods, echinoids; minor to abundant quartz grains; trace red algae, bryozoans, charophytes **Helium porosity (percent):** Common pore types include skeletal moldic porosity, burrow-related vugs, irregular vugs, interparticle porosity, pelmoldic porosity, root-mold porosity, and intraparticle. Mean porosity is 27.1, n = 85, range from 10.8 to 48.3 **Air permeability (millidarcies):** Mean maximum horizontal is 3,279, n = 84, range from 0.2 to 19,318; mean vertical is 3,102, n = 83, range from 0 to 20,140 **Paleoenvironment:** Mainly grain-rich middle shelf **Pore class:** II and uncommonly I
Coral boundstone	**Color:** Very pale orange 10YR 8/2, grayish orange 10YR 7/4 **Depositional texture:** Coral framestone, bafflestone, and (or) bindstone **Ichnofabrics:** Massive with borings and vugs, and uncommon rhizoliths **Carbonate and accessory grains:** *Monastrea annularis*, *Porites porites*, *Acropora cervicornis*, *Manicina*, benthic foraminifera (including archaiasinids, miliolids, peneroplids, *Elphidium*), peloids, pelecypods, gastropods, ostracods, bryozoans **Helium porosity (percent):** Common pore types include intraparticle porosity, irregular vugs, and uncommon root-mold porosity. Mean porosity is NDA **Air permeability (millidarcies):** Mean maximum horizontal is NDA and mean vertical is NDA **Paleoenvironment:** Shallow-shelf coral patch reefs **Pore class:** I and II

Table 4. Summary of lithofacies of the Miami Limestone, Fort Thompson Formation, and selected lithofacies of the Tamiami Formation in north-central Miami-Dade County including the Snapper Creek Well Field (updated data originally developed for the Lake Belt area from Cunningham and others, 2006a).—Continued.

[Color, based on Geological Society of America rock color chart (1995); Ichnofabric, based on index developed by Droser and Bottjer (1986); NDA, no laboratory measurements available; mm, millimeter; cm, centimeter; *, lithology applies to Tamiami Formation only]

Lithofacies	Description
Pelecypod floatstone and rudstone	**Color:** Very pale orange 10YR 8/2, very light gray N8 **Depositional texture:** Pelecypod floatstone and rudstone with skeletal wackestone, packstone or grainstone matrix **Sedimentary structures/textures:** Thickly to very thickly bedded **Ichnofabrics:** Abundant ichnofabrics probably produced by thalassinidean and (or) thalassinidean-like crustaceans and much less common rhizoliths **Carbonate and accessory grains:** Mainly mollusks (*Chione*, *Turritella*, *Trachycardium*, *Bellucina*, *Cerithium*, *Diodora*, *Muricid*, *Brachidontes*, *Modulus*, *Anomalocardia*?, *Divaricella*, *Bulla*, pectenids, arcids, *Glycymeris*, muricids, ostreids, *Phacoides*, *Vermicularia*, *Anodontia*, *Codakia*, *Conus*, *Lithopoma*, *Oliva*, *Turbo*, *Anadara*, *Carolinapecten*, *Nuculana*, *Parastarte*) benthic foraminifera (including archaiasinids, peneroplids, miliolids, *Parasorites*, soritids, *Ammonia*, *Elphidium*, *Androsina*, rotaliforms, *Gypsina*?, *Nonion*?, amphistiginids, agglutinating foraminifera, *Bolivina*, *Cyclorbiculina*, *Cycloputeolina*), peloids, ostracods; minor quartz grains; trace echinoids, *Manicina*, red algae, charophytes, globigerinids **Helium porosity (percent):** Common pore types include fossil moldic, interparticle, burrow-related magaporosity, irregular vugs, and intraparticle. Mean porosity is 26.8, n = 89, range from 10.0 to 50.2 **Air permeability (millidarcies):** Mean maximum horizontal is 6,922, n = 90, range from 0.3 to 27,411; mean vertical is 3,485, n = 90, range is 0 to 18,551 **Paleoenvironment:** Grain-rich middle shelf **Pore class:** II and I
Touching-vug pelecypod floatstone and rudstone	**Color:** Very pale orange 10YR 8/2, very light gray N8 **Depositional texture:** Pelecypod floatstone and rudstone with peloid and skeletal fragment wackestone and packstone matrix **Sedimentary structures/textures:** Medium to very thickly bedded **Ichnofabrics:** Abundant ichnofabrics probably produced by thalassinidean and (or) thalassinidean-like crustaceans **Carbonate and accessory grains:** Mainly peloids, mollusks (including *Chione*, *Modulus*, *Turritella*, *Codakia*, *Lucina*, *Cerithium*, *Trachycardium*, *Lucinisca*, *Pecten*, *Diplodonta*, *Strombus*, *Pleuromeris*, *Carditimera*, *Anadara*, *Glycymeris*, *Anodonita*, *Cardium*, *Dosinia*, *Nucula*, *Turbo*, *Glycymeris*, *Pecten*?, *Astralium*, *Nuculana*, *Phacoides*, *Divaricella*), skeletal fragments, benthic foraminifers (including soritids, archaiasinids, miliolids, *Ammonia*, *Parasorites*, amphistiginids, *Elphidium*, peneroplids, rotaliforms, *Androsina*), ostracods, echinoids; trace *Porites* coral, red algae, bryozoans **Helium porosity (percent):** Common pore types include fossil moldic, burrow-related megaporosity, irregular vugs, interparticle and intraparticle porosity, 5 to 100 percent separate and touching vugs. Mean porosity is 36.4, n = 5, range from 32.0 to 42.1 **Air permeability (millidarcies):** Mean maximum horizontal is 8,358, n = 4, range from 2,731 to 16,478; mean vertical is 7,881, n = 7, range from 1,387 to 16,468 **Paleoenvironment:** Grain-rich inner shelf **Pore class:** I
Quartz sandstone and skeletal quartz sandstone*	**Color:** Very pale orange 10YR 8/2, very light gray N8 **Depositional texture:** Quartz sandstone and skeletal quartz sandstone **Sedimentary structures/textures:** Thickly to very thickly bedded **Ichnofabrics:** Typically abundant ichnofabrics probably produced by thalassinidean and (or) thalassinidean-like crustaceans, *Ophiomorpha*, uncommon rhizoliths **Carbonate and accessory grains:** Mainly quartz sand, peloids, pelecypods, skeletal fragments, gastropods, echinoids; foraminifera can include archaiasinids, soritids, peneroplids, globigerinids, amphistiginids, *Ammonia*, *Elphidium*, miliolids **Helium porosity (percent):** Common pore types include interparticle and fossil moldic porosity, and minor irregular vugs and burrow-related megaporosity. Mean porosity is 14.0, n = 5, range from 8.3 to 19.7 **Air permeability (millidarcies):** Mean maximum horizontal is 609, n = 4, range from 0.67 to 1,736; mean vertical is 1,088, n = 5, range from 0 to 3,333 **Paleoenvironment:** Mainly middle-shelf Fort Thompson Formation or inner ramp of the Tamiami Formation **Pore class:** II

Table 4. Summary of lithofacies of the Miami Limestone, Fort Thompson Formation, and selected lithofacies of the Tamiami Formation in north-central Miami-Dade County including the Snapper Creek Well Field (updated data originally developed for the Lake Belt area from Cunningham and others, 2006a).—Continued.

[Color, based on Geological Society of America rock color chart (1995); Ichnofabric, based on index developed by Droser and Bottjer (1986); NDA, no laboratory measurements available; mm, millimeter; cm, centimeter; *, lithology applies to Tamiami Formation only]

Lithofacies	Description
Skeletal quartz sand*	**Color:** Mainly greenish gray 5GY 8/1, light greenish gray 5GY 8/1, yellowish gray 5Y 8/1, and minor light gray N7 and very pale orange 10YR 8/2 for the skeletal quartz sand of the Tamiami Formation **Depositional texture:** Skeletal quartz sand **Sedimentary structures/textures:** Thickly to very thickly bedded **Ichnofabrics:** Typically abundant ichnofabrics probably produced by thalassinidean and (or) thalassinidean-like crustaceans, *Ophiomorpha*, *Thalassinoides*?, *Teichichnus*? Ichnofacies: In some cases *Glossifungites* occurs **Carbonate and accessory grains:** Mainly peleycpod fragments and minor articulated pelecypods, skeletal fragments, gastropods (including *Turritella*), foraminifera include amphistiginids (very minor miliolids, *Elphidium*, *Ammonia*, biserial, *Pyrgo*?), echinoid spines, barnacles (*Balanus*), cheilostome bryozoans, planktic foraminifera, *Ostrea*, intraclasts **Helium porosity (percent):** Common pore types include interparticle and very minor fossil moldic porosity. Visually estimated porosity ranges between 5-25 percent **Air permeability (millidarcies):** Mean maximum horizontal is NDA and mean vertical is NDA **Paleoenvironment:** Mainly inner ramp of the Tamiami Formation **Pore class:** II
Quartz sand*	**Color:** Light greenish gray 5GY 8/1, yellowish gray 5Y 8/1 **Depositional texture:** Quartz sand **Sedimentary structures/textures:** Thickly to very thickly bedded **Ichnofabrics:** Commonly bioturbated **Carbonate and accessory grains:** Minor skeletal fragments and pelecypod fragments **Helium porosity (percent):** Pore types dominated by interparticle porosity. Visually estimated porosity averages about 25 percent **Air permeability (millidarcies):** Mean maximum horizontal is NDA and mean vertical is NDA **Paleoenvironment:** Mainly inner ramp of the Tamiami Formation **Pore class:** II

not recognized in the SCWF and SWWF study area and are not included in table 4. Carbonate lithofacies can be composed of a substantial amount of quartz grains, and in instances in which the quartz grain content of the rock is between 25 and 50 percent, "arenaceous" is added as a prefix to the lithofacies type. Carbonate-rich rock with quartz-grain content of greater than 50 percent is considered a quartz sandstone. "Touching-vug," a prefix to a lithofacies type, refers to a vuggy porosity that forms an interconnected pore system (Lucia, 1999).

Cyclostratigraphy

Cyclostratigraphy—the study of rocks and sediments in relation to their cyclic deposition and erosion—was used to organize vertical and lateral changes in lithofacies into high-frequency cycles (HFCs). The HFCs provided the fundamental building blocks of the geologic framework. Cyclostratigraphy can be used to correlate horizontally connected groundwater flow between wells and, thus, helps define the hydrogeologic framework. The HFCs are delineated by vertical lithofacies successions bounded by surfaces where there is evidence for an increase in sea level (Kerans and Tinker, 1997). Four recurring lithofacies successions represent four ideal HFCs within the study area. The four ideal HFCs identified for the Lake Belt area by Cunningham and others (2006b, 2009; fig. 2) are (1) an upward-shallowing subtidal cycle, (2) an aggradational subtidal cycle, (3) an upward-shallowing paralic cycle, and (4) an upward-shallowing peritidal cycle. Paralic environmental facies cap the upward-shallowing paralic cycles (Cunningham and others, 2004a, 2004c, 2006a, 2006b). The principal characteristic of paralic depositional environments is that they occur at the transitional areas or zones between marine and terrestrial realms, including estuaries, coastal lagoons, marshes, and coastal zones subject to high freshwater input (Debenay and others, 2000). The two upward-shallowing ideal cycle types are present only within the Fort Thompson Formation, and the aggradational subtidal cycle is present only within the Miami Limestone. In the study area, the ideal peritidal cycle is unique in its occurrence within the Fort Thompson Formation.

Four orders of cycle hierarchy (modified from Kerans and Tinker, 1997, fig. 1.11) are identified for the cycles of the Pinecrest Member of the Tamiami Formation, Fort Thompson Formation, and Miami Limestone: third-order sequences, fourth-order high-frequency sequences (HFSs), fifth-order composite high-frequency cycles (CHFCs), and sixth-order HFCs (plate 2). (Note that HFSs include, or consist of, both CHFCs and HFCs.) The delineation of the hierarchical order of cycles and bounding surfaces within the Fort Thompson Formation and Miami Limestone is based on two criteria: (1) the extent and physical attributes of cycles and the magnitude of change at subordinate bounding surfaces compared to that at the major regional unconformity that separates the Tamiami Formation and Fort Thompson Formation and (2) the extent and characteristics of cycles and degree of physical change of bounding surfaces compared to those generated by glacio-eustatic sea-level cyclic variation of approximately 100,000 years during the Pleistocene epoch (Perkins, 1977; Multer and others, 2002). Thus, the SCWF and SWWF study area cycle hierarchy is not strictly a cycle-duration-based hierarchy (for example, see Mitchum and Van Wagoner, 1991) nor one established solely on the basis of boundary extent and physical characteristics (Embry, 1995), but is grounded on the two criteria above, which are important to the unique geologic context of the Pliocene-Pleistocene rocks and sediments of south Florida (Catuneanu, 2006).

The lowest order cycle boundary present is the major subaerial exposure surface and unconformity identifiable at the top of the Pinecrest Member of the Tamiami Formation and the base of the Fort Thompson Formation. This sequence boundary is a third-order boundary because it separates two successions of rock and sediment, with bounding unconformities that probably represent intervals of 1 million years or more. Cycles and bounding surfaces within the upper part of the Pinecrest Member of the Tamiami Formation are poorly defined in terms of duration and physical character relative to the overlying Pleistocene cycles, and thus are not discussed further. The high frequency sequences of the Fort Thompson Formation and the Miami Limestone are equivalent to the five Q units of Perkins (1977), which accumulated during major Pleistocene interglacial periods. The unconformity separating the Q1 and Q2 units of Perkins (1977), however, has not been identified in the SCWF, SWWF, and Lake Belt areas (fig. 6); (Cunningham and others 2004b, 2006a, 2006b). The CHFCs and HFCs may be related to glacio-eustatic sea-level changes or may be autocyclic.

The accumulation of HFS 2–HFS 5 of the Fort Thompson Formation and Miami Limestone (plate 2) was controlled by eustacy and thus defined by the approximate 100,000-year duration of major Pleistocene glacio-eustatic sea-level changes (Perkins, 1977). The HFSs likely have a duration of accumulation of only about 10,000 to 30,000 years. For example, the rocks equivalent to HFS 5 are reported by Multer and others (2002) as having a range in age of only about 25,000 years. On the Great Bahamas Bank, the duration of accumulation of sediment during Marine Isotope Stage (MIS) 5e has been reported between 131,000 and 119,000 years (Chen and others, 1991) or even shorter, between 124,000 and 115,000 years (Thompson and others, 2011). The HFS duration is based on the time hypothesized that the south Florida carbonate platform was flooded during major Pleistocene interglacial high stands of sea level. Assuming that the HFSs have accumulated over 9,000 to 25,000 years, then the CHFCs and HFCs have cycle durations of 1,000 to 20,000 years. Because groundwater flow units commonly are defined by concentrated flow within only one or two HFCs or a single HFS, they occur within rocks representing 1,000 to 20,000 years of sediment accumulation bounded by unconformities that represent periods of up to about 100,000 years. The study area hydrostratigraphy and karst pore system are products of the cumulative duration for paleo-vadose karstic processes on the stack of Pleistocene carbonate cycles. The cycle durations are on the scale of several hundreds of thousands of years as opposed to cumulative durations for paleo-phreatic dissolution on the order of many tens of thousands of years. The cumulative time that each HFS was subjected to cyclic vadose and phreatic karst processes could affect, for example, the present-day spatial distribution of vertical solution pipes within the volume of rock constituting the Biscayne aquifer and, thus, its vertical permeability.

Ichnology

Ichnology is the study of trace fossils, such as tracks, traces, burrows, and borings, that are structures produced in sedimentary rock or sediments by organism activity (Bromley, 1996). Preferential dissolution of these structures (McIlroy, 2004) has caused development of megaporous and highly permeable limestone in many areas of the Biscayne aquifer (Cunningham and others, 2009; Cunningham and Sukop, 2011; Cunningham and others, 2012).

Ichnogenic megaporosity produced by preferential dissolution of *Ophiomorpha*-dominated ichnofabrics is the most prominent contributor to concentrated flow in groundwater flow zones identified in the Biscayne aquifer at the SCWF and SWWF study area (plate 2). Choquette and Pray (1970) define megapores as equant to equant-elongate pores whose average diameter is larger than 4 millimeters (mm), and for tubular or platy pores whose average cross-sectional diameter or thickness, respectively, is larger than 4 mm. Ichnogenic megaporosity is any pore greater than 4 mm associated with preferential dissolution of ichnofabrics or surrounding host rock. It is not uncommon for both major and minor flow zones to be dominated by or have a contribution from ichnogenic megaporosity (plate 2). Ichnogenic megaporosity is present in all four ideal cycle types of the Biscayne aquifer in the study area (fig. 6). Droser and Bottjer (1986) established a semiquantitative classification of ichnofabric (ichnofabric index) to determine the amount of bioturbation recorded in the stratigraphic record. The index is based on percentage of original sedimentary fabric that has been disrupted by biogenic reworking from no bioturbation (ichnofabric index 1)

to complete homogenization (ichnofabric index 6; Droser and Bottjer, 1989). Cunningham and others (2009, 2012) and Cunningham and Sukop (2011) present a more extensive discussion of the application of ichnology to the hydrogeology of the Biscayne aquifer.

Depositional Environments

Depositional environments are geographic areas (for example, bays or beaches) where sediment accumulates and that are characterized by specific physical, chemical, and biological conditions. The mapping of depositional facies, rock units that accumulated within specific depositional environments, can help predict the spatial distribution and properties of groundwater flow. In the study area, the Pinecrest Member of the Tamiami Formation, Fort Thompson Formation, and Miami Limestone can be characterized by 11 depositional environments. A mixed-carbonate siliciclastic-influenced inner ramp depositional environment is found in the Tamiami Formation. Seven depositional environments are found in the Fort Thompson Formation: grain-rich middle shelf, middle-shelf patch reefs, middle-shelf quartz sandstone, micrite-rich middle shelf, tidal flat, brackish inner shelf, and freshwater terrestrial areas of paralic settings. The Miami Limestone is characterized by two additional depositional environments, middle-shelf ooid shoals and inner shelf peloidal lagoons, as well as by micrite-rich middle shelf. Subaerial exposure, although a diagenetic environment (Scholle and others, 1983), is represented herein as a depositional environment in the Tamiami Formation, Fort Thompson Formation, and Miami Limestone, where evidence of the upper bounding surface or upper zone of a rock unit has been altered due to chemical, physical, or biological effects associated with subaerial exposure.

Mixed carbonate-siliciclastic inner ramp—The mixed carbonate-siliciclastic inner ramp depositional environment (Burchette and Wright, 1992) is represented throughout the upper part of the Pinecrest Member of the Tamiami Formation that was penetrated in the coreholes of the study area. Representative lithofacies include skeletal quartz sand and skeletal quartz sandstone, and subordinate arenaceous skeletal wackestone and packstone, arenaceous skeletal packstone and grainstone, skeletal packstone and grainstone, and arenaceous pelecypod floatstone and rudstone (plate 2). A restricted, low-energy depositional environment that received a large terrigenous influx is indicated by the assemblage of grain types dominated by quartz sand and pelecypods with lesser occurrences of gastropods (including *Turritella*), miliolids, echinoids, amphisteginids, cheilostome bryozoans, and sparsely disseminated globular planktic foraminifera. This assemblage suggests a shallow-marine setting such as a bay or marine lagoon. *Ostrea*, *Elphidium*, *Balanus*, and *Ammonia* could be indicative of a brackish bay or lagoon, such as that in the Charlotte Harbor area in southwestern Florida described by Dubar (1962). In most cases, the rock and sediment are intensely bioturbated, with a typical ichnofabric-index value of 5. Ichnofabrics are dominated by burrows that were probably created by thalassinideans or thalassinidean-like crustaceans, but the trace fossil *Ophiomorpha* is abundant and widespread, and in some places *Thalassinoides* is present.

The mixed carbonate-siliciclastic inner ramp depositional environment grain types constitute a heterozoan association of particle types (James, 1997). This association is in contrast to a photozoan association of particles found in most of the overlying Fort Thompson Formation and Miami Limestone (plate 2), and could represent a shift from temperate waters prevailing during deposition of the Pinecrest Member of the Tamiami Formation to tropical conditions throughout that part of the Pleistocene when the Fort Thompson Formation and Miami Limestone accumulated. The exception would be the lowermost part of the Fort Thompson Formation in the study area, where the transition from a heterozoan to photozoan association of particles is found (plate 2). Alternatively, water salinity values or nutrient production, and changes in water temperature could have created the upward shift from a heterozoan to the photozoan association of particle types within the lower part of the Fort Thompson Formation.

Grain-rich middle shelf—Lithofacies characteristic of a grain-rich middle shelf are present in the Fort Thompson Formation. These include touching-vug pelecypod floatstone and rudstone, skeletal packstone and grainstone lithofacies, and arenaceous varieties of these two lithofacies. Common grain types are pelecypods and benthic foraminifera (soritids, archaiasinids, and peneroplids). The grain assemblage suggests open-marine, tropical conditions similar to those in the modern inner-shelf margin of southern Florida that is seaward of the present-day islands of the Florida Keys (Enos, 1977; Rose and Lidz, 1977; Lidz and Rose, 1989). These lithofacies are commonly highly bioturbated with a common ichnofabric index value of 5.

Middle-shelf patch reefs—The coral boundstone lithofacies is characteristic of the middle-shelf patch-reef depositional environment and is observed only in the Fort Thompson Formation. Three types of patch reefs are present and have the following depositional textures: *Acropora cervicornis* bafflestone, *Porites porites* bafflestone, and *Montastrea* framestone. Small heads of *Manicina* and other types of unidentified small head-shaped corals are commonly associated with the patch reefs. These patch reefs, which are indicative of shallow, open-marine, tropical conditions on the middle shelf of the Fort Thompson Formation, are present in the middle and lowermost CHFCs of HFS 2. Abundant small *Manicina* corals extend over a broad area between coreholes G–3883 and G–3878 along the hardened surface near the base of the uppermost HFC of HFS 3, but are scattered and did not form patch reefs. The *Montastrea* coral typically are fixed to the upper boundary of HFCs, which provided a hard substrate at the time the corals began to grow on the sea floor. The *Acropora cervicornis* and *Porites porites* patch reefs commonly established growth within sand-rich or micrite-rich sediment.

Middle-shelf quartz sandstone—The skeletal quartz sandstone lithofacies is characteristic of a middle-shelf quartz sand. The quartz sand accumulated in this open-marine environment is generally thick sand bodies continuous over distances of about 0.5 to 2 miles. Two prominent occurrences of middle-shelf quartz sandstone were delineated in the uppermost HFC of HFS 2 and in an HFC that occurs in the middle of the central CHFC of HFS 2. Common grain types in the sandstones indicative of open-marine conditions include archaiasinids, soritids, and echinoids. Pelecypods are widespread throughout both bodies of the quartz sandstone. *Manicina* and *Schizoporella* were present in the upper quartz sandstone of corehole G–3878. Quartz grains are mostly very fine to fine sand size, angular to subrounded, and moderately to poorly sorted. In almost all cases, the sandstone is intensively burrowed with an ichnofabric index value of 5. These two sandstone bodies could have accumulated as a result of long-shore transport of quartz sands within subtidal middle-shelf environments. Only a few other occurrences of skeletal quartz sandstone of limited extent were found in the core samples of the Fort Thompson Formation.

Micrite-rich middle shelf—The peloid wackestone and packstone lithofacies characterizes the micrite-rich middle shelf and is present in the lower part of the Miami Limestone (HFS 4). The skeletal wackestone and packstone lithofacies is common in the Fort Thompson Formation. The interparticle space in wackestones and mud-dominated packstones is entirely or mostly occluded by micrite. Burrowing in this lithofacies is intensive, and it commonly has an ichnofabric index value of 5. The burrows resemble many of the types described by Shinn (1968) and Halley and Evans (1983). The ichnofabric of HFS 4 is dominated by *Thalassinoides*, which contributes to a *Thalassinoides*-dominated *Cruziana* Ichnofacies (Cunningham and others, 2012). The peloid wackestone and packstone lithofacies commonly contains a benthic foraminiferal assemblage of archaiasinids, soritids, and peneroplids (Rose and Lidz, 1977; Lidz and Rose, 1989), which is similar to the present-day muddy interior bottom sediments of the inner shelf margin on the shallow shelf in the Florida Keys (Enos, 1977). Alternatively, the archaiasinid, soritid, and peneroplid assemblage could suggest shallow, restricted, hypersaline or euryhaline conditions (Hallock and Glenn, 1986). *Schizoporella* bryozoa are common in some areas. The peloid wackestone and packstone lithofacies corresponds to the lower part of the bryozoan facies of Hoffmeister and others (1967), which they interpreted to represent an open-marine shelf lagoon. Later, both Perkins (1977) and Evans (1984) indicated that deposition of the bryozoan facies was on an open-marine platform.

Tidal flat—A single tidal flat depositional environment is present in the HFS 3 of the Fort Thompson Formation (plate 2). This depositional environment is characterized by the laminated peloid packstone and grainstone lithofacies. Peloids are overwhelmingly the dominant grain type. Thin to thick laminations are typically horizontal, but commonly have a wavy geometry. In a few places in the Lake Belt area, the laminations, probably generated by algal stromatolites, have a hemispheroidal shape. Mud cracks and rip-up clasts are common.

Brackish inner shelf, and freshwater terrestrial—Lithofacies representative of brackish inner shelf and freshwater terrestrial environments are common in all test coreholes reported on in the study area. Mudstone and wackestone lithofacies commonly distinguish the brackish inner shelf environment, and *Planorbella* floatstone and rudstone with a mudstone or wackestone matrix are characteristic of the freshwater terrestrial environment. The lithofacies of the brackish inner shelf is principally micrite and has an abundance of the benthic foraminifer *Ammonia* and smooth-shelled ostracodes. Charophytes and the benthic foraminifer *Elphidium* are less commonly present, Other types of benthic foraminifers are not common. The *Planorbella* floatstone and rudstone lithofacies commonly contains abundant *Planorbella*, smooth-shelled ostracodes, and charophytes. These three fossil types are characteristic of the freshwater terrestrial environment.

Modern Florida Bay sediments with large populations of *Ammonia* and *Elphidium* and containing few other foraminiferal species are indicative of a brackish platform interior (Rose and Lidz, 1977; Lidz and Rose, 1989). Ishman and others (1997) and Brewster-Wingard and others (1997) found *Ammonia*-*Elphidium* assemblages to be present in hyposaline-influenced areas of modern Biscayne Bay and Florida Bay, respectively. In many cases, interpretation indicates deposition of the *Planorbella*-rich beds in freshwater ponds or marshes (Galli, 1991).

The restricted platform interior and brackish platform interior of Cunningham and others (2006a, 2006b) is herein termed brackish inner shelf. Both the brackish inner shelf and freshwater terrestrial depositional environments are considered paralic environments (plate 2).

Middle-shelf ooid shoals—Middle-shelf ooid shoals are represented by the ooid grainstone and packstone lithofacies within the upper Miami Limestone or HFS 5e in the eastern part of the study area (figs. 2 and 6). The ooid grainstone and packstone lithofacies accumulated in an ooid-shoal complex that forms the Atlantic Coastal Ridge in Miami-Dade County (Halley and others, 1977). Grain types include ooids; peloids; *Halimeda*; large benthic, discoidal foraminifera (archaiasinids are dominant); bivalves; miliolids; *Schizoporella*; and gastropods. This diverse assemblage is indicative of tropical-marine conditions. Bedding is thinly cross laminated or very thinly cross bedded, and in many cases grades into thick, heavily bioturbated beds. The cross-laminated and cross-bedded oolite was generated in active shoals and the bioturbated oolite deposited in stabilized shoals. *Ophiomorpha* dominates the trace-fossil assemblage in this environment with minor *Conichnus* and *Planolites*. This trace-fossil assemblage characterizes an *Ophiomorpha*-dominated *Skolithos* Ichnofacies (Cunningham and others, 2012). The oolite of the stabilized shoal typically has a maximum ichnofabric index value of 5 (Droser and Bottjer, 1986).

Inner-shelf peloidal lagoon—The inner-shelf peloidal lagoon is characterized by the peloid packstone and grainstone lithofacies, which is found mainly in the upper part of the Miami Limestone (HFS 5e) and uncommonly in the lower part of the Miami Limestone (HFS 4). Within the upper part

of the Miami Limestone, the peloidal lagoon was protected by the middle-shelf ooid-shoal complex to the east. Peloids are the main grain type. Subordinate grain types are bivalves, *Halimeda*, *Schizoporella*, miliolids, gastropods, archaiasinids, and ostracods. Thick beds that are riddled with the trace fossil *Ophiomorpha* characterize this depositional environment. The *Ophiomorpha* produce a maximum ichnofabric index value of 5 (Droser and Bottjer, 1986), indicating an *Ophiomorpha*-dominated *Skolithos* Ichnofacies.

Subaerial exposure—The subaerial exposure environment is represented by the pedogenic limestone lithofacies, which in most cases in the SCWF and SWWF study area is represented by laminated calcrete. In some cases, pedotubule calcrete (Wright and Tucker, 1991) can extend as much as 3 ft downward from an upper bounding surface of a cycle. Uncommonly, the calcretes are associated with an autobreccia that developed during soil-forming processes.

Hydrogeologic Framework of the Biscayne Aquifer in Central Miami-Dade County

In the study area, the Biscayne aquifer consists almost entirely of the lithostratigraphic units of the Fort Thompson Formation and Miami Limestone; however, up to several feet of the Pinecrest Sand Member of the Tamiami Formation is part of the Biscayne aquifer in most of the coreholes (plate 2). Thus, although the lower boundary of the Biscayne aquifer is commonly within the upper part of the Pinecrest Member of the Tamiami Formation, in some instances the base of the aquifer is at or above the base of the Fort Thompson Formation (plate 2). This finding is also true for the Lake Belt area (Cunningham and others, 2004b, 2004c, 2006a, 2006b; Renken and others, 2005). Below the Biscayne aquifer is a semiconfining unit recognized by Fish and Stewart (1991) as an upper clastic unit of the Tamiami Formation that is identified herein as the Pinecrest Sand Member of the Tamiami Formation (fig. 2). The identification is based on a comparative stratigraphic position at the top of the Tamiami Formation and lithology (a sand and shell unit) that Missimer (1992) reported as the Pinecrest Sand Member of the Tamiami Formation in southern Florida.

Hydraulic properties of the formations penetrated by the coreholes and monitoring wells at the Snapper Creek Well Field (SCWF) were determined from analysis of borehole geophysical data, examination of the collected core, and results of single-well slug tests. Stratiform flow zones in the Biscayne aquifer identified in each test corehole show that within the study area, the aquifer can be divided into three major hydrogeologic units: (1) a highly transmissive upper flow unit (upper Biscayne aquifer flow unit) that commonly includes most of the depositional sequence designated HFS 4 and the entire thickness of the sequence HFS 5e; (2) a semiconfining unit (middle semiconfining unit) with thin discontinuous stratiform groundwater flow zones that includes the lower or middle part of HFS 2, the entire HFS 3, and the lower part of or the entire HFS 4; and (3) a high-transmissivity flow unit in the lower part of the aquifer (lower Biscayne aquifer flow unit) with multiple stratiform groundwater flow zones in the uppermost Tamiami Formation to middle to lower part of HFS 2. Hydraulic characteristics were correlated with the cyclostratigraphic-based geologic framework (plate 2), which provided a template for the hydrogeologic framework (plate 3).

The Biscayne aquifer within the SCWF is also highly heterogeneous and anisotropic, and low permeability units within the well field have dissolution channels that connect flow zones above and below low permeability units. Borehole fluid temperature data (apps. 4–2 and 5) collected from the EM flowmeter during cross-hole tests in coreholes adjacent to the C–2 canal may also be important for showing that warm canal water may be recharging the aquifer within the well field.

Natural gamma data are often used for stratigraphic correlation, but gamma data from coreholes within the study area exhibit low gamma ray activity (plate 2), which is a typical response for the limestone, arenaceous limestone, quartz sandstone, and quartz sands that are the main lithologies at the SCWF (Keys and MacCary, 1971). However, some general trends in gamma activity were noted and used to confirm cyclostratigraphic and lithostratigraphic correlations. The response of the gamma log from the base of the limestone in the Pinecrest Member of the Tamiami Formation to within HFC 2h is higher than the response from within HFC 2h to the top of HFS 5e, (plates 2 and 3; app. 4–2). Below the base of the limestone in the Pinecrest Member of the Tamiami Formation, within the quartz sand and sandstone that dominate the lithology of the Pinecrest Member of the Tamiami Formation of the lower semiconfining unit, the gamma response is higher owing to the higher concentrations of phosphorite grains relative to those in the Fort Thompson Formation and Miami Limestone.

Flows zones within the study area are typically stratiform and generally correlatable between coreholes. Borehole image, flowmeter, and fluid data for all coreholes show that the Biscayne aquifer within the study area is composed of two major flow units separated by a semiconfining unit. Borehole geophysical data, mainly flowmeter data, were then used to support the ranking of each flow zone within a flow unit as major or minor with the exception of the upper Biscayne aquifer flow unit. Flow zones below the uppermost flow unit were ranked as major if flow increased across the zone and was greater than 25 percent of the total flow measured from just below the upper Biscayne aquifer flow unit. Most of the major flow zones also show some change in fluid properties including temperature, conductivity, or dissolved-oxygen concentration across the zone's depth interval, whereas minor flow zones commonly do not show any change across the flow zone. Borehole image data were used as a reference to fix the upper and lower bounding depth below land surface for each lithofacies, flow zone, and the base of the Biscayne aquifer within each corehole. Flow-zone intervals, ranking of major and minor flow zones, identification of flow-zone lithofacies and pore type, and supporting data used for each corehole at SCWF are presented in table 5.

Table 5. Flow zone information for coreholes in the Snapper Creek Well Field.

[ID, identification; BLS, below land surface; BTM, bottom; ft, feet; HU, hydrologic unit within the Biscayne aquifer; HFS, High-frequency sequence; HFC, High-frequency cycle; OBI, optical borehole image; ABI, acoustic borehole image; AMB, ambient borehole flow in test corehole; PMP, pumping from test corehole; FM, flowmeter; %, percent; X-hole, cross-hole flowmeter tests; UFU, upper Biscayne aquifer flow unit; MSU, middle semiconfining unit; LFU, lower Biscayne aquifer flow unit; TAM, Tamiami Formation; T, fluid temperature; C, fluid conductivity; WQT, water-quality tool; O, percent oxygen in fluid; R, fluid resistivity; N/A, not applicable;]

Well ID	Flow zone (BLS)		Base of Biscayne aquifer (BLS in ft)	HU	Major flow zone	Minor flow zone	Dominant lithology	HFS or HFC	Evidence for flow zone										Dominant porosity and permeability network types
	Top	BTM							OBI	ABI	AMB fluid	PMP fluid	AMB FM	PMP FM	% Change in vertical PMP flow below UFU	X-Hole FM data	Sonic porosity	Stoneley amplitude	
G–3877	4.70	17.65	91.65	UFU	X		Peloid packstone/ grainstone	4b/5	X	X	X	X	X	(a)	N/A		X		*Ophiomorpha* and thalassinidean and (or) thalassinidean-like crustacean megaporous macro-ichnofabric and irregular vugs
	33.00	34.00		MSU		X	Gastropod floatstone/ rudstone	3a		X			X	X	9		X		Fossil (gastropods and pelecypods) moldic, small irregular vugs
	35.90	37.12		MSU		X	Gastropod floatstone/ rudstone	3a	X	X			X	X	5		X	X	Fossil (gastropods and pelecypods) moldic, small irregular vugs
	45.20	47.40		MSU		X	Pelecypod floatstone/ rudstone and no recovery	2h0	X	X		T	X	X	6		X	X	Fossil moldic, bedding plane vug, small irregular vugs
	50.20	62.40		LFU		X	Pelecypod floatstone/rudstone, Arenaceous skeletal wackestone/ packstone, skeletal quartz sandstone, and no recovery	2f2/2g2	X	X			X	X	13		X	X	50.20–59.80 Fossil moldic and irregular vugs, 59.80–62.40 irregular vugs
	69.60	75.60		LFU	X		Skeletal packstone/ grainstone and no recovery	2e2			T, C	C	X	X	54		X	X	Thalassinidean and (or) thalassinidean-like crustacean megaporous macro-ichnofabric
	89.90	91.65		LFU		X	Skeletal wackestone/ packstone and skeletal quartz sandstone	TAM/2d2	X	X	T, C	C	X	X	5		X	X	Thalassinidean and (or) thalassinidean-like crustacean megaporous macro-ichnofabric

Table 5. Flow zone information for coreholes in the Snapper Creek Well Field.—Continued

[ID, identification; BLS, below land surface; BTM, bottom; ft, feet; HU, hydrologic unit within the Biscayne aquifer; HFS, High-frequency sequence; HFC, High-frequency cycle; OBI, optical borehole image; ABI, acoustic borehole image; AMB, ambient borehole flow in test corehole; PMP, pumping from test corehole; FM, flowmeter; %, percent; X-hole, cross-hole flowmeter tests; UFU, upper Biscayne aquifer flow unit; MSU, middle semiconfining unit; LFU, lower Biscayne aquifer flow unit; TAM, Tamiami Formation; T, fluid temperature; C, fluid conductivity; WQT, water-quality tool; O, percent oxygen in fluid; R, fluid resistivity; N/A, not applicable;]

Well ID	Flow zone (BLS)		Base of Biscayne aquifer (BLS in ft)	HU	Major flow zone	Minor flow zone	Dominant lithology	HFS or HFC	Evidence for flow zone										Dominant porosity and permeability network types
	Top	BTM							OBI	ABI	AMB fluid	PMP fluid	AMB FM	PMP FM	% Change in vertical PMP flow below UFU	X-Hole FM data	Sonic porosity	Stoneley amplitude	
G–3878	3.50	16.17	86.40	UFU	X		Peloid packstone/grainstone, peloid wackestone/packstone, and no recovery	4b/5	X	X	T, C		X	(a)	N/A		X	X	*Ophiomorpha* megaporous macro-ichnofabric and irregular vugs
	20.80	22.80		MSU		X	Arenaceous skeletal packstone/grainstone	3a	X	X				X	9			X	Fossil moldic, interparticle, bedding plane vug, small irregular vugs
	31.00	33.03		MSU		X	Arenaceous touching-vug, gastropod floatstone/rudstone, and no recovery	3a	X	X		T	X	X	8		X	X	31.00–31.30 Fossil (pelecypods) moldic, 31.30–33.03 fossil (Turritella gastropods) moldic and irregular vugs
	40.00	41.70		MSU		X	Arenaceous skeletal wackestone/packstone	2h1-2	X	X				X	9			(b)	Irregular vugs
	50.52	51.78		LFU		X	Skeletal quartz sandstone?	2g2	X	X				X	8		X	(b)	Uncertain, but possibly intergranular
	63.68	72.17		LFU		X	Arenaceous pelecypod floatstone/rudstone, arenaceous and skeletal wackestone/packstone, and no recovery	2e2/2f1	X	X			X	X	11	X	X	X	63.68–64.42 Fossil (pelecypods) moldic, 64.42–65.00 irregular vugs, 65.00–72.17 thalassinidean and (or) thalassinidean-like crustacean megaporous macro-ichnofabric and fossil (pelecypods) moldic, uncertain
	74.13	78.87		LFU	X		Coral boundstone and arenaceous skeletal packstone/grainstone	2d2/2e2	X	X	T, C	T, R		X	51	X	X	X	74.13–78.87 Fossil (*Montastrea* coral) moldic and irregular vugs
	80.60	86.40		LFU		X	Arenaceous skeletal packstone/grainstone	2d2	X	X	T, C	T, R		X	<5	X	X	X	Thalassinidean or thalassinidean-like crustacean megaporous macro-ichnofabric and irregular vugs

Table 5. Flow zone information for coreholes in the Snapper Creek Well Field.—Continued

[ID, identification; BLS, below land surface; BTM, bottom; ft, feet; HU, hydrologic unit within the Biscayne aquifer; HFS, High-frequency sequence; HFC, High-frequency cycle; OBI, optical borehole image; ABI, acoustic borehole image; AMB, ambient borehole flow in test corehole; PMP, pumping from test corehole; FM, flowmeter; %, percent; X-hole, cross-hole flowmeter tests; UFU, upper Biscayne aquifer flow unit; MSU, middle semiconfining unit; LFU, lower Biscayne aquifer flow unit; TAM, Tamiami Formation; T, fluid temperature; C, fluid conductivity; WQT, water-quality tool; O, percent oxygen in fluid; R, fluid resistivity; N/A, not applicable;]

Well ID	Flow zone (BLS)		Base of Biscayne aquifer (BLS in ft)	HU	Major flow zone	Minor flow zone	Dominant lithology	HFS or HFC	Evidence for flow zone										Dominant porosity and permeability network types
	Top	BTM							OBI	ABI	AMB fluid	PMP fluid	AMB FM	PMP FM	% Change in vertical PMP flow below UFU	X-Hole FM data	Sonic porosity	Stoneley amplitude	
G–3879	2.50	15.85	85.60	UFU	X		Peloid packstone/ grainstone and no recovery	4b/5	X	X	WQT-T, C, O	T, R		(a)	N/A			(b)	*Ophiomorpha* megaporous macro-ichnofabric and vertical solution pipe
	22.30	25.10		MSU		X	Arenaceous pelecypod floatstone/ rudstone	3a2	X	X	C		X	X	8			(b)	Irregular vugs and fossil (pelecypods) moldic
	29.80	32.90		MSU		X	Arenaceous pelecypod floatstone/ rudstone	3a1	X	X	WQT-T,O		X	X	7		X	(b)	Fossil moldic
	40.20	41.50		MSU		X	Skeletal quartz sandstone	2h1-2	X	X				X	9		X	(b)	Irregular vugs and fossil (pelecypods) moldic
	46.41	47.40		MSU		X	Skeletal wackestone packstone and mudstone/wackestone	2g2b	X	X			X		4		X	(b)	46.41–47.10 Thalassinidean or thalassinidean-like crustacean megaporous macro-ichnofabric and fossil (pelecypods) moldic, 47.10–47.40 irregular vugs
	49.90	56.10		LFU		X	No recovery, skeletal quartz sandstone, and quartz sandstone	2f2/2g2a	X	X	WQT-T, C		X	X	1	X	X	(b)	49.90–51.41 Uncertain, 51.41–53.60 irregular vugs, 53.60–56.10 uncertain
	63.60	74.12		LFU	X		Arenaceous pelecypod floatstone/ rudstone, Skeletal packstone/grainstone. Coral boundstone, skeletal wackestone/ packstone, and no recovery	2e2/2f1	X	X	T, C	T, R	X	X	39	X	X	(b)	63.60–64.40 Fossil (pelecypods) moldic, 64.40–64.90 small vertical solution pipes, 64.90–69.97 thalassinidean or thalassinidean-like crustacean megaporous macro-ichnofabric, 69.97–70.57 irregular vugs, 70.57–72.40 thalassinidean or thalassinidean-like crustacean megaporous macro-ichnofabric, 72.40–74.12 Fossil (coral) moldic and thalassinidean or thalassinidean-like crustacean megaporous macro-ichnofabric and irregular vugs
	84.84	85.60		LFU	X		Arenaceous pelecypod floatstone/ rudstone	TAM	X	X	C	T, R	X	X	35	X	X	(b)	Irregular vugs and fossil (pelecypods) moldic

Table 5. Flow zone information for coreholes in the Snapper Creek Well Field.—Continued

[ID, identification; BLS, below land surface; BTM, bottom; ft, feet; HU, hydrologic unit within the Biscayne aquifer; HFS, High-frequency sequence; HFC, High-frequency cycle; OBI, optical borehole image; ABI, acoustic borehole image; AMB, ambient borehole flow in test corehole; PMP, pumping from test corehole; FM, flowmeter; %, percent; X-hole, cross-hole flowmeter tests; UFU, upper Biscayne aquifer flow unit; MSU, middle semiconfining unit; LFU, lower Biscayne aquifer flow unit; TAM, Tamiami Formation; T, fluid temperature; C, fluid conductivity; WQT, water-quality tool; O, percent oxygen in fluid; R, fluid resistivity; N/A, not applicable;]

Well ID	Flow zone (BLS)		Base of Biscayne aquifer (BLS in ft)	HU	Major flow zone	Minor flow zone	Dominant lithology	HFS or HFC	Evidence for flow zone										Dominant porosity and permeability network types
	Top	BTM							OBI	ABI	AMB fluid	PMP fluid	AMB FM	PMP FM	% Change in vertical PMP flow below UFU	X-Hole FM data	Sonic porosity	Stoneley amplitude	
G-3880	4.00	14.00	88.40	UFU	X		Peloid packstone/ grainstone, peloid wackestone/ packstone, and no recovery	4b/5	X	X	WQT-T, C		X	X	N/A		X	(b)	Ophiomorpha megaporous macro-ichnofabric and vertical solution pipe
	26.50	29.00		MSU		X	No recovery	3a	X	X	T, R	T	X	X	9		X	(b)	Uncertain
	42.20	45.64		MSU		X	Skeletal quartz sandstone, arenaceous skeletal packstone/ grainstone, and no recovery	2h0/2h1-2	X	X			X	X	19			X	42.20–44.00 Irregular vugs, 44.00–45.64 thalassinidean or thalassinidean-like crustacean megaporous macro-ichnofabric
	52.62	58.76		LFU		X	No recovery and skeletal quartz sandstone	2f2/2g2	X	X			X	X	9	Xz	X	X	52.62–53.60 Fossil (coral) moldic and irregular vugs, 53.60–55.00 irregular vugs, 55.00–58.76 thalassinidean or thalassinidean-like crustacean megaporous macro-ichnofabric and irregular vugs
	65.50	79.00		LFU		X	No recovery, arenaceous and pelecypod floatstone/ rudstone, and arenaceous and skeletal wackestone/ packstone	2d2/2e2/2f1	X	X	R	T, R		X	16	X	X	X	65.50–66.89 Irregular vugs, 66.98–67.31 small vertical solution pipes, 67.31–70.10 intergranular (quartz sand), 70.10–72.30 thalassinidean or thalassinidean-like crustacean megaporous macro-ichnofabric and irregular vugs, 72.30–73.05 intergranular (quartz sand), 73.05–79.00 thalassinidean or thalassinidean-like crustacean megaporous macro-ichnofabric and irregular vugs
	82.90	88.40		LFU	X		No recovery, arenaceous pelecypod floatstone/rudstone, and skeletal quartz sandstone	TAM/2d2	X	X	T, R	T, R	X	X	28	X	X	X	Thalassinidean or thalassinidean-like crustacean megaporous macro-ichnofabric

Table 5. Flow zone information for coreholes in the Snapper Creek Well Field.—Continued

[ID, identification; BLS, below land surface; BTM, bottom; ft, feet; HU, hydrologic unit within the Biscayne aquifer; HFS, High-frequency sequence; HFC, High-frequency cycle; OBI, optical borehole image; ABI, acoustic borehole image; AMB, ambient borehole flow in test corehole; PMP, pumping from test corehole; FM, flowmeter; %, percent; X-hole, cross-hole flowmeter tests; UFU, upper Biscayne aquifer flow unit; MSU, middle semiconfining unit; LFU, lower Biscayne aquifer flow unit; TAM, Tamiami Formation; T, fluid temperature; C, fluid conductivity; WQT, water-quality tool; O, percent oxygen in fluid; R, fluid resistivity; N/A, not applicable;]

Well ID	Flow zone (BLS)		Base of Biscayne aquifer (BLS in ft)	HU	Major flow zone	Minor flow zone	Dominant lithology	HFS or HFC	Evidence for flow zone										Dominant porosity and permeability network types
	Top	BTM							OBI	ABI	AMB fluid	PMP fluid	AMB FM	PMP FM	% Change in vertical PMP flow below UFU	X-Hole FM data	Sonic porosity	Stoneley amplitude	
G–3881	3.75	16.50	88.30	UFU	X		Arenaceous peloid wackestone/packstone and Peloid packstone/grainstone	7b/5	X	X	WQT-T, C, O		X	(a)	N/A		X	X	4.00–14.00 *Ophiomorpha* and Thalassinoides? megaporous macro-ichnofabric, and vertical solution pipe
	21.48	25.50		MSU		X	Arenaceous skeletal wackestone/packstone	3a	X	X	T, C		X	X	18		X		Thalassinidean or thalassinidean-like crustacean megaporous macro-ichnofabric and irregular vugs
	29.60	34.00		MSU		X	Arenaceous pelecypod floatstone/rudstone and no recovery	2h1-2 /3a	X	X	T, C WQT-C, O		X	X	18		X	X	Fossil moldic
	49.48	51.06		MSU		X	No recovery	2g2	X	X	T,C			X	8	X	X		Irregular vugs and uncertain origin of permeability
	55.15	56.95		LFU		X	Pelecypod floatstone/rudstone and no recovery	2f2	X	X					11		X	X	Fossil moldic
	64.60	72.61		LFU		X	Arenaceous and pelecypod packstone, skeletal packstone/grainstone and no recovery	2e2/2f1	X	X	WQT-T, O		X	X	10	X	X	X	Irregular vugs, fossil moldic, bedding plan vugs, and thalassinidean or thalassinidean-like crustacean megaporous macro-ichnofabric
	82.65	88.30		LFU	X		Pelecypod floatstone/ rudstone, Arenaceous skeletal wackestone/packstone, and no recovery	TAM/ 2d2	X	X	WQT-T, O	T, R	X	X	26	X	X	X	Fossil moldic and thalassinidean or thalassinidean-like crustacean megaporous macro-ichnofabric

Table 5. Flow zone information for coreholes in the Snapper Creek Well Field.—Continued

[ID, identification; BLS, below land surface; BTM, bottom; ft, feet; HU, hydrologic unit within the Biscayne aquifer; HFS, High-frequency sequence; HFC, High-frequency cycle; OBI, optical borehole image; ABI, acoustic borehole image; AMB, ambient borehole flow in test corehole; PMP, pumping from test corehole; FM, flowmeter; %, percent; X-hole, cross-hole flowmeter tests; UFU, upper Biscayne aquifer flow unit; MSU, middle semiconfining unit; LFU, lower Biscayne aquifer flow unit; TAM, Tamiami Formation; T, fluid temperature; C, fluid conductivity; WQT, water-quality tool; O, percent oxygen in fluid; R, fluid resistivity; N/A, not applicable;]

Well ID	Flow zone (BLS)		Base of Biscayne aquifer (BLS in ft)	HU	Major flow zone	Minor flow zone	Dominant lithology	HFS or HFC	Evidence for flow zone										Dominant porosity and permeability network types
	Top	BTM							OBI	ABI	AMB fluid	PMP fluid	AMB FM	PMP FM	% Change in vertical PMP flow below UFU	X-Hole FM data	Sonic porosity	Stoneley amplitude	
G–3882	2.75	19.50	85.00	UFU	X		Ooid grainstone/ packstone and arenaceous skeletal packstone/ grainstone	5	X	X		T, R	X	X	N/A	X	X	X	6.90–19.50 *Ophiomorpha* megaporous macro-ichnofabric and vertical solution pipe (approximate length of solution pipe from 13 to 19.50 feet)
	38.21	39.82		MSU		X	No recovery	2h1-2	X	X		T, R		X	18	X	X	X	38.21–39.82 Probably thalassinidean or thalassinidean-like crustacean megaporous macro-ichnofabric
	45.02	47.50		MSU		X	Arenaceous skeletal packstone/grainstone and no recovery	2g2		X				X	14	X			45.02–47.50 Fossil moldic and irregular vugs
	61.75	66.00		LFU		X	Arenaceous and pelecypod floatstone/ rudstone and no recovery	2e2/2f1	X	X				X	3	X	X	X	Irregular vugs and fossil moldic
	71.00	72.40		LFU	X		No recovery	2d2	X	X			X	X	26	X	X	X	Irregular vugs and thalassinidean or thalassinidean-like crustacean megaporous macro-ichnofabric
	82.27	83.00		LFU		X	No recovery	2d2	X	X	T, C, R	T, R	X		10	X	X	X	Fossil moldic
	84.42	85.00		LFU		X	No recovery	TAM	X	X	T, C, R	T, R	X		3	X	X	X	Thalassinidean or thalassinidean-like crustacean megaporous macro-ichnofabric

(a) No flowmeter data due to pump suction in flow zone.

(b) Stoneley amplitude not determined due to low signal strength.

The flow zones were readily defined for the lower Biscayne aquifer flow unit (app. 4–2; plate 3), but the presence of laterally extensive flow zones in the upper Biscayne aquifer flow unit is uncertain as the flow unit is too close to the surface for the flowmeter to pass across the entire flow unit. Due to suction pipe placement within the corehole, flowmeter logging was stopped midway within the flow unit. Flowmeter tests of stressed steady-state conditions (while pumping from a production well; table 2, phase 1) and unstressed ambient conditions (with no pumping from any well in the well field; table 2, phase 2 test type 1) showed that the upper Biscayne aquifer flow unit was a major interval of either inflow or outflow (app. 4–2) depending on the head difference between the lower and upper Biscayne aquifer flow units. During stressed steady-state conditions while pumping from the corehole (table 2, phase 2 test type 2), the amount of flow originating from the upper Biscayne aquifer flow unit was similar to that originating from the lower Biscayne aquifer flow unit, and it could not be determined which unit was more transmissive.

After a 16-hour period without production well pumping to allow the well field to return to ambient conditions, production wells were pumped to test flow in the coreholes (cross-hole flowmeter testing; table 2, phase 2 test type 3). Most of the downward flow measured during the tests when pumping from a SCWF production well originated from the interval above the uppermost test depth to the surface except in test corehole G–3882 (table 3; plate 1). There are only minor flow zones for the interval between the base of the uppermost Biscayne aquifer flow unit and the upper test depth in the middle semiconfining unit (table 6). Thus most of the inflow to the borehole during production well pumping likely originates from the upper flow unit. Slug-test results of the upper Biscayne aquifer flow unit in coreholes G–3881 and G–3882 (table 3; app. 5) show this flow unit to have the highest transmissivity. Within HFS 4 and 5e of the Miami Limestone, vertical solution pipes contribute to the megapore system of the upper Biscayne aquifer flow unit, making identification of individual flow zones within the flow unit difficult. Accordingly, the upper Biscayne aquifer flow unit is considered as one continuous unit, although it may be composed of several flow zones.

Minor flow zones are present as thin, discontinuous, and stratiform flow zones in the middle semiconfining unit, which comprises the upper part of HFS 2 and HFS 3 of the Fort Thompson Formation. Slug tests (table 3) indicate that transmissivities of the minor flow zones are less than transmissivities of the major flow zones within the lower Biscayne aquifer flow unit. Minor flow units within the lower Biscayne aquifer flow unit and the middle semiconfining unit commonly show no change in fluid properties and little change in vertical borehole flow across the flow zone (table 5; app. 4–2).

The base of the Biscayne aquifer in the study area is defined as the base of the lowest flow zone, which in most cases is the base of a flow zone in the lower part of HFS 2. In some instances the aquifer base is a flow zone within the uppermost limestone part of the Pinecrest Sand Member of the Tamiami Formation and the lowermost Fort Thompson

Table 6. Geometric means for horizontal hydraulic conductivity and transmissivity from slug tests of monitoring-well completion zones entirely within designated flow units, aquifer matrix, or semiconfining units.

(ft/d, feet per day; ft^2/d, feet squared per day; n, number of slug-test values; <, values are less than)

Hydrologic unit	Hydraulic conductivity (ft/d)	n	Transmissivity (ft^2/d)
Upper Biscayne aquifer flow unit	8,200	2	87,000
Minor flow zone in middle semiconfining unit	2,600	4	19,000
Matrix (pore class II) of middle semiconfining unit	40	1	70
Major flow zone in lower Biscayne aquifer flow unit	5,900	4	44,000
Minor flow zone in lower Biscayne aquifer flow unit	2,900	4	33,000
Lower semiconfining unit	< 350	3	< 3300

Formation (app. 4–2; plate 3). Borehole fluid properties also help define the base of the Biscayne aquifer as below the base of the lower Biscayne aquifer flow unit. In the lower semiconfining unit of the Tamiami Formation (plate 3), there is no inflow or outflow of groundwater, so little mixing by vertical flow occurs within the borehole. Few changes in fluid temperature and specific conductance values were recorded under both unstressed ambient and stressed steady-state conditions in the interval of the lower semiconfining unit with no vertical fluid flow from below the base of the aquifer to total depth of the borehole.

Borehole image data show examples of several foot-scale vertical solution pipes and thick (up to about 20 ft) zones containing substantial volumes of megaporosity, suggesting it may be possible for groundwater to flow upward or downward as conduit flow (U.S. Environmental Protection Agency, 2002) through a complex arrangement of megaporosity between the three flow units and multiple flow zones identified in the Biscayne aquifer (plate 3). However, no single vertical passageway or maze of connected megaporosity from the top of the upper flow unit to the lower flow unit has been identified in the study area. At the G–3889 test corehole, located about 4 miles south of the study area (fig. 1), however, an assemblage of vertical solution pipes and areas of well-connected touching-vug megaporosity form a 35-ft vertical flow passageway (fig. 8*A*). The vertical passageway crosses several horizontal flow zones present in rocks equivalent to the upper flow unit and uppermost part of the middle semiconfining unit in the study area.

No vertical passageways with as much vertical connectivity as corehole G–3889 have been observed in Miami-Dade County, but 4 of the 11 test coreholes (G–3879, G–3880, G–3881, and G–3882) in the study area did have vertical solution pipes that cut across HFS 4 and 5e of the Miami Limestone with vertical extents up to 11 ft (fig. 8*B*). Additionally, an interval containing touching-vug megaporosity with a vertical connectivity of about 6 ft, was observed cutting across HFCs within HFS 2 of the Fort Thompson Formation (fig. 8*C*) in corehole G–3884. Other notable examples of vertical connectivity are found in HFS 3 of G–3884 and HFS 3 and 5e in G–3840 (plates 2 and 3). The identification of various types of vertical flow passageways in SCWF borehole image data suggests conduit flow between the upper flow unit and lower flow unit is possible, but this hypothesis has not been fully explored. The middle semiconfining unit between the upper Biscayne aquifer flow unit and the lower Biscayne aquifer flow unit may act to reduce the connectedness between well-field pumping and the C–2 canal.

Additional information as to the degree of confinement provided by the semiconfining unit comes from modeling of cross-hole flowmeter data. The change in flow measured between the lower and upper Biscayne aquifer flow units was simulated with the Paillet (1998) cross-borehole model as a two aquifer-zone system, with the six coreholes at SCWF open to both Biscayne aquifer flow units and the production wells pumping from the lower Biscayne aquifer unit. The lower Biscayne aquifer flow unit was simulated as connected between the corehole and production well and isolated from the upper Biscayne aquifer. The measured and simulated change in flow for corehole G–3881 is shown in figure 9. Initially the isolated (zero leakage) model provides a reasonable match between the measured and simulated response; however, the simulated and measured responses quickly diverge, suggesting that the upper and lower Biscayne aquifer flow units do not act as isolated zones and that leakage stabilizes the head difference and flow. Application of the cross-borehole model with leakage (Paillet, 2011) allows simulation of leakage between the upper and lower Biscayne aquifer flow units. The leaky two-aquifer model with a head decay time of 10 or 20 minutes (0.1 or 0.05 minutes^{-1}) provides a better match between the simulated and measured flow response than that of the isolated model (fig. 9). The inability of the model to accurately match the measured response indicates that a uniform leakage rate is not representative of the leaky interval between the upper and lower Biscayne aquifer flow units and that spatial variability of the rate of leakage exists.

Hydraulic Properties of the Biscayne Aquifer

Hydraulic properties of the Biscayne aquifer—porosity, permeability, transmissivity, and connectivity—were estimated from visual analysis and examination of thin sections of recovered core (apps. 1 and 2), and analysis of borehole geophysical data, mainly OBI and flowmeter data (app. 4–2). In addition, values for hydraulic conductivity and transmissivity were computed from the results of single-well slug tests (table 3). These hydraulic properties are summarized below, and descriptions of the results of the steady-state and transient flowmeter data analyses for each test corehole at SCWF are presented in appendix 5.

Porosity and Permeability

Sonic-porosity values for the Biscayne aquifer in coreholes outside of the study area were calculated from compressional-wave velocities by using the Raymer-Hunt equation (equation 1) (Raymer and others, 1980), and show a slight (r^2=0.271) trend with laboratory-measured whole-core porosity values of core taken from the same coreholes (fig. 10). Laboratory measurements of porosity of the SCWF core were not made. Sonic-porosity values for coreholes in the SCWF calculated using the Raymer-Hunt equation ranged between 17 and 81 percent. In general, where sonic-porosity data are correlated with borehole image data, higher values of porosity correspond to vertical intervals with vuggy megaporosity, and lower values of porosity correspond to vertical intervals dominated by matrix porosity (app. 4–2). Intervals of high porosity also correspond with the flow zones identified within the limestone strata of the Biscayne aquifer and the quartz sand, sandstone, and vuggy limestone of the Pinecrest

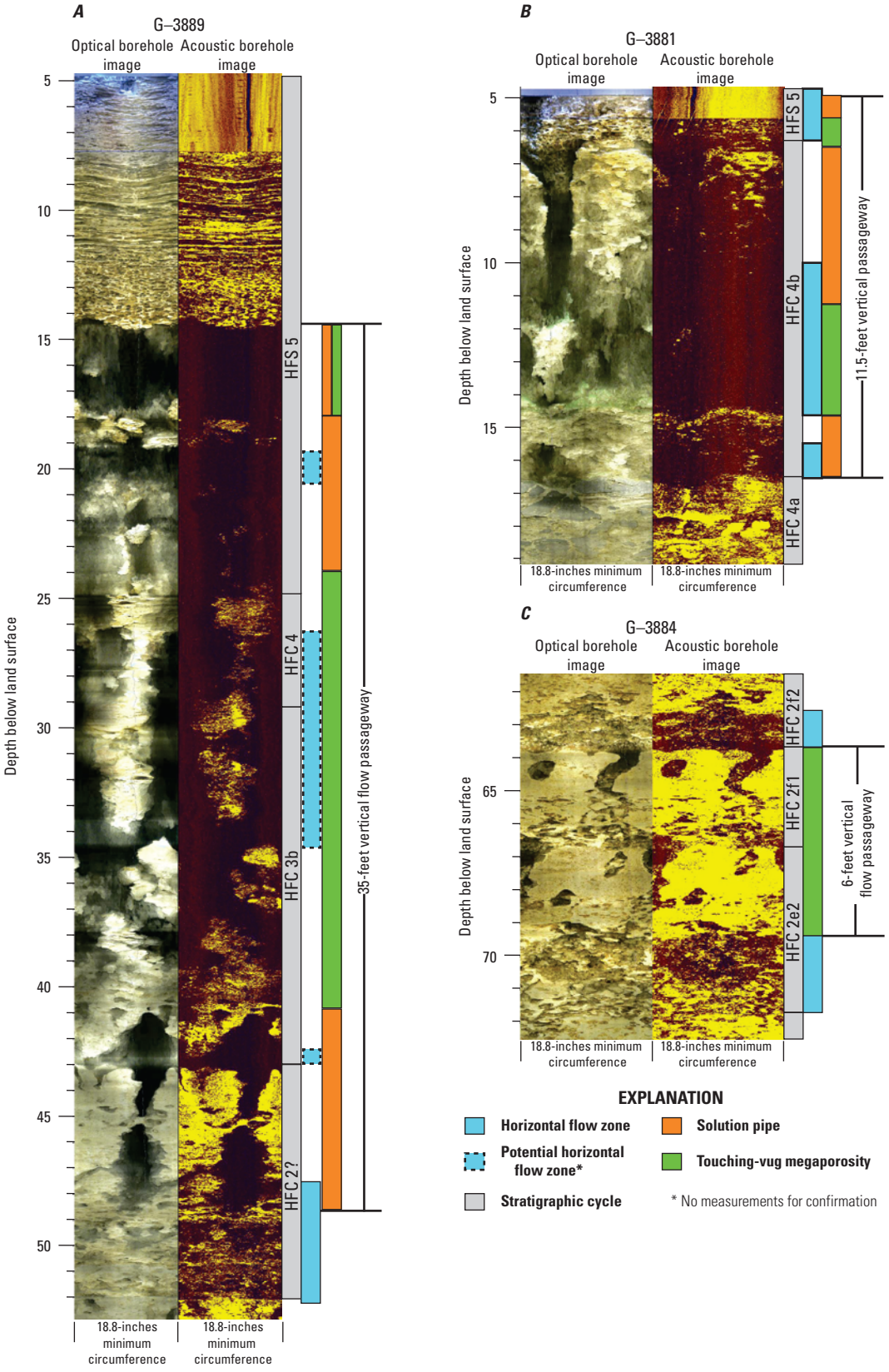

Figure 8. Examples of vertical connectivity through an assemblage of vertical solution pipes and touching-vug megaporosity found in three coreholes (*A*) borehole image of test corehole G-3889, (*B*) borehole image of test corehole G-3881, and (*C*) borehole image of test corehole G-3884.

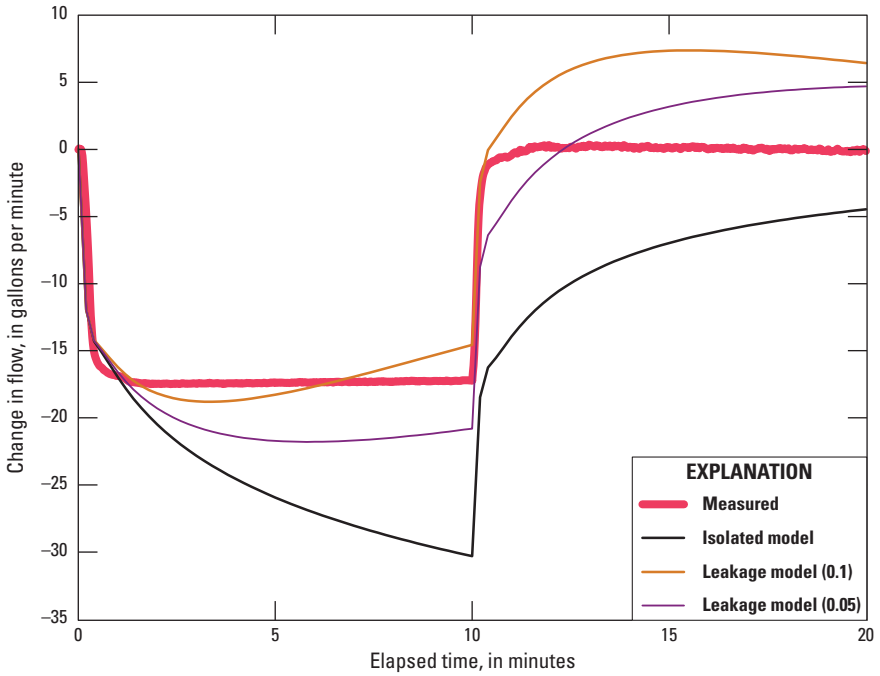

Figure 9. Simulated and measured transient change in flow at the 62-foot depth in corehole G–3881 in response to pumping and recovery in production well S–3014; the leakage model parameter given in parentheses is the inverse of the time in minutes for a head difference between aquifer units to decay to one-third of its initial value (Paillet, 2011).

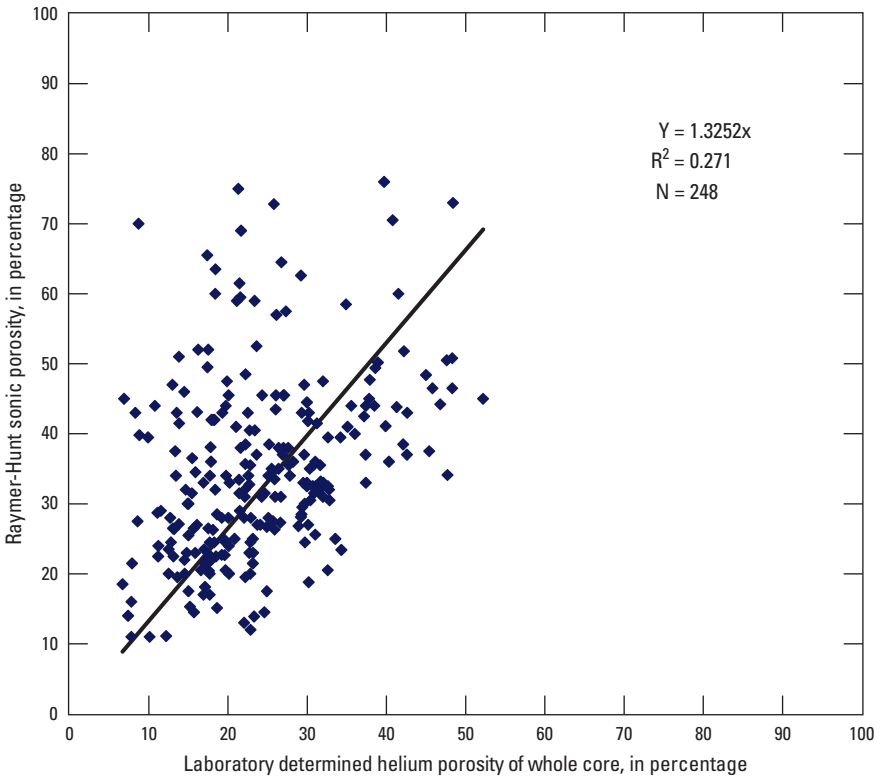

Figure 10. Laboratory-determined values of helium porosity from core collected from coreholes in the Lake Belt area of Miami-Dade County versus Raymer-Hunt equation sonic-porosity values determined using compressional-wave velocities from full waveform sonic data.

Member of the Tamiami Formation. In a cross section of the sonic-porosity values derived from the six coreholes at SCWF, the greatest composite thickness of high values of sonic porosity is beneath the general area of the C–2 canal (fig. 5).

Permeability of flow zones in a corehole was determined mainly by examination of flowmeter and borehole fluid data, and by analysis of Stoneley and ABI amplitude data (app. 4). Stoneley-wave sonic data were used to define the base of the Biscayne aquifer in coreholes (G–3877 and G–3880). Qualitative estimates of permeability are presented for coreholes at SCWF in appendix 1. Table 4 provides permeability values for each lithofacies based on air-permeameter measurements of Lake-Belt area samples (Cunningham and others, 2006b).

Pore System of the Limestone of the Biscayne Aquifer

Karst aquifers are commonly characterized by three types of porosity: interparticle matrix porosity, fracture porosity, and cavernous porosity (Martin and Screaton, 2001). This representation of carbonate karst porosity suggests a conceptualization of karst aquifers as two-component systems, in which most of the groundwater is stored in the matrix porosity or in fractures, or both, and groundwater flow and transport take place primarily in the large dissolutional conduits. Martin and Screaton's (2001) conceptualization includes both intergranular and fracture porosity within matrix porosity. In many areas of the young eogenetic karst of the Biscayne aquifer, a fourth type of porosity, touching-vug porosity, contributes substantially to focused conveyance of groundwater (Vacher and Mylroie, 2002; Cunningham and others, 2006b). The triple porosity of the Biscayne aquifer consists of (1) a matrix of interparticle and separate-vug porosity that provides considerable storage; (2) touching-vug porosity that forms stratiform groundwater flow passageways; and (3) conduit porosity composed mainly of bedding-plane vugs, vertical solution pipes, and cavernous vugs (Cunningham and others, 2006a, 2006b). Vertical solution pipes with diameters up to 1 ft are prominent in the Miami Limestone at the SCWF, both in the coreholes (plate 2) and in surface exposures.

Pore Classes and Groundwater Flow Types

The 18 lithofacies (table 4) of the uppermost Tamiami Formation, Fort Thompson Formation, and Miami Limestone have unique stratigraphic spatial distributions and distinct porosity, permeability, and storage characteristics. Each of the 18 lithofacies has been assigned to one of three pore classes (I, II, and III; table 4). Cunningham and others (2006a, 2006b) discuss how the three pore classes relate to three major types of groundwater flow: (I) concentrated flow in conditions of high-permeability, (II) diffuse flow in carbonate or mixed siliciclastic-carbonates with moderate permeability, and (III) leaky flow in conditions of low permeability (plate 3). These three pore classes conform to what was observed within the study area and link the hydrology of the study area to the previous studies.

Transmissivity and Connectivity

Application of the FLASH computer program (Day-Lewis and others, 2011) to the analysis of steady-state, single-hole flowmeter data under nonpumping and pumping conditions provided information on flow-zone transmissivity and hydraulic connectedness to production wells at the SCWF. The change in rate of steady-state flow in coreholes under unstressed ambient and stressed borehole conditions (app. 4–2) was used to compute the percentage contribution of flow zones to pumpage exclusive of the upper Biscayne aquifer flow unit in the Miami Limestone (fig. 11). Computed transmissivities from the slug-test results (app. 6; table 3) were included for comparison and generally support the transmissivities estimated using the FLASH program.

In all coreholes (apps. 4–2, 5, and 6), the upper and lower Biscayne aquifer flow units are highly transmissive and are the intervals for most of the groundwater flow. Minor flow zones within the middle semiconfining unit have lower transmissivity than the upper and lower flow units and contribute only minor flow to or from the borehole (app. 4–2). Borehole flowmeter and fluid data collected provided information on the connectivity of individual production wells and the C–2 canal to the coreholes at SCWF (app. 5).

Groundwater flow within the Biscayne aquifer at SCWF is highly heterogeneous and anisotropic, and in some cases low permeability units within the well field have dissolution channels that connect flow zones above and below them. Borehole fluid temperature data (apps. 4–2 and 5) collected using the EM flowmeter during cross-hole tests in coreholes adjacent to the C–2 canal may also be important for showing that warm canal water may be recharging the aquifer within the well field.

Slug Tests

Results for 60 slug tests performed at 19 monitoring-well locations within the SCWF indicate that horizontal hydraulic conductivity for each monitoring zone ranged from 40 to 9,900 feet per day (ft/d), with a median of 3,500 ft/d and a geometric mean of 4,000 ft/d (table 3). Computed transmissivity values from slug tests ranged from 70 to 100,000 ft^2/d, with a median of 36,000 ft^2/d and a mean of 35,000 ft^2/d. The geometric mean of horizontal hydraulic conductivity and transmissivity of flow units, aquifer matrix, or semiconfining units were also calculated from slug-test results for all monitoring-well completion zones that are entirely within the designated unit (table 6).

The uppermost Biscayne aquifer flow unit in HFS 4 and 5e is continuous and highly permeable across the SCWF, with a mean hydraulic conductivity of 8,200 ft/d and range of 6,600 to 9,900 ft/d (table 3). Minor flow zones in the middle semiconfining unit in the upper cycles of HFS 2 and HFS 3 are not continuous across the SCWF; these flow zones have a mean hydraulic conductivity of 2,600 ft/d, with a range of 660 to 6,400 ft/d. The lower Biscayne aquifer flow unit in the lower cycles of HFS 2 and the permeable limestone of the Pinecrest Member of the Tamiami Formation in the Biscayne aquifer was not tested as a flow unit, only individual

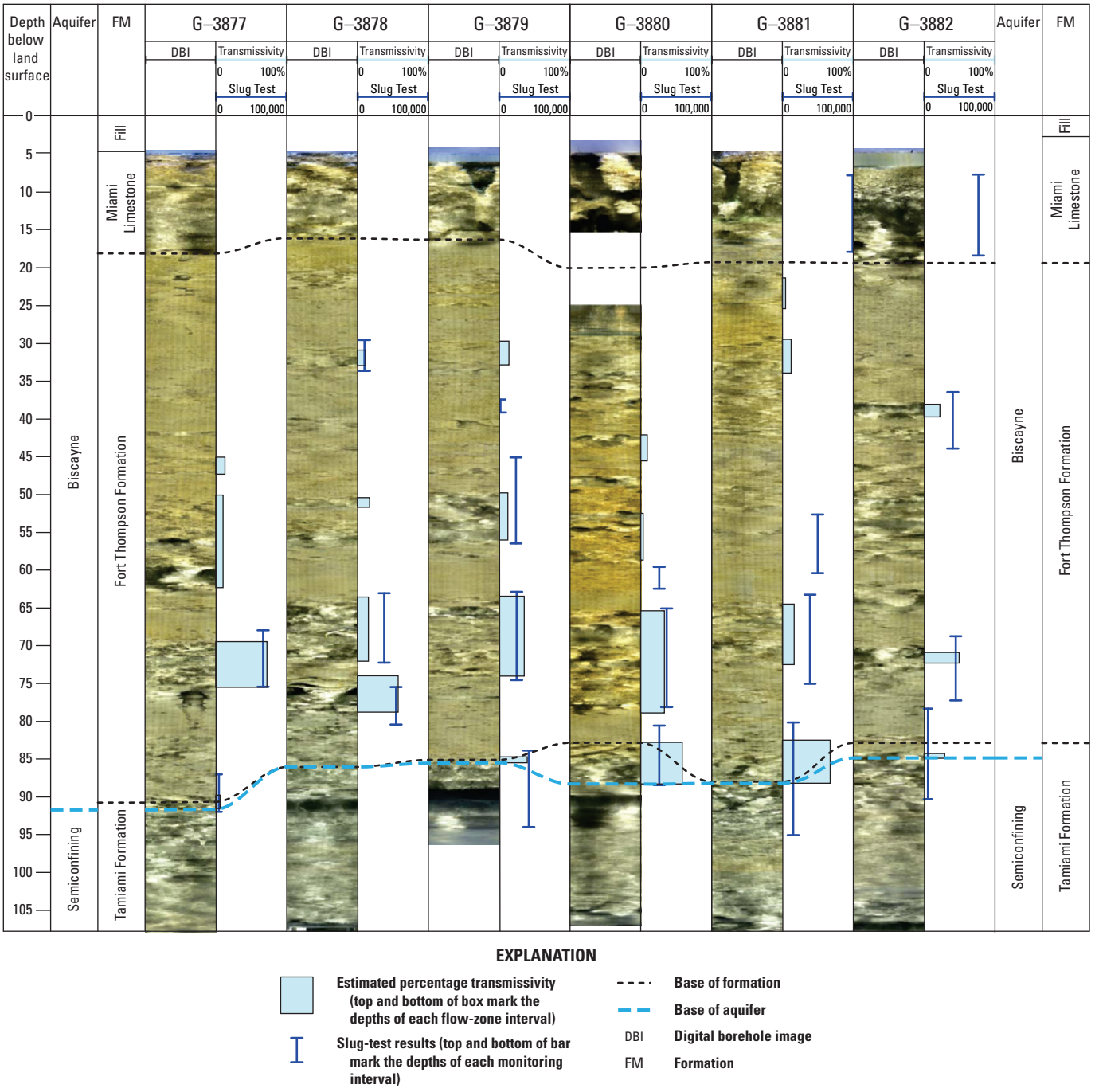

Figure 11. Estimated percentage transmissivity (blue boxes) calculated from flowmeter data for selected flow zones exclusive of the major flow unit within the Miami Limestone. Transmissivity values (in feet squared per day) calculated from slug-test results for open-hole and screened intervals in monitoring wells are shown by blue bars.

flow zones within the flow unit were tested. Flow zones that compose the lower flow unit within the lower cycles of HFS 2 are generally continuous across the SCWF. Major flow zones in the lower Biscayne aquifer flow unit had a mean hydraulic conductivity of 5,900 ft/d and a range of 3,500 to 8,900 ft/d. Minor flow zones had a mean hydraulic conductivity of 2,900 ft/d, and a range of 2,000 to 3,900 ft/d.

The only monitoring well open to a zone of matrix porosity material in the middle semiconfining unit had a hydraulic conductivity of 40 ft/d. No monitoring well screened interval was entirely within the lower semiconfining unit of the Tamiami Formation below the base of the Biscayne aquifer. Of the three monitoring wells completed mostly in the lower semiconfining unit, the lowest hydraulic conductivity was 100 ft/d, the highest was 1,000 ft/d, and a third well had a hydraulic conductivity of 400 ft/d. The three monitoring wells completed mostly in the lower semiconfining unit were found to have at least one flow zone in the final screened interval. The hydraulic

conductivity for the semiconfining unit, assuming no flow units, is defined as having below 100 ft/d (Fish and Stewart, 1991). The average value for all three wells was 500 ft/d.

Summary and Conclusions

To improve the understanding of the geologic and hydrogeologic frameworks of the Biscayne aquifer, enhance understanding of the interaction of surface water with groundwater near production well fields in central Miami-Dade County, and provide hydrogeologic properties of the aquifer for groundwater flow models, six test coreholes were drilled across the Snapper Creek Well Field. Each corehole was continuously cored through the Biscayne aquifer and into the lower semiconfining unit within the Tamiami Formation. Borehole geophysical and flowmeter data were collected in each corehole, the core was examined and described, and the cyclostratigraphy of the aquifer was determined. Additional monitoring wells were installed next to each of the original test coreholes and instrumented on the basis of a hydrogeologic framework developed for the study area. Monitoring well open intervals were completed in representative flow units, flow zones, matrix, and semiconfining units. Single-well aquifer slug tests were completed in the open intervals of each monitoring well to define the hydraulic properties of each interval. Data from other coreholes in the study area in central Miami-Dade County were then linked to the geologic and hydrogeologic frameworks developed by the U.S. Geological Survey for areas mostly to the west and northwest of the study area.

Lithostratigraphy, lithofacies, paleontology, ichnology, depositional environments, and cyclostratigraphy of the rocks and sediments penetrated by 11 coreholes were linked to geophysical interpretations and to the results of slug tests of the hydraulic properties of the materials in the six test coreholes at Snapper Creek Well Field, to construct geologic and hydrogeologic frameworks for the study area. These frameworks are consistent with those recently described for the Biscayne aquifer in the nearby Lake Belt area and link the Lake Belt area with the Snapper Creek Well Field. Three major pore types characterize the pore system of the hydrogeologic framework: (1) matrix porosity (mainly mesoporous interparticle porosity, moldic porosity, and megaporous separate vugs), which under dynamic conditions produces diffuse flow; (2) megaporous touching vug porosity that commonly forms stratiform groundwater passageways; and (3) conduit porosity, including bedding-plane vugs, up to decimeter-scale diameter vertical solution pipes, and meter-scale cavernous vugs. The various pore types and distribution of permeability generally fit into a predictable vertical succession within various cycle types that form a foundation for correlation among test coreholes in the study area.

The hydrogeologic framework shows that the Biscayne aquifer within the study area can be divided into two major flow units, one near the surface (upper Biscayne aquifer flow unit) and the other at the base of the Biscayne aquifer (lower Biscayne aquifer flow unit), of which both are continuous across the study area. These two major flow units are separated by a semiconfining unit that has relatively lower permeability compared to the two major flow units. This "middle semiconfining unit" contains some interbedded minor flow zones that are not continuous across the study area. In most cases, minor flow zones within the upper part of the middle semiconfining unit did not produce any substantial inflow to the corehole during flowmeter testing. The upper and lower Biscayne aquifer flow units consist of several vuggy flow zones and have a hydraulic conductivity that is up to two orders of magnitude higher than that of limestone with matrix porosity or of the middle semiconfining unit. Although the middle semiconfining unit has a relatively low horizontal permeability, it is possible the two major flow units are connected vertically by a network of vertical solution pipes and touching-vug megaporosity, and thus there may be substantial leakance between the major flow units; however, proof of this conceptualization has not been explored.

The upper flow unit is mainly within the Miami Limestone and is continuous throughout the study area. The lower flow unit, which is mainly within limestone of the uppermost part of the Pinecrest Sand Member of the Tamiami Formation and the lower half of the Fort Thompson Formation, forms the base of the Biscayne aquifer. The lower flow unit is continuous throughout the study area, and includes several minor flow zones and at least one major flow zone. The most productive zones of groundwater flow within the two Biscayne aquifer flow units have a characteristic pore system dominated by stratiform megaporosity related to selective dissolution of an *Ophiomorpha*-dominated ichnofabrics. The lower flow unit is the main production zone for the Snapper Creek Well Field production wells, but cross-hole flowmeter data indicate that the zone is not equally connected to each production well. Also, in some areas, flow zones that occur in the limestone of the uppermost Pinecrest Sand Member of the Tamiami Formation, especially in the test coreholes northeast of the C–2 canal, may be more permeable and better connected to production wells than flow zones entirely within the Fort Thompson Formation. Thus, indicating that the distribution of vuggy megaporosity, matrix porosity, and permeability within the Biscayne aquifer of the Snapper Creek Well Field is heterogeneous and anisotropic. Model simulations of flowmeter and water-level data showed that estimates of the transmissivity of the lower flow zones in the lower flow unit were greater in all of the coreholes than estimates for flow zones within the middle semiconfining unit.

Slug-test results indicate that the upper flow unit has a geometric mean hydraulic conductivity value of 8,200 feet per day (ft/d). Slug tests were not conducted in the entire middle semiconfining unit or lower flow unit. But flow zones within the middle semiconfining unit have a geometric mean hydraulic conductivity value of 2,600 ft/d, and a single test of aquifer matrix within this semiconfining unit had a hydraulic conductivity value of 40 ft/d. Major flow zones in the lower flow unit have a geometric mean hydraulic conductivity of 5,900 ft/d, and minor flow zones within the lower flow unit have a geometric mean hydraulic conductivity value of 2,900 ft/d. In the monitoring wells completed mostly in the lower semiconfining unit below the base of the Biscayne aquifer, the geometric mean hydraulic conductivity value was 350 ft/d.

References Cited

Bennett, G.D., Kontis, A.L., and Larson, S.P., 1982, Representation of multiaquifer well effects in three-dimensional ground-water flow simulation: Ground Water, v. 20, no. 3, p. 334–341.

Bouwer, Herman, and Rice, R.C., 1976, A slug test for determining hydraulic conductivity of unconfined aquifers with completely or partially penetrating wells: Water Resources Research, v. 12, no. 3, p. 423–428.

Brewster-Wingard, G.L., Ishman, S.E., Edwards, L.E., and Willard, D.A., 1997, Preliminary report on the distribution of modern fauna and flora at selected sites in north-central and north-eastern Florida Bay: U.S. Geological Survey Open-File Report 96–732, 34 p.

Bromley, R.G., 1996, Trace fossils—Biology, taphonomy and applications (2d ed.): London, Chapman and Hall, 361 p.

Brown and Caldwell Environmental Engineers and Consultants, 1998, Remedial action-plan—Old South Dade Landfill: Report prepared for Miami-Dade County Department of Solid Waste Management [variously paged].

Burchette, T.P., and Wright, V.P., 1992, Carbonate ramp depositional systems: Sedimentary Geology, v. 79, p. 3–57.

Burns, D.R., Cheng, C.H., Schmitt, D.P., and Toksöz, M.N., 1988, Permeability estimation from full waveform acoustic logging data: The Log Analyst, v. 29, no. 2, p. 112–122.

Catuneanu, O., 2006, Principles of sequence stratigraphy: Amsterdam, Elsevier, 375 p.

Chen, J.H., Curran, H.A., White, B., and Wasserburg, G.J., 1991, Precise chronology of the last interglacial period—^{234}U–^{230}UTh data from fossil coral reefs in the Bahamas: Geological Society of America Bulletin, v. 103, p. 82–97.

Choquette, P.W., and Pray, L.C., 1970, Geologic nomenclature and classification of porosity in sedimentary carbonates: American Association of Petroleum Geologists Bulletin, v. 54, p. 207–250.

Cunningham, K.J., 2004, Application of ground-penetrating radar, digital optical borehole images, and cores for characterization of porosity hydraulic conductivity and paleokarst in the Biscayne aquifer, southeastern Florida, U.S.A.: Journal of Applied Geophysics, v. 55, p. 61–76.

Cunningham, K.J., Carlson, J.L., and Hurley, N.F., 2004a, New method for quantification of vuggy porosity from digital optical borehole images as applied to the karstic Pleistocene limestone of the Biscayne aquifer, southeastern Florida: Journal of Applied Geophysics, v. 55, p. 77–90.

Cunningham, K.J., Carlson, J.L., Wingard, G.L., Robinson, Edward, and Wacker, M.A., 2004b, Characterization of aquifer heterogeneity using cyclostratigraphy and geophysical methods in the upper part of the karstic Biscayne aquifer, southeastern Florida: U.S. Geological Survey Water-Resources Investigations Report 03–4208, 66 p., 5 apps. (on CD), 5 pls.

Cunningham, K.J., Renken, R.A., Wacker, M.A., Zygnerski, M.R., Robinson, Edward, Shapiro, A.M., and Wingard, G.L., 2006a, Application of carbonate cyclostratigraphy and borehole geophysics to delineate porosity and preferential flow in the karst limestone of the Biscayne aquifer, SE Florida, *in* Harmon, R.S., and Wicks, C., eds., Perspectives on karst geomorphology, hydrology, and geochemistry—A tribute volume to Derek C. Ford and William B. White: Geological Society of America Special Paper 404, p. 191–208, doi: 10.1130/2006.2404(16).

Cunningham, K.J., and Sukop, M.C., 2011, Multiple technologies applied to characterization of the porosity and permeability of the Biscayne aquifer, Florida: U.S. Geological Survey Open-File Report 2011–1037, 8 p.

Cunningham, K.J., Sukop, M.C., and Curran, H.A., 2012, Chapter 28 - Carbonate aquifers, in Knaust, D. and Bromley, R.G., eds., Trace fossils as indicators of sedimentary environments—Developments in Sedimentology, v. 26: Elsevier, New York, p. 869–896.

Cunningham, K.J., Sukop, M.C., Huang, Haibo, Alvarez, P.F., Curran, H.A., Renken, R.A., and Dixon, J.F., 2009, Prominence of ichnologically influenced macroporosity in the karst Biscayne aquifer—Stratiform "super-K" zones: Geological Society of America Bulletin, v. 121, no. 1/2, p. 164–180.

Cunningham, K.J., Wacker, M.A., Robinson, Edward, Dixon, J.F., and Wingard, G.L., 2006b, A cyclostratigraphic and borehole-geophysical approach to development of a three-dimensional conceptual hydrogeologic model of the karstic Biscayne aquifer, southeastern Florida: U.S. Geological Survey Scientific Investigations Report 2005–5235, 69 p., plus CD.

Cunningham, K.J., Wacker, M.A., Robinson, Edward, Gefvert, C.J., and Krupa, S.L., 2004c, Hydrology and ground-water flow at Levee 31N, Miami-Dade County, Florida, July 2003 to May 2004: U.S. Geological Survey Scientific Investigations Map I–2846, 1 pl.

Day-Lewis, F.D., Johnson, C.D., Paillet, F.L., and Halford, K.J., 2011, A computer program for flow-log analysis of single holes (FLASH): Groundwater, v. 49, no. 6, p. 926–931, doi: 10.1111/j.1745–6584.2011.00798.x.

Debenay, J.P., Guillou, J.J., Redois, F., and Geslin, E., 2000, Distribution trends of foraminiferal assemblages in paralic environments—A base for using foraminifera as bioindicators, *in* Martin, R.E., ed., Environmental micropaleontology—The application of microfossils to environmental geology: Topics in Geobiology, v. 15, p. 39–67.

Droser, M.L., and Bottjer, D.J., 1986, A semiquantitative field classification of ichnofabric: Journal of Sedimentary Petrology, v. 56, p. 558–559.

Droser, M.L., and Bottjer, D.J., 1989, Ichnofabric of sandstones deposited in high-energy nearshore environments: Measurement and utilization: Palaios, v. 4, p. 598–604.

DuBar, J.R., 1962, Neogene biostratigraphy of the Charlotte Harbor area in southwestern Florida: Florida Geological Survey Bulletin 43, 83 p.

Embry, A.F., 1995, Sequence boundaries and sequence hierarchies—Problems and proposals, *in* Steel, R.J., Felt, V.L., Johannessen, E.P., and Mathieu, C., eds., Sequence stratigraphy on the Northwest European Margin: Norwegian Petroleum Society Special Publication 5, p. 1–11.

Enos, P., 1977, Holocene sediment accumulations of the South Florida shelf margin, *in* Enos, P., and Perkins, R.D., eds., Quaternary sedimentation in South Florida: Geological Society of America Memoir 147, p. 115.

Evans, C.C., 1984, Development of an ooid sand shoal complex—The importance of antecedent and syndepositional topography, *in* Harris, P.H., ed., Carbonate sands—A core workshop: Society of Economic Petrologists and Mineralogists Core Workshop 5, p. 392–428.

Federal Register Notice, October 11, 1979, v. 44, no. 198.

Fish, J.E., and Stewart, M., 1991, Hydrogeology of the surficial aquifer system, Dade County, Florida: U.S. Geologic Survey Water-Resources Investigations Report, 90–4108, 50 p.

Galli, Gianni, 1991, Mangrove-generated structures and depositional model of the Pleistocene Fort Thompson Formation (Florida Plateau): Facies, v. 25, p. 297–314.

Genereux, D.P., and Guardiario, J.D.A., 1998, A canal drawdown experiment for determination of aquifer parameters: Journal of Hydrologic Engineering, v. 3, no. 4, p. 294–302.

Geological Society of America, 1995, Rock color chart: Baltimore, Md., Munsell color.

Goodson, John, 2005, Stream gauging at the C–2 canal to investigate the influence of groundwater well pumping on the SW/GW interaction: West Palm Beach, Fla., SCADA and Hydro Management Department, South Florida Water Management District.

Guardiario, J.D.A., 1996, Determination of hydraulic conductivity and dispersivity in the Biscayne aquifer, Taylor Slough, Everglades National Park: Miami, Florida International University, M.S. Thesis, 195 p.

Halford, Keith, 2009, AnalyzeHOLE—An integrated wellbore flow analysis tool: U.S. Geological Survey Techniques and Methods 4–F2, 46 p.

Halford, K.J., and Kuniansky, E.L., 2002, Documentation of spreadsheets for the analysis of aquifer-test and slug-test data: U.S. Geological Survey Open-File Report 02–197, 51 p.

Halley, R.B., and Evans, C.C., 1983, The Miami Limestone—A guide to selected outcrops and their interpretation: Miami Geological Society, 67 p.

Halley, R.B., Shinn, E.A., Hudson, J.H., and Lidz, B.H., 1977, Pleistocene barrier bar seaward of ooid shoal complex near Miami, Florida: American Association of Petroleum Geologists, v. 61, p. 519–526.

Hallock, Pamela, and Glenn, E.C., 1986, Larger foraminifera—A tool for paleoenvironmental analysis of Cenozoic carbonate depositional facies: Palaios, v. 1, no. 1, p. 55–65.

Harrison, R.S., Cooper, L.D., and Coniglio, Mario, 1984, Late Pleistocene carbonates of the Florida Keys, *in* Carbonates in subsurface and outcrop: Canadian Society of Petroleum Geologists Core Conference, p. 291–306.

Hickey, J.J., 1993, Characterizing secondary porosity of carbonate rocks using borehole video data [abs.]: Geological Society of America Abstracts with Programs, v. 25, Southeastern Section, p. 23.

Hickey, T.D., 2004, Geologic evolution of south Florida Pleistocene-age deposits with an interpretation of the enigmatic rockridge development: St. Petersburg, University of South Florida, M.S. Thesis, 125 p.

Hickey, T.D., Hine, A.C., Shinn, E.A., Kruse, S.E., and Poore, R.Z., 2010, Pleistocene carbonate stratigraphy for high-frequency sea-level cyclicity: Journal of Coastal Research, v. 26, p. 605–614.

Hoffmeister, J.E., Stockman, K.W., and Multer, H.G., 1967, Miami Limestone of Florida and its recent Bahamian counterpart: Geological Society of America Bulletin, v. 79, no. 2, p. 175–190.

Hurley, N.F., Pantoja, David, and Zimmerman, R.A., 1999, Flow unit determination in a vuggy dolomite reservoir, Dagger Draw Field, New Mexico: Oslo, Norway, Transactions, June 1999.

Hurley, N.F., Zimmerman, R.A., and Pantoja, David, 1998, Quantification of vuggy porosity in a dolomite reservoir from borehole images and core, Dagger Draw Field, New Mexico: Annual Technical Conference and Exhibition, New Orleans, Society of Petroleum Engineers, Paper 49323, p. 789–802.

Ishman, S.E., Graham, Ian, and d'Ambrosio, Jill, 1997, Modern benthic foraminifer distributions in Biscayne Bay—Analogs for historical reconstructions: U.S. Geological Survey Open-File Report 97–34, 23 p.

James, N.P., 1997, The cool-water carbonate depositional realm, *in* James, N.P., and Clarke, J.A.D., eds., Cool-water carbonates: SEPM (Society for Sedimentary Geology) Special Publication 56, p. 1–20.

Jervey, M.T., 1988, Quantitative geological modeling of siliciclastic rock sequences and their seismic expression, *in* Wilgus, C.K., Hastings, B.S., Kendall, C.G.St.C., Posamentier, H.W., Ross, C.A., and Van Wagoner, J.C., eds., Sea-level changes—An integrated approach: Society of Economic Paleontologists and Mineralogists, Special Publication 42, p. 47–69.

Kaufman, R.S., and Switanek, M.P., 1998, Confinement of the Biscayne aquifer in northwest Dade County, Florida: Geological Society of America Abstracts with Programs, 47th Annual Meeting Southeastern Section, March 30–31, Charleston, W.Va., p. 20.

Kerans, Charles, and Tinker, S.W., 1997, Sequence stratigraphy and characterization of carbonate reservoirs: Society of Economic Paleontologists and Mineralogists, Short Course Notes 40, 130 p.

Keys, W.S., 1990, Borehole geophysics applied to groundwater investigations: U.S. Geological Survey Techniques of Water-Resources Investigations, book 2, chap. E2, 150 p.

Keys, W.S., and MacCary, L.M., 1971, Application of borehole geophysics applied to water-resources investigations: U.S. Geological Survey Techniques of Water-Resources Investigations, book 2, chap. E1, 126 p.

Klein, Howard, and Sherwood, C.B., 1961, Hydrologic conditions in the vicinity of Levee 30, northern Dade County, Florida: Tallahassee, Florida Bureau of Geology Report of Investigations 24, 24 p.

Krupa, Amanda, and Mullen, V.T., 2005, Extent of a dense limestone layer in the upper portion of the Biscayne aquifer in the Pennsuco Wetlands, Miami-Dade County: West Palm Beach, South Florida Water Management District, Technical Publication HESM–1, 33 p.

Lidz, B.H., and Rose, P.R., 1989, Diagnostic foraminiferal assemblages of Florida Bay and adjacent shallow water—A comparison: Bulletin of Marine Science, v. 44, p. 399–418.

Lucia, F.J., 1995, Rock-fabric/petrophysical classification of carbonate pore space for reservoir characterization: American Association of Petroleum Geologists, v. 79, p. 1275–1300.

Lucia, F.J., 1999, Carbonate reservoir characterization: Berlin, Springer-Verlag, 226 p.

Martin, J.B., and Screaton, E.J., 2001, Exchange of matrix and conduit water with examples from the Floridan aquifer, *in* Kuniansky, E.L., ed., U.S. Geological Survey Karst Interest Group Proceedings, Water-Resources Investigations Report 01–4011, p. 38–44.

McIlroy, D., 2004, Some ichnological concepts, methodologies, and applications and frontiers, *in* McIlroy, D., ed., The application of ichnology to paleoenvironmental and stratigraphic analysis: London, Geological Society, Special Publications, v. 228, p. 3–27.

Mercury Geophysics, 2009, LogCruncher Web page, accessed October 13, 2011, at *http://www.mercurygeophysics.com/wiki/tiki-index.php?page=LogCruncher*.

Middleton, G.V., 1973, Johannes Walther's law of the correlation of facies: Geological Society of America Bulletin, v. 84, p. 979–988.

Missimer, T.M., 1992, Stratigraphic relationships of sediment facies within the Tamiami Formation of southwest Florida—Proposed intraformational correlations, *in* Scott, T.M., and Allmon, W.D., eds., Plio-Pleistocene stratigraphy and paleontology of southern Florida: Florida Geological Survey Special Publication 36, p. 63–92.

Missimer, T.M., 1993, Pliocene stratigraphy of southern Florida—Unresolved issues of facies correlation in time, *in* Zullo, V.A., Harris, W.B., Scott, T.M., and Portall, R.W., eds., The Neogene of Florida and adjacent regions: Florida Geological Survey Special Publication 37, p. 33–42.

Mitchum, R.M., Jr., and Van Wagoner, J.C., 1991, High-frequency sequences and their stacking patterns—Sequence stratigraphic evidence of high-frequency eustatic cycles: Sedimentary Geology, v. 70, p. 131–160.

Multer, H.G., Gischler, E., Lundberg, J., Simmons, K.R., and Shinn, E.A., 2002, Key Largo Limestone revisited—Pleistocene shelf-edge facies, Florida Keys, U.S.A.: Facies, v. 46, p. 229–272.

Nemeth, M.S., Wilcox, W.M., and Solo-Gabriele, H.M., 2000, Evaluation of the use of reach transmissivity to quantify leakage beneath Levee 31N, Miami-Dade County, Florida: U.S. Geological Survey Water-Resources Investigations Report 00–4066, 80 p.

Neuendorf, K.E., Mehl, J.P., Jr., and Jackson, J.A., (5^{th} ed.), 2005, Glossary of geology: American Geological Institute, 799 p.

Newberry, B.M., Grace, L.M., and Stief, D.D., 1996, Analysis of carbonate dual porosity systems from borehole electrical images: Permian Basin Oil and Gas Recovery Conference, Midland, Tex., Society of Petroleum Engineers Paper 35158, p. 123–125.

Paillet, F.L., 1993, Using borehole geophysics and cross-borehole flow testing to define hydraulic connections between fracture zones in bedrock aquifers: Journal of Applied Geophysics, v. 30, no. 3, p. 261–279.

Paillet, F.L., 1998, Flow modeling and permeability estimation using borehole flow data in heterogeneous fractured formations: Water Resources Research, v. 34, no. 5, p. 997–1010.

Paillet, F.L., 2000, A field technique for estimating aquifer parameters using flow log data: Ground Water, v. 38, no. 4, p. 510–521.

Paillet, F.L., 2011, Accounting for the effects of hydraulic diffusivity, indirect connections, and leakage in cross-borehole flowmeter experiments [abs.]: NGWA Focus Conference on Fractured Rock and Eastern Groundwater Regional Issues, September 26–27, Burlington, Vt.

Paillet, F.L., and White, J.E., 1982, Acoustic modes of propagation in the borehole and their relationship to rock properties: Geophysics, v. 74, no. 8, p. 1215–1228.

Paillet, F.L., Williams, J.H., Urik, J., Lukes, J., Kobr, M., and Mares, S., 2012, Cross-borehole flow analysis to characterize fracture connections in the Melechov Granite, Bohemian-Moravian Highland, Czech Republic: Hydrogeology Journal, v. 20, no. 1, p. 143–154.

Parker, G.G., Ferguson, G.E., Love, S.K., and others, 1955, Water resources of southeastern Florida: U.S. Geological Survey Water-Supply Paper 1255, 965 p.

Perkins, R.D., 1977, Depositional framework of Pleistocene rocks in south Florida, *in* Enos, Paul, and Perkins, R.D., eds., Quaternary sedimentation in south Florida: Geological Society of America Memoir 147, p. 131–198.

Prensky, S.E., 1999, Advances in borehole imaging technology and applications, *in* Lovell, M.A., Williamson, G., and Harvey, P.K., eds., Borehole imaging—Applications and case histories: London, Geological Society, Special Publications 159, p. 1–43.

Raymer, L.L., Hunt, E.R., and Gardner, J.S., 1980, An improved sonic transit time-to-porosity transform, paper P, *in* 21st Annual Logging Symposium Transactions: Society of Professional Well Log Analysts, 12 p.

Reese, R.S., and Cunningham, K.J., 2000, Hydrogeology of the gray limestone aquifer in southern Florida: U.S. Geological Survey Water-Resources Investigations Report 99–4213, 244 p.

Renken, R.A., Cunningham, K.J., Shapiro, A.M., Harvey, R.W., Zygnerski, M.R., Metge, D.W., and Wacker, M.A., 2008, Pathogen and chemical transport in the karst limestone of the Biscayne aquifer—1. Revised conceptualization of groundwater flow: Water Resources Research, v. 44, W08429, doi:10.1029/2007WR006058.

Renken, R.A., Cunningham, K.J., Zygnerski, M.R., Wacker, M.A., Shapiro, A.M., Harvey, R.W., Metge, D.W., Osborn, C.L., and Ryan, J.N., 2005, Assessing the vulnerability of a municipal well field to contamination in a karst aquifer: Environmental & Engineering Geoscience, v. XI, no. 4, p. 319–331.

Richter, R., 1936, Marken und Spuren im Hunsrückschiefer 2. Schichtung und Grundleben: Senckenbergiana, v. 18, p. 215–244.

Rose, P.R., and Lidz, Barbara, 1977, Diagnostic foraminiferal assemblages of shallow-water modern environments—South Florida and the Bahamas—Sedimenta VI: Comparative Sedimentology Laboratory, Division of Marine Geology and Geophysics, University of Miami, 55 p.

Scholle, P.A., Bebout, D.G., and Moore, C.H., 1983, Carbonate depositional environments: American Association of Petroleum Geologists Memoir 33, 708 p.

Sherwood, C.B., and Leach, S.D., 1962, Hydrologic studies in the Snapper Creek Canal area, Dade County, Florida: Florida Geological Survey Report of Investigations 24, part 2, 32 p.

Shinn, E.A., 1968, Burrowing in recent lime sediments of Florida and the Bahamas: Journal of Paleontology, v. 42, no. 4, p. 879–894.

Shinn, E.A., and Corcoran, Eugene, 1988, Contamination by landfill leachate, south Biscayne Bay, Florida: Gainesville, University of Florida, Final Report to Sea Grant, 11 p.

Sonenshein, R.S., 2001, Methods to quantify seepage beneath Levee 30, Miami-Dade County, Florida: U.S. Geological Survey Water-Resources Investigations Report 01–4074, 36 p.

South Florida Water Management District, 2000, Lower east coast water supply plan: West Palm Beach, Fla., Water Supply Department, South Florida Water Management District.

Sunderland, S.A., and Krupa, S.L., 2007, Groundwater-surface water interaction along the C–2 canal, Miami-Dade County, Florida: West Palm Beach, Fla., Water Supply Department, South Florida Water Management District.

Swain, E., 2012, Stochastic analyses to identify wellfield withdrawal effects on surface-water and groundwater in Miami-Dade County, Florida: Journal of Environmental Management, v. 113, p. 15–21.

Tang, X.M., and Cheng, C.H., 1988, Wave propagation in a fluid filled fracture, and experimental study: Geophysical Research Letters, v. 15, no. 13, p. 1463–1466.

Tang, X.M., and Cheng, C.H., 1993, Fast inversion of formation permeability from Stoneley wave logs using a simplified Biot-Rosenbaum model: Cambridge, Mass., Earth Resources Laboratory, Department of Earth, Atmospheric, and Planetary Sciences, Massachusetts Institute of Technology, p. 209–226.

Thiem, G., 1906, Hydologische methoden: Leipzig, J. M. Gebhardt, 56 p.

Thompson, W.G., Curran, H.A., Wilson, M.A., and White, B., 2011, Sea-level oscillations during the last interglacial highstand recorded by Bahamian corals: Nature Geoscience, v. 4, p. 684–687.

U.S. Environmental Protection Agency, 2002, A lexicon of cave and karst terminology with special reference to environmental karst hydrology: EPA/600/R–02/003, 214 p.

Vacher, H.L., and Mylroie, J.E., 2002, Eogenetic karst from the perspective of an equivalent porous medium: Carbonates and Evaporites, v. 17, no. 2, p. 182–196.

Van der Kamp, Garth, 1976, Determining aquifer transmissivity by means of well response tests—The underdamped case: Water Resources Research, v. 12, no. 1, p. 71–77.

Wacker, M.A., and Cunningham, K.J., 2003, Linking full-waveform sonic logs to the hydrology of the karstic Biscayne aquifer, SE Florida [abs.]: Geological Society of America Abstracts with Programs, v. 29, no. 6, p. 454.

Wacker, M.A., and Cunningham, K.J., 2008, Borehole geophysical logging program—Incorporating new and existing techniques in hydrologic studies: U.S. Geological Survey Fact Sheet 2008–3098, 4 p.

Williams, J.H., and Johnson, C.D., 2000, Borehole-wall imaging with acoustic and optical televiewers for fractured-bedrock aquifer investigations: Proceedings 7th Minerals and Geotechnology Logging Symposium, October 24–26, Golden, Colo., p. 43–53.

Williams, J.H., and Johnson, C.D., 2004, Acoustic and optical borehole wall imaging for fractured-rock aquifer studies: Journal of Applied Geophysics, v. 55, p. 151–159.

Williams, J.H., and Paillet, F.L., 2002, Using flowmeter pulse tests to define hydraulic connections in the subsurface—A fractured shale example: Journal of Hydrology, v. 265, p. 100–117.

Wright, V.P., and Tucker, M.E., 1991, Calcretes—An introduction, *in* Wright, V.P., and Tucker, M.E., eds., Calcretes: Oxford, Blackwell Scientific Publications, Reprint Series Volume 2 of the International Association of Sedimentologists, 352 p.

Wyllie, M.R.J., Gregory, A.R., and Gardner, L.W., 1956, Elastic wave velocities in heterogeneous and porous media: Geophysics, v. 21, p. 41–70.

Glossary

Accommodation "The space made available for potential sediment accumulation" (Jervey, 1988).

Bioturbation Displacement (reworking) within sediments and soils by the activities of organisms and plants (Richter, 1936).

Conduit flow In this report, refers to groundwater flow through "relatively large dissolution voids, including enlarged fissures and tubular tunnels…. Conduits may include all voids greater than 1 cm [centimeter] in diameter" (U.S. Environmental Protection Agency, 2002).

Cyclostratigraphy The study of stratified rock in relation to cyclic formation and destruction.

Eogenetic Young limestones undergoing meteoric diagenesis and porosity development in the vicinity of their deposition (Choquette and Pray, 1970; Vacher and Mylroie, 2002).

Heterozoan association An association of benthic carbonate particles including (1) organisms that are light-independent or (2) red calcareous algae or both (James, 1997).

High-frequency cycle The smallest set of sediment deposited during a single relative rise and fall of sea level.

Ichnology The study of trace fossils, such as tracks, traces, burrows, and borings, that are structures produced in sedimentary rock or other substrate by organism activity (Bromley, 1996).

Ideal high-frequency cycle A conceptual high-frequency cycle and its abstracted vertical succession of lithofacies and upper and lower bounding surfaces.

Karst Type of topography that is formed on limestone, gypsum, and other rocks, primarily by dissolution, and that is characterized by sinkholes, caves, and underground drainage (Neuendorf and others, 2005).

Lithoclasts A mechanically formed and deposited fragment of a carbonate rock, normally larger than 2 mm in diameter, derived from an older lithified rock, adjacent to, or outside the depositional site.

Paralic The principal characteristic of paralic environments is that they occur at the transition between marine and terrestrial realm—estuaries, coastal lagoons, marshes, and coastal zones subject to high freshwater input (Debenay and others, 2000).

Pedotubule calcrete A near surface, terrestrial, accumulation of predominately calcium carbonate where all, or nearly all, the secondary carbonate forms encrustations around roots or fills roots or other tubes (Wright and Tucker, 1991).

Peritidal Referring to depositional environments in a zone from somewhat above highest storm or spring tides to somewhat below lowest tides. Peritidal is a broader term than intertidal (Neuendorf and others, 2005).

Photozoan association An association of benthic carbonate particles including (1) skeletons of light-dependent organisms, or (2) non-skeletal particles (for example, ooids and peloids) or both, and in some cases (3) skeletons from the heterozoan association (James, 1997).

Stratiform Having the form of a layer, bed, or stratum.

Vug A "pore space that is within grains or crystals or that is substantially larger than grains or crystals," but does not include interparticle pore space (Lucia, 1995). Vugs are commonly present as leached fossils or other grains, fractures, dissolution along bedding planes, and large, irregular cavities.

Appendix 1. Detailed Lithologic Descriptions

Appendix 1 provides detailed lithologic descriptions by Kevin Cunningham of recovered 4-inch core from Snapper Creek Well Field, West Well Field, and G-3889 coreholes drilled for this study. Borehole image logs and thin sections were used to supplement the recovered core for missing intervals or intervals of poor recovery. Included in each description are lithofacies, depositional texture, color, sedimentary structures and textures, ichnofabrics, carbonate grains, accessory grains, estimates of porosity and permeability, and any relative comments.

See supplemental file available at *http://pubs.usgs.gov/sir/2014/5138/.*

Appendix 2. Core Photographs

Appendix 2 provides core-box photographs of recovered 4-inch core from Snapper Creek Well Field, West Well Field, and G-3889 coreholes drilled for this study. Boxed core samples were prepared for analysis by first slabbing the core using a 10 inch diameter blade rock saw to cut each core section in half lengthwise, followed by acid washing with a 10 percent hydrochloric acid solution. The boxed core was then photographed with a high resolution camera. Thin sections were cut from the slabbed core and sent out for processing. Photographs of the collected, boxed core are presented in appendix 2.

See supplemental file available at *http://pubs.usgs.gov/sir/2014/5138/.*

Appendix 3. Monitoring-Well Construction Methods and Completion Data

Drilling of each test corehole, later completed as a deep monitoring well (except test corehole G–3880, which was completed as a shallow monitoring well), began by using a 14-inch (in.) diameter auger or tri-cone roller bit to drill a hole to the top of bedrock at each site, followed by placing a 10-in. internal diameter (ID) Schedule 40, polyvinyl chloride (PVC) surface casing in the hole produced by drilling, and then grouting the surface casing into place. Next the well was cored downward in 5-foot (ft) intervals cutting a nominal 5 7/8-in. diameter test corehole from the approximate top of the bedrock using a wire-line coring system to collect 4-in. diameter core samples to a depth below the base of the Biscayne aquifer and into the uppermost part of the underlying semiconfining unit.

A liquid polymer drilling additive was added at times to the drilling fluid to facilitate collection of unconsolidated sand and soft sediment in the core barrel, allow their extrusion from the barrel at the surface, and provide lubrication and more effective removal of cuttings. The polymer, unlike bentonite-clay drilling mud, breaks down within a few days, is easily removed from the column of test corehole fluid during the airlifting process, and is safe for use within a production well field. Bentonite-clay drilling mud also leaves a residue on the borehole wall that is scraped off by the centralizer during digital optical logging and becomes suspended in the borehole fluid, which reduces image quality. Once coring was completed to the desired total depth (TD) below the Biscayne aquifer, the wire-line coring casing was removed. The test corehole was prepared for logging by evacuating loose clay, silt, sand, and cobble-sized (up to 3-in. diameter) material from the test corehole using an airlift device constructed by the drilling contractor. This device is a 3-in. diameter metal drill casing with an air hose duct taped to the outside and connected at one end to an air compressor at the surface; the opposite end of the air hose is connected to a steel elbow welded to the casing side at the base of the drill casing. By using an airlift, water is also pulled from the surrounding formation so that drilling fluids are removed from an uncertain volume of the aquifer surrounding the test corehole. During airlifting, any useful samples brought to the surface by the airlift were archived in core boxes, and the estimated depth, in known, was indicated with wood blocks. Airlifting was continued until the hole was free of any obstructions and the fluid in the hole was clear of particulate to TD. The test corehole was first logged with a digital optical logging tool after a 24-hour waiting period that allowed most of the fine suspended sediment in the fluid to settle and for recovery borehole flow to return to static conditions. In test corehole G–3980, a sand layer between 15 and 25 ft below land surface (bls) necessitated that a 30-ft section of slotted 6-in. ID, PVC casing be temporarily installed to a depth of 29.1 ft so the test hole would remain open for geophysical logging.

Monitoring-well clusters were constructed after all six of the test coreholes were drilled and geophysical logging was completed in each. Monitoring-well clusters at each of the six test coreholes were designed on the basis of information provided by the geophysical logs and recovered core to determine the base of the Biscayne aquifer, characteristics of the lithologic and stratigraphic units, and hydrologic properties throughout the aquifer. All monitoring wells were cased with 4-in. ID, Schedule 40, PVC casing. The deepest monitoring well in each cluster was constructed in the test corehole, except at corehole G–3880, which filled in with formation sand after removal of the temporary casing and was then completed as a shallow monitoring well. Monitoring-well completion intervals within or near the Pinecrest Sand Member of the Tamiami Formation were screened to prevent infilling of the interval, but all other completed zones were left as open hole with the exception of shallow monitoring well G–3903, which was also infilled with soft sediment. For

the additional monitoring wells in each cluster, a 7 7/8-in. roller-bit was used to drill to the top of the planned open interval and a 4-in. ID, PVC casing was cemented in place. Then a smaller 3 7/8-in. roller bit was used to drill the open interval below the casing to the specified depth. Cuttings and sand were removed using reverse air circulation until the open interval was clear of cuttings to the planned depth. Digital borehole image and caliper logs were run in each completed monitoring well to verify completion within the desired interval. Monitoring wells (G–3914, G–3916, and G–3917) in three of the clusters were not considered acceptable, so a replacement well for each was drilled, completed, and the original well abandoned. When the temporary casing in test corehole G–3880 was removed, sand infilled the well to a depth below the surface of about 18 ft, making it difficult to construct the deep monitoring well. A decision was made to construct the shallow monitoring well in the G–3880 test corehole and to drill and construct a new well, G–3912, as the replacement deep monitoring well in that cluster. The drilling contractor was also unable to clear the open interval of the shallow monitoring well (G–3903) in the G–3877, westernmost cluster due to infilling of the hole; therefore, the well was screened with 3-in. ID, 0.010-in. slot PVC casing installed inside the 4-in. ID, PVC casing. Monitoring wells were completed by pumping until the flow was clear of particulate, and a surface manhole was constructed for access through a 2-ft square cement pad. Electrical conduit was inserted prior to cementing the manhole to provide a pathway for instrumentation of the monitoring well. After the wells were completed, the top of each casing and the manhole were surveyed. Figure 3–1 shows each completed monitoring well cluster. Field notes collected during monitoring-well drilling, logging, and construction were entered in the Groundwater Site Identification (GWSI) system for future retrieval.

Appendix 4. Borehole Geophysical Data Displays

Borehole geophysical data were collected and displayed as described previously in this report. These data were then displayed in a manner that best portrays the type of data being shown. Section A–4–1, Cluster Logs, contains borehole geophysical data for each of the six Snapper Creek Well Field (SCWF) test coreholes and the monitoring wells adjacent to each of the test coreholes that form six clusters. These data are displayed at a 1:12 scale so as to best display the image data for each corehole and open section of each monitoring well. Only the flowmeter data collected using the electromagnetic (EM) flowmeter during phase 2, test types 1 and 2, for the test corehole are displayed. Section A–4–2, Combo Logs, contains all of the borehole geophysical data collected in each of the six SCWF test coreholes and the three coreholes drilled outside the SCWF for this study. These data are displayed at a 1:96 scale to best display all logs other than the image logs. Section A–4–3, Cross-hole Logs, contains the EM flowmeter data collected during phase 2, test type 3 (cross-hole), in five of the SCWF test coreholes. No display was made for corehole G–3877 because there was no response to pumping from SCWF production wells. The cross-hole EM flowmeter data (borehole fluid flow and temperature) are plotted as a function of the time elapsed since the production well operator was told to turn on the well. Each data display shows the effect turning each well on and off has on groundwater flow and temperature at specific test depths below land.

See supplemental files:

Section A–4–1 - Cluster Logs
Section A–4–2 - Combo Logs
Section A–4–3 - Cross-hole Logs

See supplemental file available at *http://pubs.usgs.gov/sir/2014/5138/.*

The abbreviations used in each borehole geophysical data display in order of presentation are as follows:

GPS	Global positioning system
NAD 83	North American Datum of 1983
NGVD 29	National Geodetic Vertical Datum of 1929
TD	Total depth drilled or cored
FM	Formation
LITH	Lithology
Cycle	High-frequency cycle or sequence
CORE	Percentage of core collected over that interval. “100 percent” indicates 100 percent of the whole core was collected; “50 percent” indicates less than 100 percent of the whole core, rubble, or sand was collected
DBI	Digital borehole image
OBI	Optical borehole image
ABI	Acoustic borehole image
Amplitude	Amplitude of the return acoustic signal
Deg. C	Degrees Celsius
uS/cm	Microsiemens per centimeter
mV	Millivolt
Ohm-m	Ohm meter
Deg. F	Degrees Fahrenheit
EMFM	Electromagnetic flowmeter
GPM	Gallons per minute
Troll	The process of continually recording data while moving up or down in a borehole
DN	down
UP	up
FZ	Flow zone. 100 percent is a major flow zone and 50 percent is a minor flow zone
FM	Flowmeter
FT/MIN	Foot per minute
cps	Counts per second
mS/m	Millisiemens per meter
EM	Electromagnetic
SP	Spontaneous potential
SPR	Single-point resistance

Figure 3–1. Photographs showing (*A*) G–3877 monitoring-well cluster looking southwest, (*B*) G–3878 monitoring-well cluster looking southwest, (*C*) G–3879 monitoring-well cluster looking west-southwest, (*D*) G–3880 monitoring-well cluster looking west-southwest, (*E*) G–3881 monitoring-well cluster looking southeast, (*F*) G–3882 monitoring-well cluster looking east.

C

D

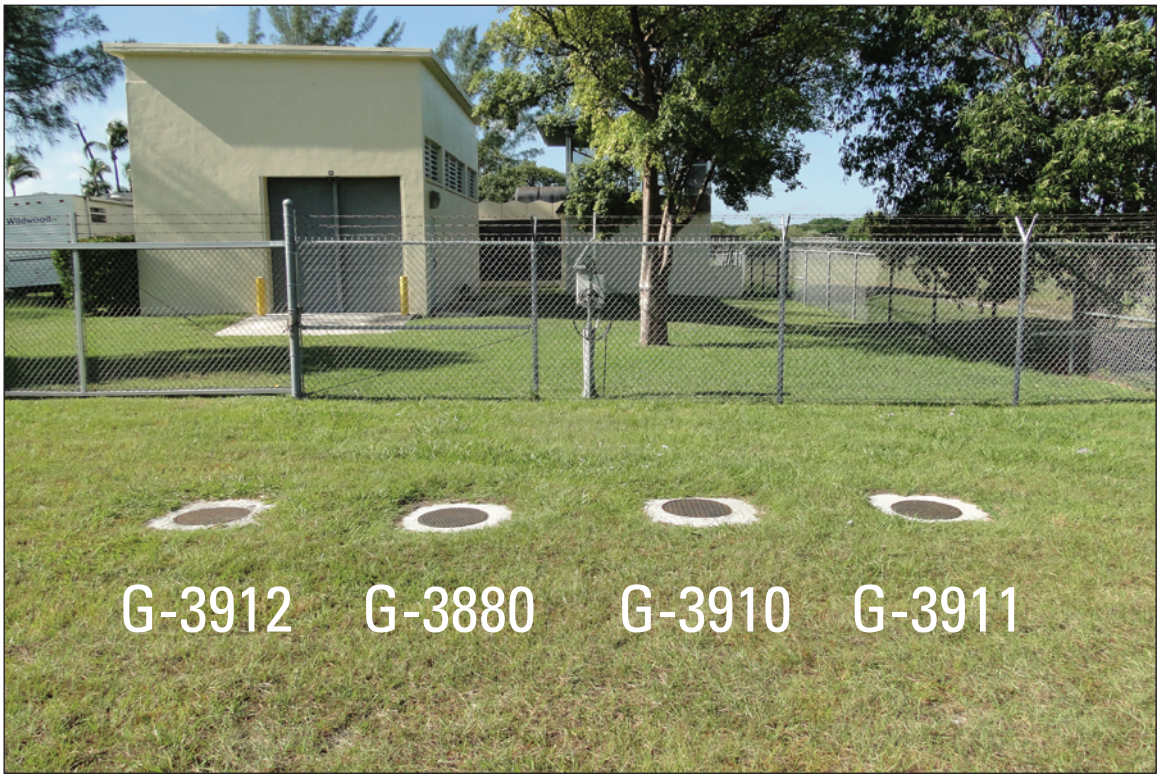

Figure 3–1. Photographs showing (*A*) G–3877 monitoring-well cluster looking southwest, (*B*) G–3878 monitoring-well cluster looking southwest, (*C*) G–3879 monitoring-well cluster looking west-southwest, (*D*) G–3880 monitoring-well cluster looking west-southwest, (*E*) G–3881 monitoring-well cluster looking southeast, (*F*) G–3882 monitoring-well cluster looking east.—Continued

E

F

Figure 3–1. Photographs showing (*A*) G–3877 monitoring-well cluster looking southwest, (*B*) G–3878 monitoring-well cluster looking southwest, (*C*) G–3879 monitoring-well cluster looking west-southwest, (*D*) G–3880 monitoring-well cluster looking west-southwest, (*E*) G–3881 monitoring-well cluster looking southeast, (*F*) G–3882 monitoring-well cluster looking east.—Continued

Appendix 5. Flowmeter Data Analysis of Coreholes at Snapper Creek Well Field

Qualitative analyses of steady-state flow measured using borehole flowmeters in test coreholes within the study area under both unstressed ambient and stressed borehole conditions showed that in all coreholes, the upper and lower Biscayne aquifer flow units are highly transmissive and are the intervals for most of the groundwater flow. The flowmeter data also indicated that minor flow zones within the middle semiconfining unit have lower transmissivity than the upper and lower flow units and that these zones contribute only minor flow of groundwater to or from the borehole (app. 4–2). Analyses of borehole flowmeter measurements and borehole fluid data collected in each Snapper Creek Well Field (SCWF) corehole under transient conditions (while pumping from production wells, production zone from 50 feet below land surface (ft bls) to 108 ft bls, at different distances and directions from the corehole) provided information on the connectivity of individual production wells and the C–2 canal to the coreholes at SCWF. A summary of the steady-state and transient flowmeter analysis follows for each corehole at the SCWF.

Test Corehole G–3877

Under steady-state unstressed ambient (nonpumping) conditions in the SCWF (table 2), flow in corehole G–3877 was downward, with major inflow to the borehole from the upper Biscayne aquifer flow unit and major outflow from the lower Biscayne aquifer flow unit (app. 4–2). When pumping from corehole G–3877 during steady-state stressed conditions at an approximate rate of 86 gallon per minute (gal/min), the upper Biscayne aquifer flow unit provided most of the inflow to the borehole with only about 10 gal/min from the flow zones penetrated by the borehole below the upper Biscayne aquifer flow unit. These results are similar to those observed when pumping from each of the other five SCWF coreholes. The large difference in contribution to groundwater inflow to the borehole between the upper Biscayne aquifer flow unit and the lower Biscayne aquifer flow unit is indicative of the high transmissivity of the Biscayne aquifer as a whole, in which most pumps used for flowmeter testing do not fully stress the aquifer despite each flow unit having similar transmissivity values. Analysis of flowmeter data identified a major flow zone in the lower Biscayne aquifer flow unit (69.6 to 75.6 ft bls) that accounted for about 70 percent of the transmissivity exclusive of the upper Biscayne aquifer flow unit as computed using the computer program FLASH (Flow-Log Analysis of Single Holes) (Day-Lewis and others, 2011) (fig. 11). Remaining flow zones identified in corehole G–3877 below the upper Biscayne aquifer flow unit were minor flow zones contributing less than 12 percent of the transmissivity exclusive of the upper Biscayne aquifer flow unit.

During transient (cross-hole) flowmeter data collection, no vertical flow (plate 1) or water-level response (fig. 5–1) was detected within corehole G–3877 when two production wells (S–3012 at 1,806 ft and S–3013 at 1,527 ft measured distance from corehole G–3877) were being pumped for a 10-minute period. All other five coreholes at SCWF showed an immediate response when any single production well was pumped (app. 4–3). During subsequent aquifer testing with all monitoring-well clusters recording water-level data during well field operation and with all production wells being pumped or with stressed steady-state conditions throughout the well field, water levels in monitoring wells in the G–3877 cluster showed only negligible drawdown compared with drawdown in the monitoring wells in the other five clusters. The difference in water-level response between the monitoring wells at the G–3877 cluster and those at the other five clusters suggests that corehole G–3877 either is not as hydraulically well-connected to the production wells as are the other five coreholes in SCWF or is too far away from the production wells to be under their hydraulic influence.

Test Corehole G–3878

Under unstressed ambient, steady-state borehole conditions with no pumping in the SCWF, fluid flow was upward as measured by the EM flowmeter in corehole G–3878, with the major inflow from and higher head in the lower Biscayne aquifer flow unit, and major outflow from the borehole and lower head in the upper Biscayne aquifer flow unit. Under steady-state stressed borehole conditions while pumping from production well S–3014 (app. 4–2), flowmeter data showed that fluid flow was downward in the corehole, with the upper Biscayne aquifer flow unit as the major interval of inflow with the highest head. The interval of greatest outflow was the major flow zone (74.13 to 78.87 ft bls) in the lower Biscayne aquifer flow unit, indicating that this flow zone had the lowest head and greatest degree of hydraulic connection to the production well. Computed estimates of transmissivity using the FLASH program showed that this major flow zone (74.13 to 78.87 ft bls) in the lower Biscayne aquifer flow unit accounted for about 60 percent of the transmissivity exclusive of the upper Biscayne aquifer flow unit with the remaining 40 percent distributed almost equally among the minor flow zones in the lower Biscayne aquifer flow unit and middle semiconfining unit (fig. 11).

Cross-hole testing with flowmeter measurements made at depths 38, 62, 72.5, and 83.5 ft bls in corehole G–3878 while pumping from different production wells showed that the greatest change in vertical flow rate (12.52 gal/min) in corehole G–3878 occurred when production well S–3013 was operating and the flowmeter was set at depth 62 ft bls (table 5–1; fig. 5–2). Similarly, with the S–3013 production well operating, the change in vertical flow rate at the 38-ft depth was 12.30 gal/min. This small difference in downward vertical flow rate indicated that most of the inflow into the corehole G–3878 borehole came from flow zones above the

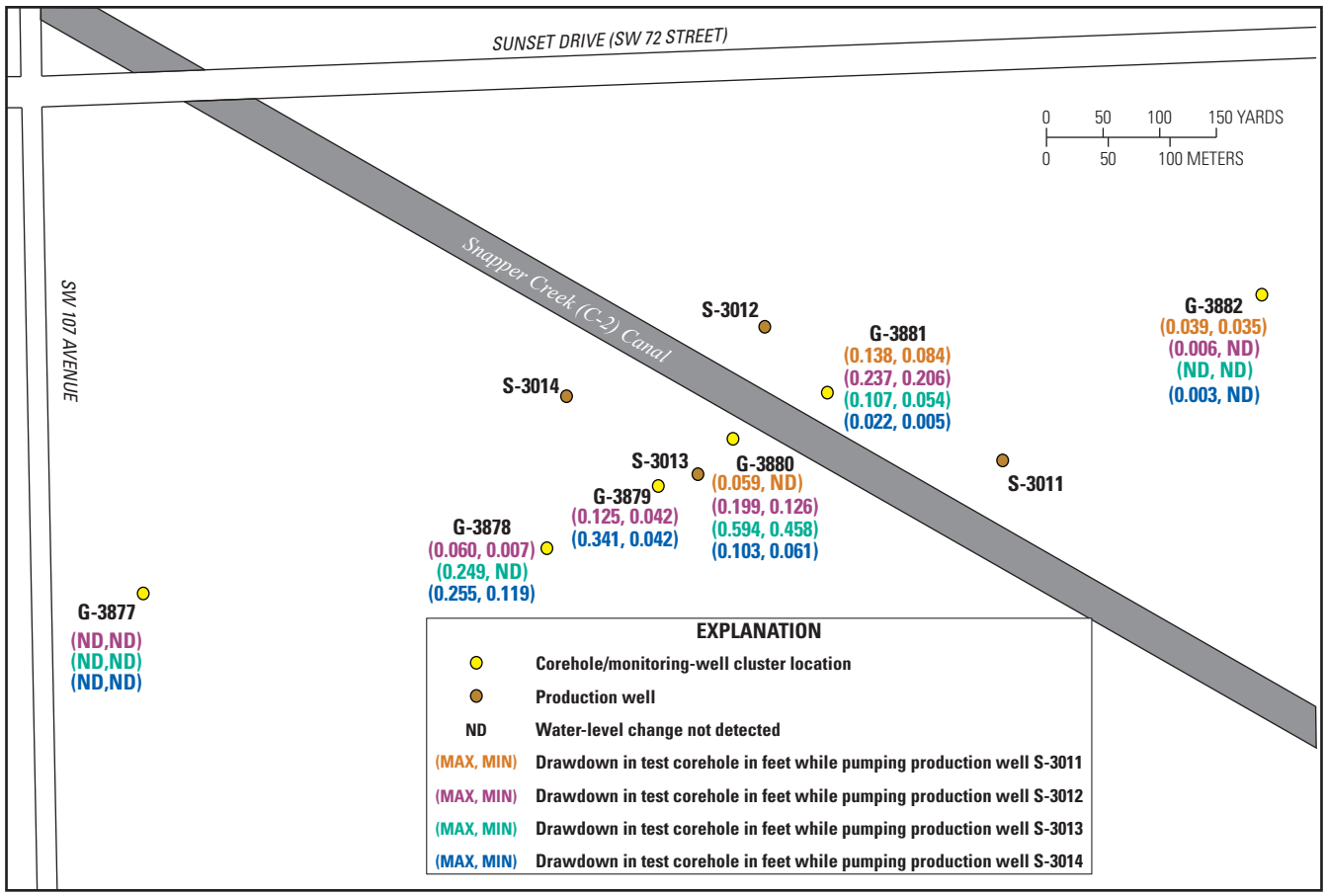

Figure 5–1. Drawdown in test coreholes during cross-hole flowmeter testing.

38-ft depth, most likely from the upper Biscayne aquifer flow unit (plate 1). The greatest outflow from this borehole was in the flow zones between depths 72.5 and 83.5 ft bls (plate 1), with production well S–3013 pumping; about three times as much water was exiting the borehole from this interval than from the interval just above it (62 and 72.5 ft bls, table 5–1).

The observation that the interval between 72.5 and 83.5 ft bls is well connected to the production wells and a major flow zone within the lower Biscayne aquifer flow unit is supported by the single-hole flowmeter testing results, which showed that 51 percent of the inflow to the borehole below the upper Biscayne aquifer flow unit came from this flow zone (table 5; app. 4–2). Below 83.5 ft bls, outflow from the borehole was less than 1 percent of the outflow from the borehole measured in the interval above (0.04 gal/min), indicating the lower most flow zone in corehole G–3878 to be a minor flow zone. Results observed while running production well S–3014 (table 5–1) suggest that the hydraulic connection between corehole G–3878 and production well S–3013 is better than between G–3778 and production well S–3013.

Pumping from the more distant production well S–3012 on the opposite side of the C–2 canal from corehole G–3878 produced similar results as reported above (table 5–1; plate 1), but the rates and volume of flows in corehole G–3878 were less than when pumping from either production well S–3013 or S–3014 for the same depths. Pumping from production well S–3012 caused no downflow in corehole G–3878, only less upflow unlike when pumping from the other two production wells, which caused reversal of vertical flow from upward to downward. This response to pumping from the more distant production well S–3012 would be expected, because the distance from corehole G–3878 to production well S–3012 is almost twice as great as that from the other two production wells (fig. 5–1), and production well S–3012 is on the opposite side of the C–2 canal. Drawdown in water levels observed in the G–3878 corehole caused by the production well showed a consistent relation between distance from the pumping production well and magnitude of the drawdown in the corehole (fig. 5–1).

Test Corehole G–3879

Under unstressed ambient, steady-state borehole conditions with no pumping in the SCWF, vertical borehole fluid in corehole G–3879 was upward, with the major inflow from and higher head in the lower Biscayne aquifer flow unit, and major outflow from the borehole and lower head in the upper Biscayne aquifer flow unit. During stressed steady-state borehole conditions while pumping from the corehole or from production well

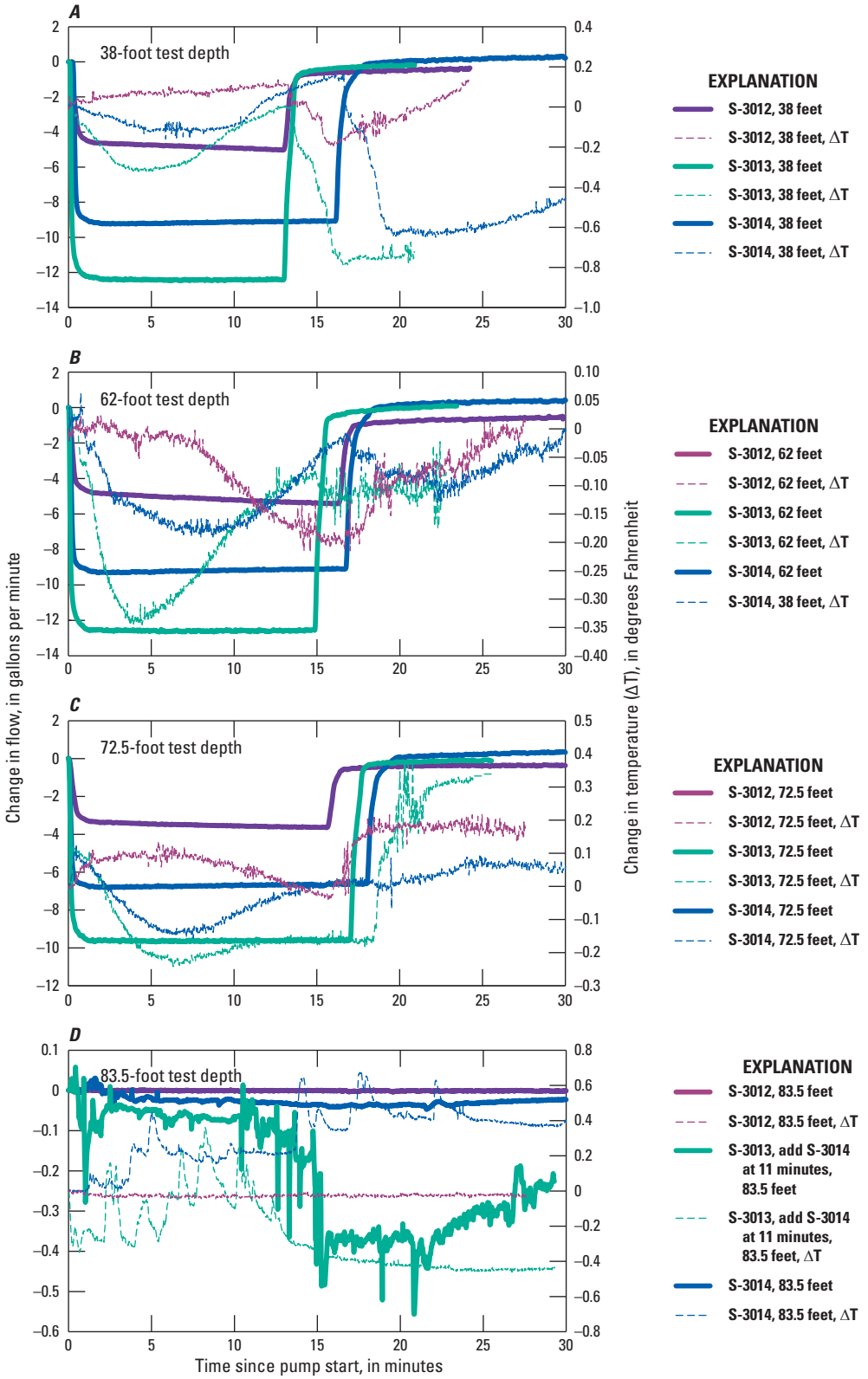

Figure 5–2. Change in flow rate and fluid temperature at tested intervals in test corehole G–3878 in response to pumping and recovery in production wells S–3012, S–3013, and S–3014.

Table 5–1. Cross-hole flowmeter test results showing net change in borehole flow in the Snapper Creek Well Field (SCWF) coreholes in response to pumping from SCWF production wells.

[Except where stated in column 7 (inflow or outflow), positive values indicate upflow in the borehole and negative values downflow in the borehole. Borehole diameter was the same at all test depths. Change in flow above the upper most test depth is equal to the inflow above that test depth. Inflow and outflow in intervals below the uppermost test depth are equal to the change in flow (column 6) between the test depth and the one above it. Outflow below the lower most test depth is equal to the change in flow between ambient and pumping (column 6) and displayed in bold red. AMB, pumping production well off; gal/min, gallons per minute; PMP, pumping from production well; ft, feet; * Depth not tested in all test coreholes]

Well ID/ Date of test	Production well pumped for cross-hole test (~6,940 gal/min)	Diverter depth below land surface (ft)	AMB flow (gal/min)	PMP flow (gal/min)	Change in flow between PMP and AMB (gal/min)	Inflow (+) or outflow (-) from interval above the test depth (gal/min)	Distance from corehole to supply well (ft)
G–3877 29JUN09	No flow detected during test time interval (nearest production well, S–3014, is 1,215 ft away)						
G–3878 29MAY09	S–3012	38	2.90	–2.02	4.92	4.92	822
	S–3013	38	2.55	–9.75	12.30	12.30	450
	S–3014	38	2.47	–6.51	8.98	8.98	423
	S–3012	62	2.82	–2.58	5.40	0.48	822
	S–3013	62	2.27	–10.25	12.52	0.22	450
	S–3014	62	2.39	–6.68	9.07	0.09	423
	S–3012	*72.5	2.02	–1.56	3.58	–1.82	822
	S–3013	*72.5	1.64	–7.98	9.62	–2.90	450
	S–3014	*72.5	1.64	–5.04	6.68	–2.39	423
	S–3012	83.5	–0.17	–0.17	**0.003**	–3.58	822
	S–3013	83.5	–0.17	–0.21	**0.04**	–9.58	450
	S–3014	83.5	–0.15	–0.19	**0.04**	–6.64	423
G–3879 20MAY09	S–3012	38	6.82	–5.53	12.35	12.35	504
	S–3014	38	7.32	–8.43	15.75	15.75	348
	S–3012	62	6.26	–6.35	12.61	0.26	504
	S–3014	62	9.97	–7.84	17.81	2.06	348
	S–3012	82	2.91	–4.96	**7.87**	–4.74	504
	S–3014	82	5.16	2.34	**2.82**	–14.99	348
G–3880 23JUN09	S–3011	46.3	1.65	–2.62	4.27	4.27	702
	S–3012	46.3	1.02	–6.72	7.74	7.74	312
	S–3013	46.3	1.20	–11.13	12.33	12.33	126
	S–3014	46.3	3.80	–4.09	7.89	7.89	465
	S–3011	64	3.54	–3.38	6.92	2.65	702
	S–3012	64	2.34	–9.50	11.84	4.10	312
	S–3013	64	2.53	–11.13	13.66	1.33	126
	S–3014	64	2.15	–7.11	9.26	1.37	465
	S–3011	80.5	0.90	–1.56	**2.46**	–4.46	702
	S–3012	80.5	1.28	–5.22	**6.50**	–5.34	312
	S–3013	80.5	1.54	–11.13	**12.67**	–0.99	126
	S–3014	80.5	1.96	–6.47	**8.43**	–0.83	465
G–3880 during canal draw down 9JUN09	S–3011	46.3	3.54	–1.56	5.10	5.10	702
	S–3012	46.3	2.29	–6.28	8.57	8.57	312
	S–3013	46.3	2.15	–11.10	13.25	13.25	126
	S–3014	46.3	2.29	–4.53	6.82	6.82	465
	S–3011	64	4.87	–2.62	7.49	2.39	702
	S–3012	64	3.47	–9.27	12.74	4.17	312
	S–3013	64	3.24	–11.08	14.32	1.07	126
	S–3014	64	3.43	–6.92	10.35	3.53	465
	S–3011	80.5	2.48	0.45	**2.03**	–5.46	702
	S–3012	80.5	2.22	–4.84	**7.06**	–5.68	312
	S–3013	80.5	2.03	–11.01	**13.04**	–1.28	126
	S–3014	80.5	2.34	–5.98	**8.32**	–2.03	465

Table 5–1. Cross-hole flowmeter test results showing net change in borehole flow in the Snapper Creek Well Field (SCWF) coreholes in response to pumping from SCWF production wells.—Continued

[Except where stated in column 7 (inflow or outflow), positive values indicate upflow in the borehole and negative values downflow in the borehole. Borehole diameter was the same at all test depths. Change in flow above the upper most test depth is equal to the inflow above that test depth. Inflow and outflow in intervals below the uppermost test depth are equal to the change in flow (column 6) between the test depth and the one above it. Outflow below the lower most test depth is equal to the change in flow between ambient and pumping (column 6) and displayed in red. AMB, pumping production well off; gal/min, gallons per minute; PMP, pumping from production well; ft, feet* Depth not tested in all test coreholes]

Well ID/ Date of test	Production well pumped for cross-hole test (~6,940 gal/min)	Diverter depth below land surface (ft)	AMB flow (gal/min)	PMP flow (gal/min)	Change in flow between PMP and AMB (gal/min)	Inflow (+) or outflow (-) from interval above the test depth (gal/min)	Distance from corehole to supply well (ft)
G–3881 22JUN09	S–3011	46	2.79	–7.16	9.95	9.95	495
	S–3012	46	–0.73	–10.89	10.16	10.16	246
	S–3013	46	2.86	–11.08	13.94	13.94	393
	S–3014	46	0.59	–4.65	5.24	5.24	690
	S–3011	62	1.35	–8.24	9.59	–0.36	495
	S–3012	62	2.67	–11.08	13.75	3.59	246
	S–3013	62	3.35	–11.08	14.43	0.49	393
	S–3014	62	1.77	–5.15	6.92	1.68	690
	S–3011	79	0.78	–5.65	**6.43**	–3.16	495
	S–3012	79	1.39	–8.24	**9.63**	–4.12	246
	S–3013	79	1.09	–9.31	**10.40**	–4.03	393
	S–3014	79	2.29	–2.81	**5.10**	–1.82	690
G–3882 2JUN09	S–3011	36	–0.73	–2.32	1.59	1.59	831
	S–3012	36	–0.75	–0.94	0.19	0.19	1338
	S–3013	36	–0.75	–0.85	0.10	0.10	1575
	S–3014	36	–0.85	–0.88	0.03	0.03	1725
	S–3011	61	–0.77	–3.69	2.92	1.33	831
	S–3012	61	–0.73	–1.14	0.41	0.22	1338
	S–3013	61	–0.41	–0.84	0.43	0.33	1575
	S–3014	61	–0.84	–0.97	0.13	0.10	1725
	S–3011	*68.5	–0.57	–3.63	3.06	0.14	831
	S–3012	*68.5	–0.60	–1.00	0.40	–0.01	1338
	S–3013	*68.5	–0.37	–0.76	0.39	–0.04	1575
	S–3014	*68.5	–0.76	–0.88	0.12	–0.01	1725
	S–3011	83.5	–0.24	–0.43	**0.19**	–2.87	831
	S–3012	83.5	–0.26	–0.27	**0.01**	–0.39	1338
	S–3013	83.5	–0.27	–0.28	**0.01**	–0.38	1575
	S–3014	83.5	–0.28	–0.28	**0.00**	–0.12	1725

S–3014 (app. 4–2), in corehole G–3879 the upper Biscayne aquifer flow unit and two flow zones (63.60 to 74.12 and 84.84 to 85.60 ft bls) within the lower Biscayne aquifer flow unit (table 5) were major intervals where groundwater flowed into or out of the borehole. The transmissivity of the two major flow zones in the lower Biscayne aquifer flow unit accounted for almost 75 percent of the transmissivity in the corehole exclusive of the upper Biscayne aquifer flow unit (fig. 11).

Most inflow of groundwater into corehole G–3879 while production well S–3012 or S–3014 were pumped originated in the upper Biscayne aquifer flow unit, with only 2.06 gal/min entering the borehole in the interval between depths 38 and 62 ft bls while production well S–3014 was pumped, compared to 15.75 gal/min inflow from the interval above the 38 ft bls depth (table 5–1; plate 1). As most inflow into the borehole is from the interval above 38 ft, and other flowmeter tests (app. 4–2) show only minor flow zones in the middle semiconfining unit contributing only a small percentage of groundwater inflow to the borehole (table 5), the most likely source for the majority of the inflow into the borehole is the upper Biscayne aquifer flow unit. Similar results were observed in corehole G–3879 when pumping from production well S–3012 (table 5–1), with 12.35 gal/min inflow of water into the borehole from the interval above the 38-ft depth, but the inflow of groundwater into the interval between 38 and 62 ft bls was at a much lower rate (0.26 gal/min while pumping from S–3012 versus 2.06 gal/min when pumping from production well S–3014), indicating that flow zones in the middle semiconfining unit may not be as well connected to production well S–3012 as to production well S–3014.

While pumping from production well S–3014, outflow from corehole G–3878 into the Biscayne aquifer was greater in the interval between depths 62 and 82 ft bls (14.99 gal/min) than from flow zones in the interval below depth 82 ft bls (2.82 gal/min). When production well S–3012 (across the C–2 canal from corehole G–3879) was being pumped (table 5–1; plate 1), less outflow occurred in corehole G–3879 in the interval between depths 62 and 82 ft bls (4.74 gal/min) than from the interval below depth 82 ft bls (7.87 gal/min), opposite of what occurred in the corehole when pumping from production well S–3014. This may indicate that the lowest flow zone in the lower Biscayne aquifer flow unit in corehole G–3879 is not as well connected to the closer production well S–3014 as it is to the more distant production well S–3012.

The vertical flow rate at the lower depth (82 ft) in corehole G–3879 showed an unusual response when production well S–3014 was pumped (fig. 5–3; app. 4–2) in that the upflow increased and then tapered off to a lower rate of upflow. The opposite occurred when pumping in production well S–3014 ended. Instead of an increase in upflow, there was a sharp decrease in upflow, followed by a sharp increase in upflow to a rate that was greater than when pumping began. This spike did not occur in corehole G–3879 at the same depth of 82 ft bls with production well S–3012 pumping, nor was it repeated in any of the other coreholes at SCWF. This may be caused by the more rapid propagation of drawdown in the flow zone in the interval above the depth of the lower Biscayne aquifer flow unit than in the flow zone found in the interval below the depth, causing the greatest head differential between these two flow zones to occur early in the test. The opposite occurred when pumping was stopped; therefore, the spikes are further indication of the differences in connectivity of each flow zone to the pumping production well, even though they are separated vertically by only a few feet.

Fluid temperature response in corehole G–3879 during pumping was dependent on which side of the C–2 canal the pumping well was located, possibly indicating influence of the C–2 canal. At the depth of 38 ft bls, fluid in the corehole G–3879 increased during pumping of production well S–3012 on the opposite side of the C–2 canal (fig. 5–3*A*) as warmer water from the canal flowed into the borehole from the upper Biscayne aquifer flow unit. During pumping of production well S–3014 on the same side of the C–2 canal at the same depth of 38 ft, fluid temperature initially increased, but then decreased for the duration of pumping (fig. 5–3*A*), possibly indicating a different source of cooler groundwater to the borehole from the upper Biscayne aquifer flow unit. In both cases, however, and as in other coreholes at SCWF, when pumping from the production wells stopped, temperature of borehole fluid rapidly decreased as the vertical flow reversed from downflow to upflow and cooler groundwater entered the borehole, and then the temperature slowly returned to its pre-test level. At a depth of 62 ft bls (fig. 5–3*B*), the fluid temperature increased slightly and slowly as production well S–3012 was being pumped. When pumping began at production well S–3014, however, fluid temperature in corehole G–3879 showed a brief increase, then decreased during the first minute of pumping before it rose again for the remainder of the period of pumping. These two examples may indicate that different sources of groundwater flowed into corehole G–3879 depending on which production well was pumping and its relation to the C–2 canal.

Test Corehole G–3880

Due to instability in corehole G–3880, the Miami Limestone portion and the upper 10 ft of the Fort Thompson Formation in the borehole were lined with slotted PVC casing (app. 4–2), which affected the borehole flow and ability to measure it. Under unstressed ambient, steady-state borehole conditions with no pumping in the SCWF, vertical borehole fluid flow in corehole G–3880 was upward, with the major inflow from and higher head in the lower Biscayne aquifer flow unit, and major outflow from the borehole and lower head in the upper Biscayne aquifer flow unit. Testing under stressed steady-state conditions while pumping from corehole G–3880 showed a major flow zone from 82.9 to 88.4 ft bls in the lower Biscayne aquifer flow unit, which accounted for 28 percent of the change in vertical flow below the upper Biscayne aquifer flow unit (table 5). This zone had a transmissivity of 60 percent exclusive of the upper Biscayne aquifer

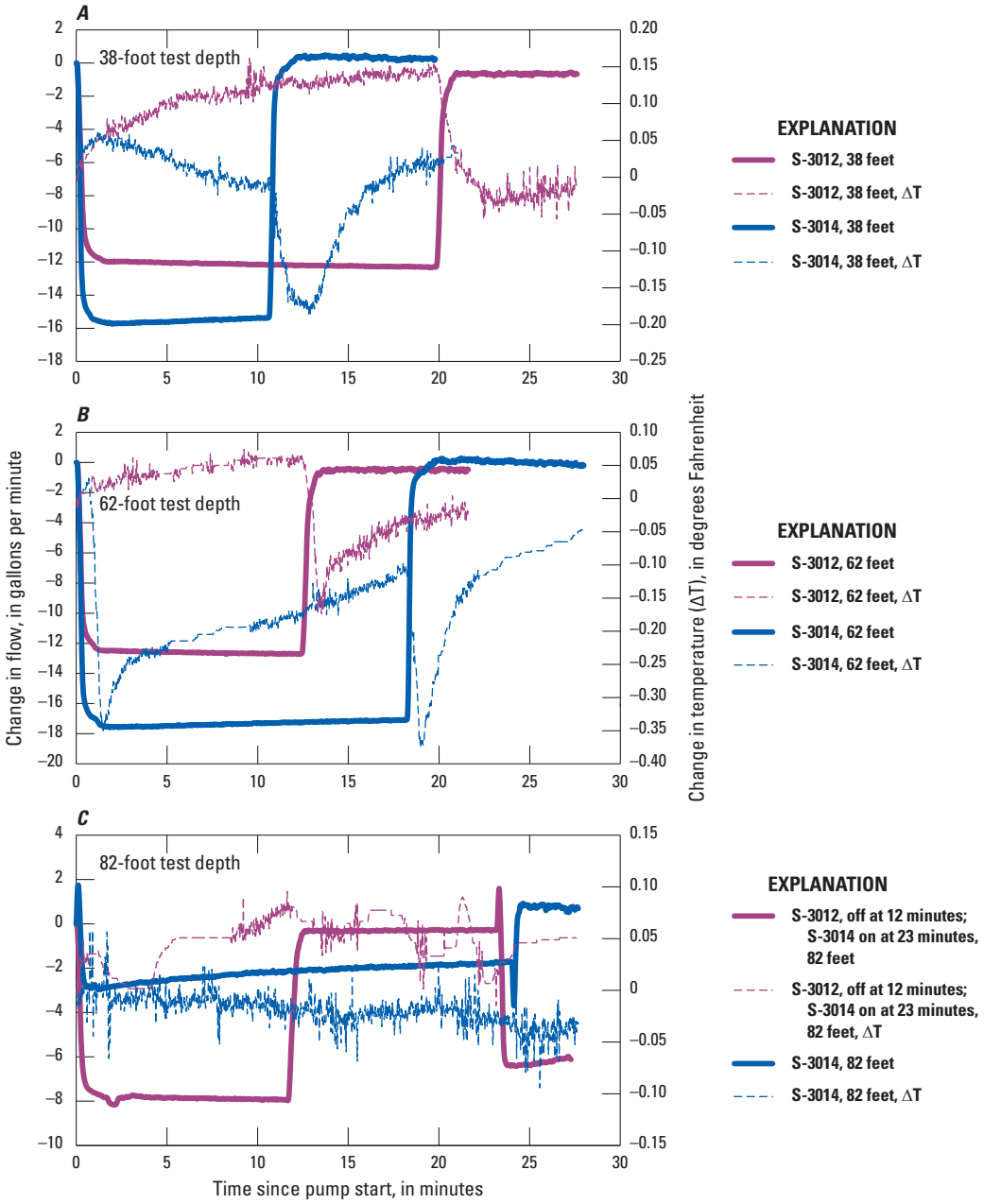

Figure 5–3. Change in flow rate and fluid temperature at tested intervals in test corehole G–3879 in response to pumping and recovery in production wells S–3012 and S–3014.

flow unit as computed using the FLASH program (fig. 11). A second minor flow zone identified from 65.5 to 79.0 ft bls with about 16 percent of the change in vertical flow below the upper Biscayne aquifer flow unit (table 5) accounted for 30 percent of the estimated transmissivity exclusive of the upper Biscayne aquifer flow unit (fig. 11).

Data were first collected in G–3880 while pumping from different SCWF production wells when the C–2 canal stage was lowered for water-management activities to observe the response in groundwater flow to a lower canal stage. A second cross-hole set of tests was then completed when the canal stage returned to a stage level that is typical for the canal. At the higher canal stage level, responses of flow and fluid temperature in the G–3880 corehole to production well pumping appear to be dependent on (1) distance from the pumping production well, (2) hydraulic connectivity of flow zones within the corehole to the pumping production well, and (3) the spatial relation of the corehole and the pumping production well to the C–2 canal. Comparison of vertical flow rates at three depths in corehole G–3880 at two different canal-stage levels showed that rate of vertical fluid flow was about the same at each depth and for each production well and not dependent on canal stage level (table 5). Temperature at three depths in corehole G–3880, however, was affected by the lowered stage level (figs. 5–4 and 5–5).

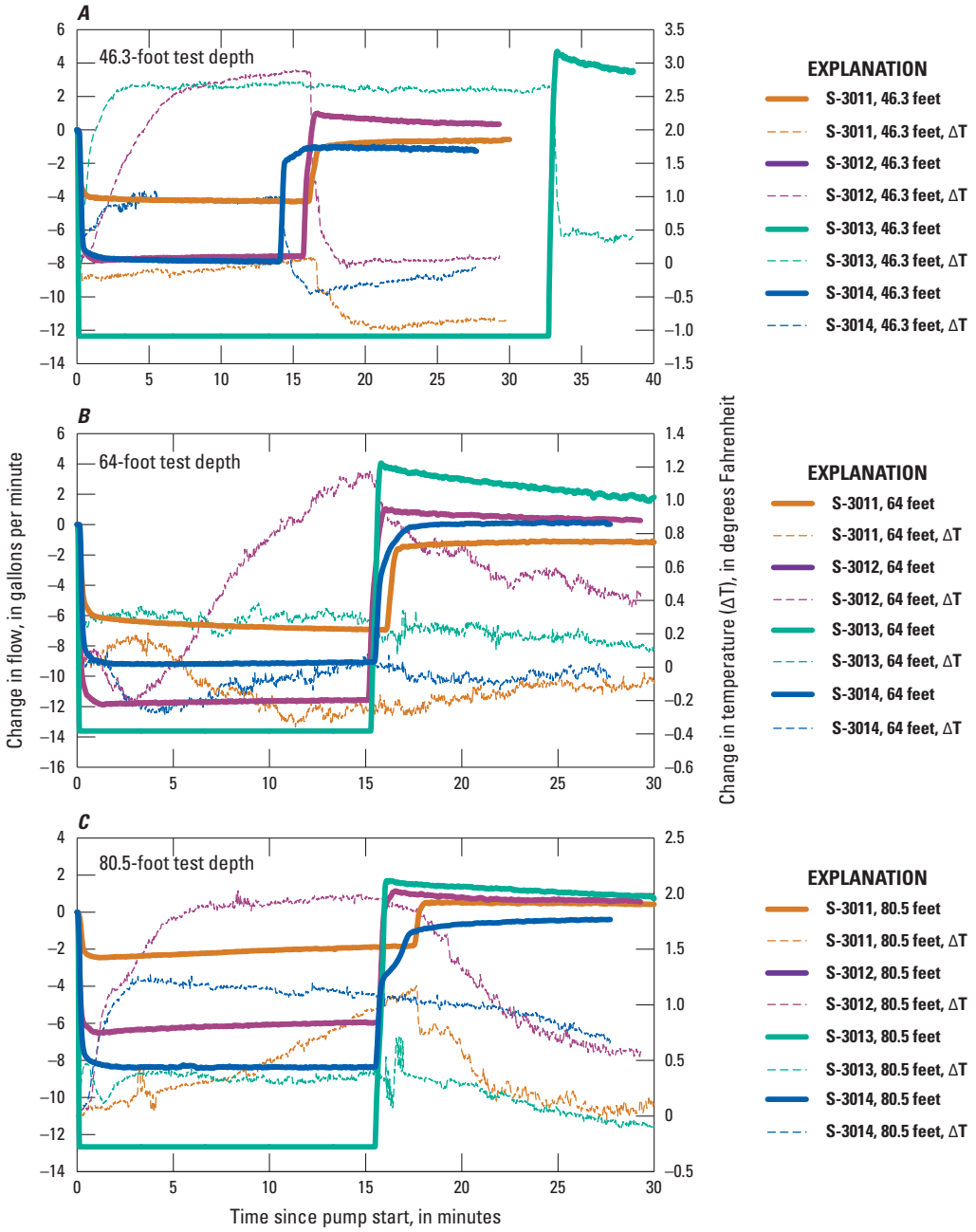

Figure 5–4. Change in flow rate and fluid temperature at tested intervals in test corehole G–3880 in response to pumping and recovery in production wells S–3011, S–3012, S–3013, and S–3014.

The majority of the inflow at normal canal stage levels in corehole G–3880 (table 5–1; plate 1) came from the uppermost Biscayne aquifer flow unit, and the variation in flow rate can be related to the distance of the pumping production well from the corehole. However, a greater amount of groundwater inflow occurred in the interval between depths 46.3 and 64 ft bls (plate 1), which appears to be related to which side of the canal the pumping production well is located. Production wells (S–3013 and S–3014) on the southwestern side of the C–2 canal produced less inflow into corehole G–3880 in the interval between 46.3 and 64 ft bls (averaging 1.35 gal/min for both production wells S–3013 and S–3014) compared to production wells on the northeastern side of the C–2 canal (2.65 gal/min for production well S–3011 and 4.10 gal/min for production well S–3012) or about 50 percent of what was contributed from the upper Biscayne aquifer flow unit in the interval above test depth 46.3 ft when pumping from the production wells on the opposite side of the C–2 canal (table 5–1; plate 1). Minor flow zones in the interval between 46.3 to 64 ft bls of the middle semiconfining unit may be better connected to production wells on the northeastern side of the canal.

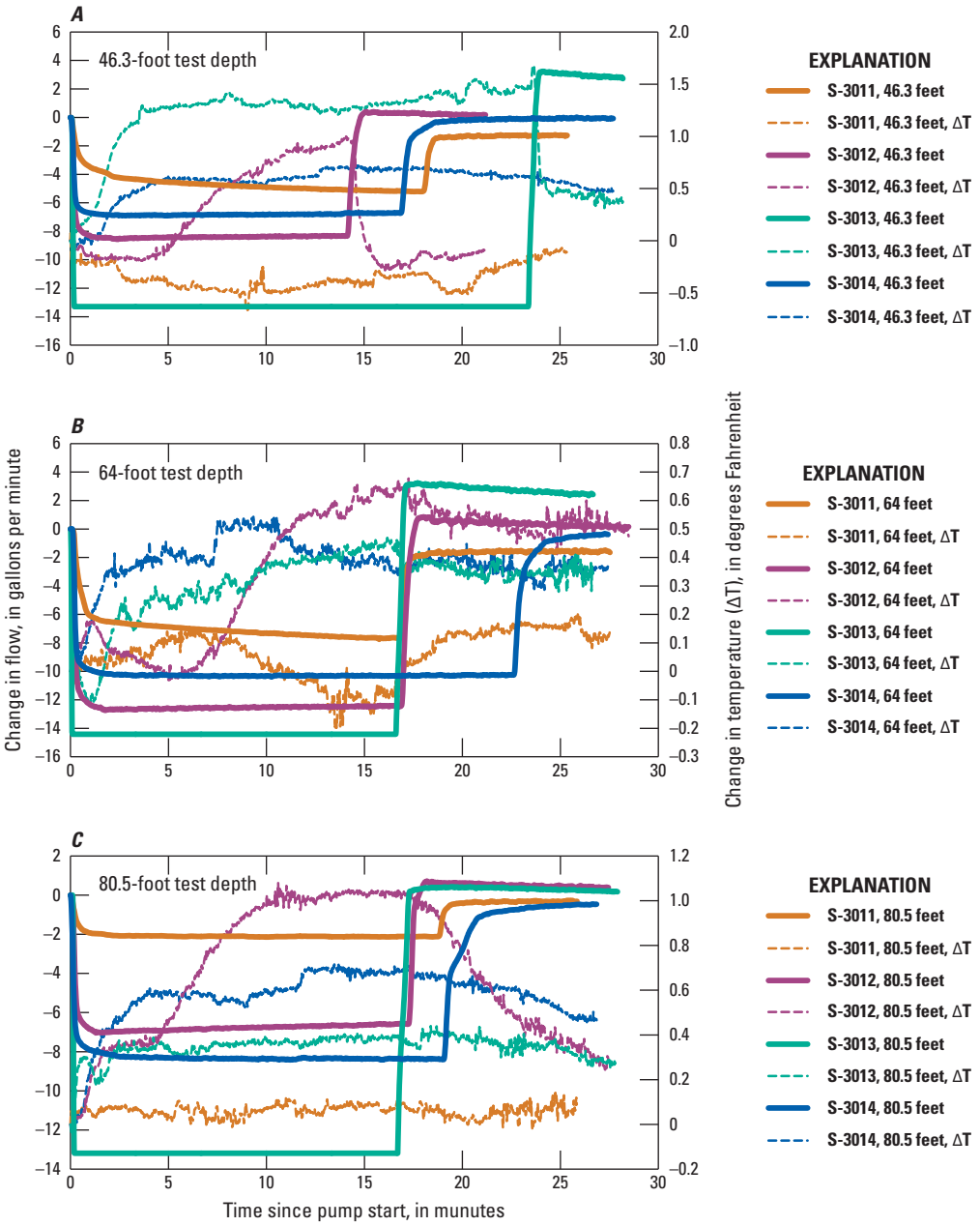

Figure 5–5. Change in flow rate and fluid temperature at tested intervals in test corehole G–3880 in response to pumping and recovery in production wells S–3011, S–3012, S–3013, and S–3014 during lowered canal stage level.

Outflow from the lower Biscayne aquifer flow unit in corehole G–3880 also varied depending on which side of the canal the pumping production well was located (plate 1). When pumping from production wells (S–3013 and S–3014) on the southwestern side of the canal, the outflow from the corehole was less than 1 gal/min in the interval between depths 64 and 80.5 ft bls (table 5–1), and most outflow occurred in the major flow zone found in the interval below 80.5 ft bls. When pumping from production wells (S–3011 and S–3012) on the northeastern side of the C–2 canal, the outflow from the corehole for production well S–3011 in the interval below 80.5 ft bls was about half (2.46 gal/min) of that in the interval between 64 to 80.5 ft bls (4.46 gal/min), but when production well S–3012 was pumped, flow in corehole G–3880 was only slightly less in the interval between 64 to 80.5 ft bls (5.34 gal/min) than in the interval below the depth of 80.5 ft bls (6.50 gal/min; table 5–1; plate 1). Therefore, flow zones in the interval below 80.5 ft may be better connected to all of the production wells except S–3011 than in the interval between 64 to 80.5 ft bls, which may be better

connected to production wells on the northeastern side of the canal. Groundwater inflow and outflow showed similar results in corehole G–3880 during cross-hole tests conducted during the lowered canal stage level (table 5–1).

The G–3880 corehole (fig. 5–4) had a greater range of fluid temperature values (almost 3 degrees Fahrehneit (°F) of temperature change) than other SCWF coreholes (up to 0.4 °F of temperature change). When a production well was pumped (except S–3011), there was a rapid increase in the fluid temperature in corehole G–3880 at depth 46.3 ft bls that was greater (almost 3 °F change in the two closest production wells, S–3012 and S–3013) than that in SCWF coreholes at a similar depth but further from the corehole (fig. 5–4*A*). The exception was when production well S–3011 was pumped, the fluid temperature in corehole G–3880 stayed about the same, dropping slightly by 0.25 °F and then slowly rising back to the starting borehole fluid temperature. When pumping from the production wells ceased at depth 46.3 ft, however, fluid temperature in corehole G–3880 decreased noticeably as the flow reversed to the static prepumping condition with upflow bringing deeper and cooler groundwater into the corehole. The increase in fluid temperature and the proximity of corehole G–3880 to the canal would seem to indicate that warmer canal water was being drawn into the test corehole when a production well was being pumped.

The increase in fluid temperature response in G–3880 at depth 64 ft bls (fig. 5–4*B*) was repeated when production well S–3012 was pumped, though the increase in borehole fluid temperature was less than half of the change at the shallower depth of 46.3 ft bls. The other three production wells when pumped showed little or no change in borehole fluid at depth 64 ft bls in the corehole. While pumping from production wells S–3012 and S–3014 at depth 80.5 ft bls, a similar change in fluid temperature as at depth 46.3 ft bls was observed in the corehole (fig. 5–4*C*). Differences in connectivity of the flow zones between the corehole and the pumping production well are most likely the cause for these variations.

The change in flow rate between unstressed ambient and stressed borehole conditions in corehole G–3880 when pumping from a production well were similar during both canal stage levels at all three depths (figs. 5–4 and 5–5; table 5–1). The fluid temperature results, however, were different for the lower canal stage level. Overall, the fluid temperature changes in corehole G–3880 caused by pumping from a production well during the lower canal stage level were lower than those recorded at the higher canal stage level (figs. 5–4 and 5–5), which could have been caused by less infiltration of warmer canal water during the lower canal stage level. Temperature change during the lower stage level was half that of when the canal was at the higher stage level at all depths, and the temporal trend when normalized was different only at test depth 64 ft bls for production wells on the southwest side of the C–2 canal (figs. 5–4*B* and 5–5*B*). These results may indicate that the canal stage level has an effect on how much water is being lost from the canal to groundwater.

Test Corehole G–3881

Under unstressed ambient, steady-state borehole conditions with no pumping in the SCWF, vertical borehole fluid flow in corehole G–3881 was upward, with the major inflow from and higher head in the lower Biscayne aquifer flow unit, and major outflow from the borehole and lower head in the upper Biscayne aquifer flow unit. During stressed steady-state borehole conditions while either pumping from the corehole or from production well S–3013 (app. 4–2), the upper Biscayne aquifer flow unit and a major flow zone (82.65 to 88.30 ft bls) within the lower Biscayne aquifer flow unit (table 5) were the major intervals where groundwater flowed into the borehole. The major flow zone in the lower Biscayne aquifer flow unit accounted for 26 percent of the change in vertical flow below the upper Biscayne aquifer flow (table 5) and has a transmissivity of almost 70 percent exclusive of the upper Biscayne aquifer flow unit (fig. 11).

Flow data collected in corehole G–3881 showed that the response of vertical flow rate and fluid temperature (fig. 5–6) and water level drawdown (fig. 5–1) to pumping from different SCWF production wells was influenced by the distance from the corehole to the pumping production well and the relation of the pumping well and the corehole to the C–2 canal. The upper Biscayne aquifer flow zone produced most of the inflow into the corehole during pumping of all four production wells (plate 1), but unlike previously discussed coreholes (G–3878, G–3879, and G–3880), two minor flow zones in the middle semiconfining unit contributed more inflow of groundwater in the interval above 46 ft bls while pumping from the test corehole (app. 4–2). The steady-state stressed flowmeter data showed these two flow zones to be responsible for 18 percentage each of the total change in vertical flow below the upper Biscayne aquifer flow unit (table 5).

Inflow of groundwater into corehole G–3881 while pumping at production well S–3013 to the southwest and across the C–2 canal (393 ft from corehole G–3881) from the corehole produced more inflow at all depths than did pumping from the closer production well S–3012 (246 ft from corehole G–3881) to the northwest and on the same side of the canal as the corehole (fig. 5–6). Because production well S–3013 produced greater vertical flow in the corehole than the closer production well S–3012, it may indicate that corehole G–3881 is better connected in the lower Biscayne aquifer flow unit to production well S–3013 or that corehole G–3881 is better connected to the canal, which is only 70 ft from corehole G–3881 and positioned between production well S–3013 and the corehole (fig. 5–1). At the two lower depths (62 and 79 ft bls), the vertical flow generated in corehole G–3881 by pumping of production well S–3012 was more than that generated by pumping from the two more distant production wells (S–3011 and S–3014), but still less than production well S–3013. Again, the relation of the C–2 canal between corehole and production well S–3013 and the proximity of the corehole to the canal may influence the rate of vertical flow in the borehole.

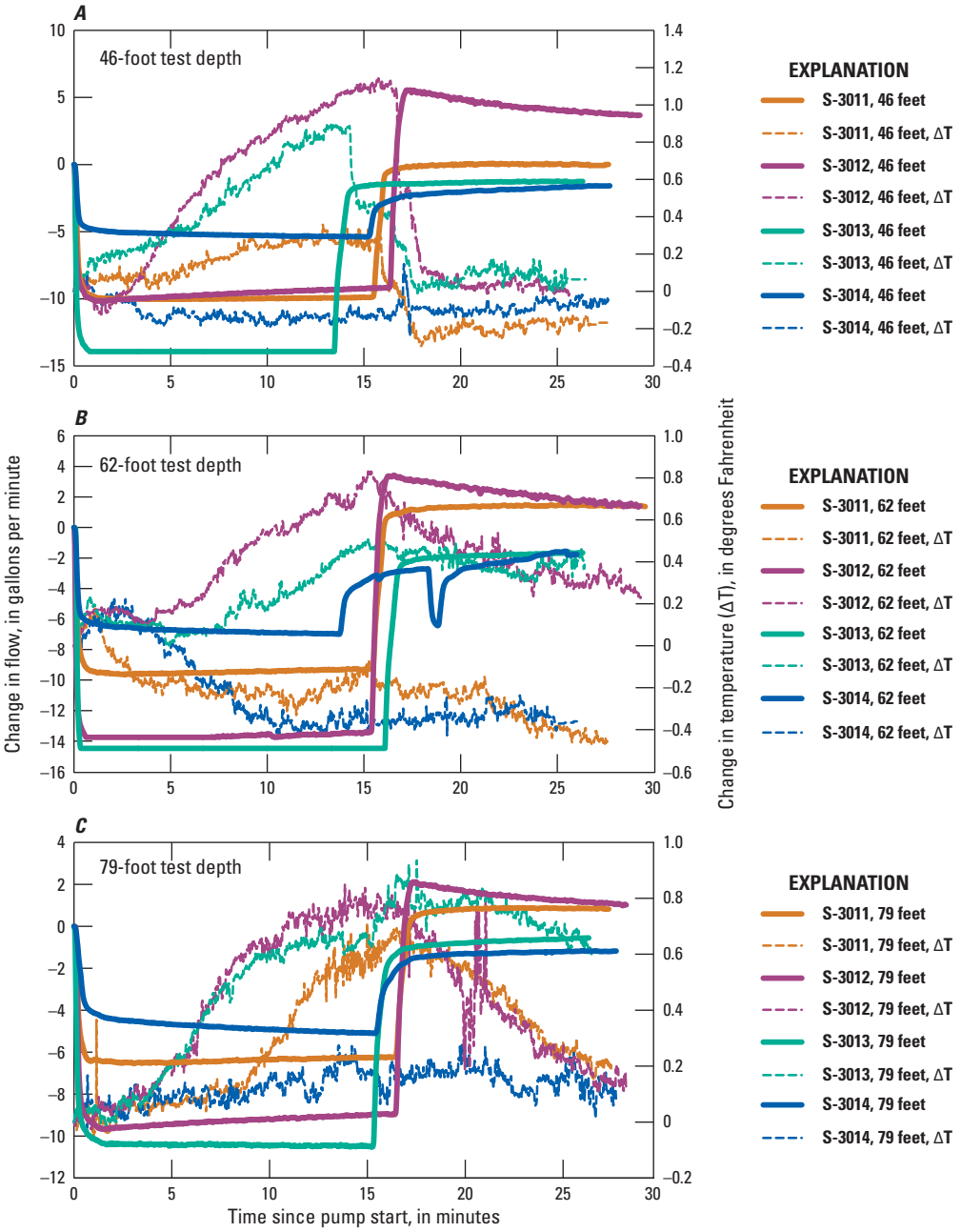

Figure 5–6. Change in flow rate and fluid temperature at tested intervals in test corehole G–3881 in response to pumping and recovery in production wells S–3011, S–3012, S–3013, and S–3014.

Flow zones in the interval between depths 46 and 62 ft bls in corehole G–3881 had greater inflow of groundwater in the borehole when pumping from the closer production well S–3012 to the northwest (3.59 gal/min) and the more distant production well S–3014 to the west (1.68 gal/min) than when pumping from production well S–3013 to the southwest (0.49 gal/min), which had greater inflow from the interval above 62 ft bls (table 5–1), and production well S–3011 to the southeast, which produced an outflow of 0.36 gal/min in this interval (plate 1). Production well S–3011 was the only production well that caused outflow from a corehole in this interval, which further demonstrates the heterogeneity in the connectivity of flow zones to pumping wells at the SCWF.

Major outflow from the G–3881 corehole was similar to that observed in test corehole G–3880 in that outflow from the borehole was greater in the interval below 79 ft bls from the lowermost flow zone in the lower Biscayne aquifer flow unit for each production well than the outflow in flow zones in the interval between 62 and 79 ft bls (plate 1). In the interval between 62 and 79 ft bls, the rate of outflow was similar to that in corehole G–3880, which also had greater outflow from this interval during pumping of production wells on the northeastern side of the C–2 canal (plate 1).

Possible inflow of canal water to corehole G–3881 was also evident in the fluid temperature data of the vertical flow at three depths (fig. 5–6). When a production well was pumped, the borehole fluid flow in corehole G–3881 reversed and brought warmer, possibly C–2 canal water into the borehole. And when pumping from a production well ceased, vertical flow in corehole G–3881 reversed and cooler water from a deeper source moved up the borehole. The C–2 canal as the source of the warmer water is based on its proximity to corehole G–3881 (70 ft) and measurements made on June, 16, 2009, during unstressed ambient, steady-state flow-meter data collection in corehole G–3881, for which the fluid temperature measurement in the upper part of the borehole of corehole G–3881 was 6.5 °F cooler than the C–2 canal measurement. The only exceptions to the observed warming trend in borehole fluid temperature were at depth 46 ft bls during pumping from the most distant production well S–3014 (fig. 5–6*A*), in which fluid temperature decreased slightly and at depth 62 ft bls (fig. 5–6*B*) when pumping from production wells S–3011 and S–3014, a cooling trend was observed in the borehole fluid temperature followed by the fluid temperature slowly increasing as pumping continued. In both of these cases, however, production wells S–3011 and S–3014 are more distant than production wells S–3012 and S–3013 and may not have cause enough stress on the corehole to draw in as much of the warmer canal water. Temperature profiles in corehole G–3881 while pumping from different production wells seem to support differences in connectivity between the corehole and the production wells in the SCWF and that the C–2 canal may supply recharge to the groundwater during production well pumping.

Test Corehole G–3882

Under unstressed ambient, steady-state borehole conditions with no pumping in the SCWF, vertical borehole fluid flow in corehole G–3882 was downward, with the major inflow from and higher head in the upper Biscayne aquifer flow unit, and major outflow from the borehole and lower head in the lower Biscayne aquifer flow unit. During stressed steady-state borehole conditions while pumping from the corehole (app. 4–2), flowmeter measurements in corehole G–3881 showed that the upper Biscayne aquifer flow unit and a major flow zone (71.00 to 72.40 ft bls) within the lower Biscayne aquifer flow unit (table 5) were major intervals where groundwater flowed into the borehole. The major flow zone in the lower Biscayne aquifer flow unit accounted for 26 percent of the change in vertical flow below the upper Biscayne aquifer flow unit (table 5) and has a transmissivity of almost 50 percent exclusive of the upper Biscayne aquifer flow unit (fig. 11).

Pumping from the SCWF production wells caused less change in flow rate between unstressed ambient and stressed borehole conditions in corehole G–3882 and minimal change in borehole fluid temperatures than in the other coreholes (except for G–3877, which showed no response to pumping). This result was expected as this corehole is the second most distant from the production wells (831 ft from the closest production well S–3011). The unstressed ambient steady-state flow in this corehole was downward rather than upward as in the other four coreholes (table 5–1). Additionally, even when pumping from two production wells (S–3013 and S–3014) simultaneously, response of borehole fluid flow to production well pumping was either negligible or below detection (table 5–1; plate 1).

The greatest response in corehole G–3882 vertical flow was caused by pumping from the nearest production well (fig. 5–7), S–3011, but unlike the other coreholes at SCWF that had a borehole flow response to production well pumping in which the greatest inflow was from the upper Biscayne aquifer flow unit in the uppermost interval, the inflow from the uppermost interval above 46 ft bls while pumping from production well S–3011 (1.59 gal/min) was about the same as the inflow from the interval between 36 and 61 ft bls (1.33 gal/min) (table 5–1; plate 1). Pumping from production wells S–3012, S–3013, and S–3014 produced a similar response, but the total inflow to the borehole from all flow zones above a depth of 61 ft bls while pumping from one of these production wells was less than 0.33 gal/min (production well S–3013). Most of the outflow from corehole G–3882 while pumping from any of the four production wells occurred between depths 68.5 and 83.5 ft bls (plate 1) supporting other flowmeter data that the flow zone between 71.0 and 72.40 ft bls is a major flow zone.

In summary, flowmeter data collection in the SCWF coreholes were useful for determining the presence and attributes of a flow zone, its connectivity to a production well, and possible hydraulic connection with the C–2 canal. In a homogeneous aquifer, flow generated in the test corehole by pumping from a production well would be most affected by the distance from the pumping production well. Cross-hole flowmeter data, however, show that in some cases distance to a pumping well was not the only, or principal, factor in determining the response of the corehole to that pumping, and that additional factors, including the corehole's spatial relation to the C–2 canal and (or) connectivity of flow zones within the corehole to the C–2 canal and production well, affected the response. Borehole fluid temperature data (app. 4–2 and figs. 5–4 and 5–5) collected from the electromagnetic (EM) flowmeter during cross-hole tests in coreholes adjacent to the C–2 canal may also be important for showing that warmer canal water may be recharging the aquifer within the well field.

Analysis of borehole flow in the test coreholes in response to pumping and recovery of the SCWF production wells provided additional information on the character of the hydraulic connection between the coreholes and the production wells. For example, the transient change in flow that was measured at selected depths in coreholes G–3879 and G–3881 is presented in figures 5–3 and 5–6, respectively. The transient response curves have a similar character, reflecting similar changes in the hydraulic-head difference between the upper Biscayne aquifer flow unit and the lower Biscayne aquifer flow unit. Pumping initially results in rapid decreases

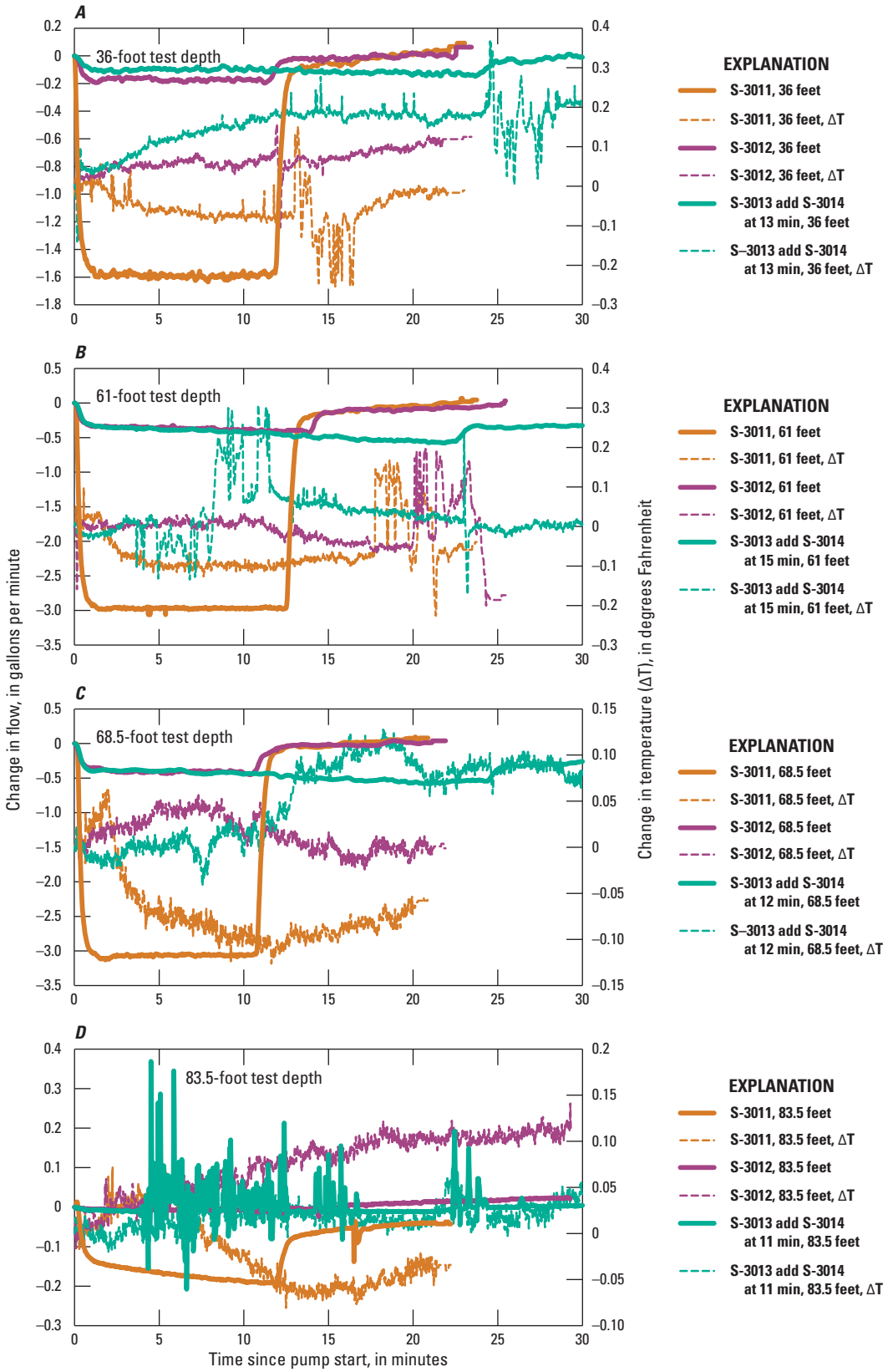

Figure 5–7. Change in flow rate and fluid temperature at tested intervals in test corehole G–3882 in response to pumping and recovery in production wells S–3011, S–3012, S–3013, and S–3014.

in head in the lower Biscayne aquifer flow unit relative to the upper Biscayne aquifer flow unit, with the head difference and flow change quickly stabilizing. When pumping is stopped, the head in the lower Biscayne aquifer flow unit increases rapidly relative to that in the upper Biscayne aquifer flow unit, with the head difference and flow response quickly trending toward stabilization.

Differences observed in flow response (to production well pumping) between flow zones within the lower Biscayne aquifer flow unit in the test coreholes reflect the degree of hydraulic connection of flow zones within the same lower Biscayne aquifer flow unit with the individual production wells (plate 1). For example, in corehole G–3879, the contrast in the flow responses to pumping at production wells S–3012 and S–3014 reflects the greater degree of connection of the major flow zone in the uppermost Tamiami Formation (84.84 to 85.60 ft bls) with production well S–3012 and a greater degree of connection of the major flow zone in the lower Fort Thompson Formation (63.60 to 74.12 ft bls) with production well S–3014 (fig. 5–3*B* and *C*; plate 1). In corehole G–3881, the contrast in the flow responses between flow zones within the lower Biscayne aquifer flow unit consistently reflects a greater degree of connection between the major flow zone in the uppermost Tamiami and lower Fort Thompson Formations (82.65 to 88.30 ft bls) and all production wells, S–3011, S–3012, and S–3013, than the minor flow zone 64.60 to 72.61 ft bls (fig. 5–6; plate 1).

Appendix 6. Slug-Test Report

See supplemental file available at *http://pubs.usgs.gov/sir/2014/5138/*.

Manuscript approved July 17, 2014

Prepared by the Raleigh Publishing Service Center
Kay Naugle, Editor
Kimberly Swidarski, Illustrations and layout

For more information about this publication, contact:
Director
U.S. Geological Survey
Florida Water Science Center
4446 Pet Lane, Suite 108
Lutz, FL 33559
(813) 498-5000

or visit our Web site at
http://fl.water.usgs.gov

USGS

Wacker and others—**Geologic and Hydrogeologic Frameworks of the Biscayne Aquifer in Central Miami-Dade County, Florida**—Scientific Investigations Report 2014–5138

ISSN 2328-0328 (online)
http://dx.doi.org/10.3133/sir20145138